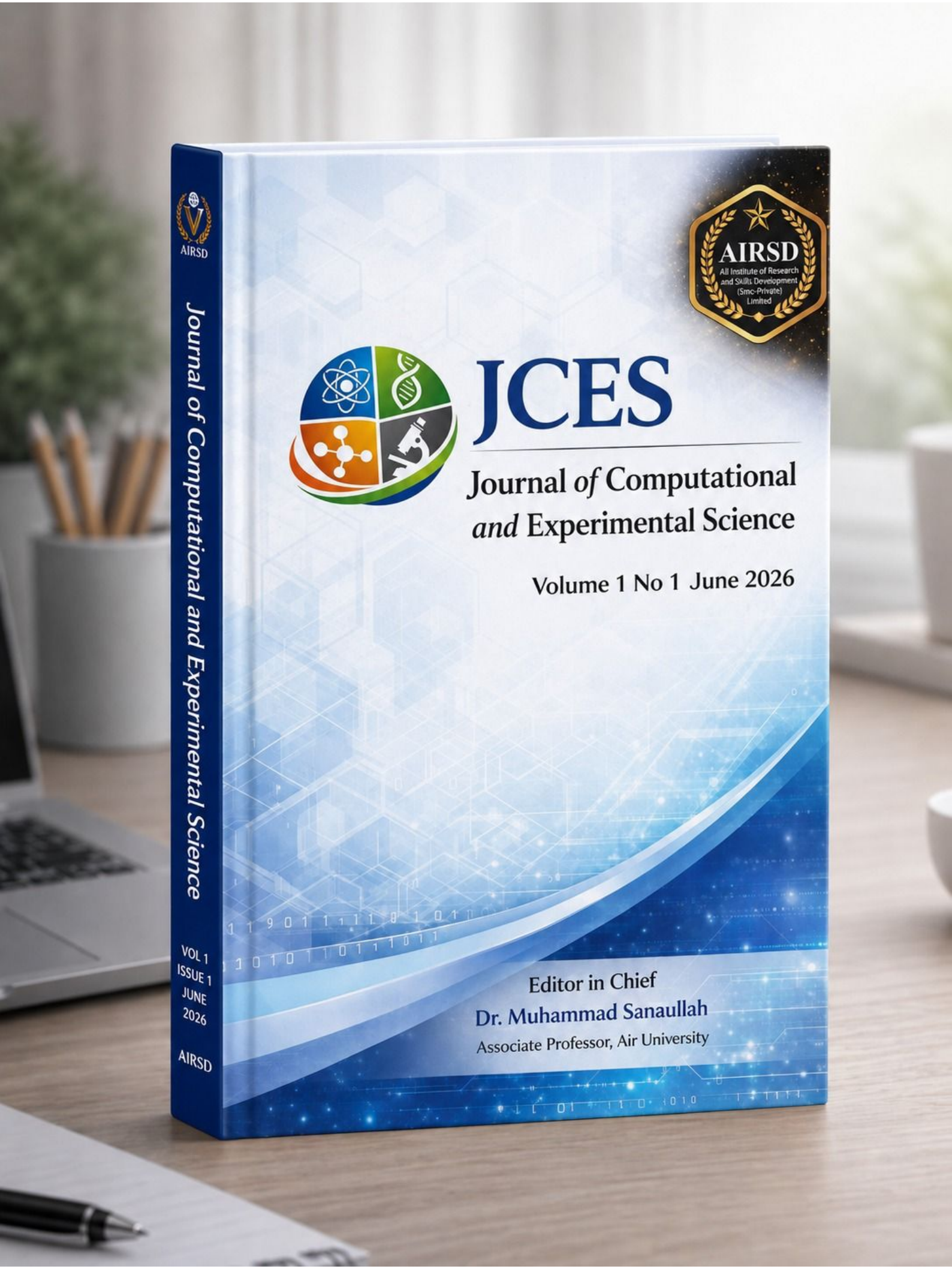
AIRSD
Journal of Computational and Experimental Science
VOL 1
ISSUE 1
JUNE
2026
AIRSD
AIRSD
All Institute of Research and Skills Development (Smc-Private) Limited
JCES
Journal of Computational and Experimental Science
Volume 1 No 1 June 2026
Editor in Chief
Dr. Muhammad Sanaullah
Associate Professor, Air University

About the Journal

The Journal of Computational and Experimental Science (JCES) publish high-quality, peer-reviewed research across physics, chemistry, biology, mathematics, engineering, and related scientific disciplines. The journal emphasizes the integration of computational modelling, theoretical analysis, and experimental validation to advance both fundamental understanding and practical applications.

The journal particularly welcomes contributions in emerging and high-impact areas, including drug discovery and design, materials science, nanotechnology, energy systems and photovoltaic technologies, as well as artificial intelligence and data-driven science.

The journal accepts original research articles, review articles, and short communications.

Scope of the journal

The journal covers a broad spectrum of scientific disciplines, including but not limited to:

Physics and applied physics

Chemistry and chemical sciences

Biology, biotechnology, and life sciences

Mathematics and computational mathematics

Engineering and applied engineering sciences

Materials science and nanotechnology

Drug discovery and design

Photovoltaics and renewable energy technologies

Environmental and energy sciences

Artificial intelligence and data-driven science

Pharmaceutical and biomedical sciences

Interdisciplinary and emerging research areas

Journal Information

Name of Journal: Journal of Computational and Experimental Science (JCES)

Journal Frequency: Bi-Annual

Editor-In-Chief: Dr. Muhammad Sanaullah

Language: English

Name of Publisher: Ali Institute of Research and Skill Development (AIRSD)

Review Type: Double Blind Peer Review

Area of Publication: Computational and Experimental Science (miscellaneous)

Journal of Computational and Experimental Science (JCES)

Ali Institute of Research and Skill Development (AIRSD)

Email: support@journals.airsd.org Phone+92 303 6411844

Editorial Team

International Advisory Board

Dr. Muhammad Habib ur Rehman

Material Engineering, Fujian Agriculture and Forestry University, Fuzhou, Fujian 350002, PR China

habibr06@hotmail.com

Dr. Faiza Farooq

Computational Chemistry, Xian, China

faizafarooq334@gmail.com

Dr. Zuhaib Nishter

North China University of water resources and Electric power, Zhengzhou China.

zuhaib.nishtar1991@gmail.com

National Advisory Board

Journal of Computational and Experimental Science (JCES)
ISSN Print: XXXX | ISSN Online: XXXX
Volume 1, Number 1, 2026, Pages 01–20
Journal Home Page: https://journals.airsd.org/index.php/jces

Hydro-Mechanical Behavior of Anisotropic Slate and Its Implications for Sustainable Slope Stability and Environmental Geo-Hazard Mitigation

Ghulam Rubab[1*], Shaista Jalbani[2], Abdul Razzaque Soomro[3], Emmy Maher[4], Fatima Gull[5]

[1] Institute of Plant Sciences, University of Sindh, Jamshoro, Sindh, Pakistan. Fisheries and Aquaculture SBBUVAS, Sakrand, Sindh, Pakistan
Email:ghulamrubabsoomro@gmail.com
[2] Fisheries and Aquaculture SBBUVAS, Sakrand, Sindh, Pakistan.
Email: jalbanishaista@gmail.com
[3] School of Resources and Environmental Engineering, Wuhan University of Technology, Wuhan, Hubei, China.
Email: soomroabdulrazaque2@gmail.com
[4] School of Environmental Engineering and Management, Mehran University of Engineering and Technology Jamshoro, Sindh, Pakistan.
Email: Emmy.mahar@gmail.com
[5] School of Sociology, University of Karachi, Pakistan.
Email: universityofkarachigull@gmail.com

ARTICLE INFO

Article History:
Received: January 10, 2026
Revised: February 15, 2026
Accepted: March 01, 2026
Available Online: March 08, 2026

Keywords:
Anisotropic slate; Hydro-mechanical coupling; Bedding angle; Discrete Element Method (DEM); Crack propagation; Slope stability

Corresponding Author:
Ghulam Rubab
Email:
ghulamrubabsoomro@gmail.com

ABSTRACT

Hydro-mechanical behavior of anisotropic slate is quite significant in regulating the stability of slopes and geo-engineering structures in water sensitive environments. The paper looks at the interaction between structural anisotropy and hydrological environment on strength, deformation and failure of slate. The suggested method to fill the gaps in the existing research involves a multi-scale methodology that will incorporate laboratory testing with the numerical model and slope-scale analysis. The standardization of uniaxial and triaxial compression tests was done using slate samples at various bedding angles, under both dry and wet conditions. The experimental results indicate that compressive strength is highly directional because it is an ordinary U-shaped curve with bedding inclination. The hydro-mechanical coupling imposes large strength and stiffness losses because of the impact of pore pressure, interlayer debilitation and along discontinuity lubrication. It was found that the saturated conditions promoted more complicated crack propagation and premature failure as compared to dry conditions. It was established that there were clear changes in failure modes, tensile-slipping, shear-slipping, and composite failure, among different bedding orientations. To study micro-mechanical behavior further, a Discrete Element Method (DEM) model based on Particle Flow Code (PFC) was built and calibrated. Patterns of initiation, propagation and coalescence of cracks observed in laboratory experiments could be replicated in the numerical models. Experimental and numerical results were synthesized to give us the most important thresholds that run the mechanisms of failures in the coupled conditions. The insights were extrapolated in hydro-mechanically coupled stability modeling to the slope scale. The results prove that the dominant factors that define slope instability are the pore water pressure and structural anisotropy. The proposed framework enhances the predictive capability in the geo-hazard assessment of reservoir banks and slopes which get rainfalls. This study will aid in bridging this gap between the laboratory level observations and field-level engineering. It gives an in-depth insight into how anisotropic rocks behave in real environmental conditions. The results present feasible suggestions on safer and more sustainable infrastructure design. Besides, the study advocates the formulation of better risk mitigation measures in geologically complicated areas. On balance, the given work contributes to the further development of combining hydro-mechanical effects in rock mechanics and the study of geo-hazards of the environment.

1. Introduction

Foliated and layered rock masses, e.g., slate, are present in large amounts in slopes, tunnels, reservoir banks, and underground engineering systems where structural anisotropy controls their mechanical behavior strongly. Due to the existence of bedding and the directions of schistosity, the response to the strength, stiffness, and deformation properties is directional. It thus does not behave much the same as an isotropic rock material (Zamanian, Mollaei-Alamouti, and Payan 2020). Existence tests have indicated that the structural planes' position with respect to the loading direction is the conclusively dominant control of compressive strength and deformation patterns (Zhang et al. 2017). Specifically, it has been recently confirmed through research on slate that the compressive strength is dependent on the bedding inclination on a typical U-shaped curve, and the mechanisms of failure switch between composite tensile-shear, shear-slip, and tensile splitting (Wen et al. 2023).

Along with anisotropy, water is another severe environmental parameter that affects the mechanical performance of rock masses. The HMC processes, such as pore pressure action, discontinuity lubrication, and degradation of inter-layer bonds, play a significant role in strengthening weaknesses in the strength of the rock and changing deformation and discontinuity failure (Qian et al. 2024). Laboratory observations reveal a decrease in compressive strength and a longer and more complicated crack propagation of saturated slate specimens under wet conditions than under dry conditions because the cementitious slates soften and become more capable of becoming deformed along structural planes (Zheng et al. 2025). These dark-oil interactions are especially applicable in water-related engineering contexts, including the slope of the reservoir, tunnels of diversions, and areas with rainfall, where seepage and redistribution of stress take place as a pair (Tian et al. 2025).

Environmentally and in an engineering sense, slope instability and geo-hazards are increasingly becoming appreciated as coupled hydro-mechanical phenomena, as opposed to mechanical failures. The interaction between water infiltration, stress concentration, and gradual fracture growth in anisotropic rock masses often leads to landslides, rockfalls, and instabilities in the banks of reservoirs (Zhu et al. 2025). Consequently, recent studies have focused on the combination of a lab experiment, numerical modeling, and field-scale tests in order to gain a superior understanding of the interplay of complex processes that determine rock mass action in the environmental loading conditions (Heinze et al. 2016). The simulated crack initiation, propagation, and coalescence of anisotropic rocks in discrete element methods (DEM) and, in particular, particle flow code (PFC) have been proven to be effective, as discrete element methods can be used to investigate the mechanisms behind failure under different hydro-mechanical settings in detail (Sun et al. 2019).

In spite of improvements, there are still substantial research gaps. The available literature is divided between laboratory-scale characterization of anisotropic rock behavior and numerical models of slope stability, but there has been a lack of integration between the two. Moreover, the application of hydro-mechanical coupling to the regulation of the failure processes and the environmental geo-hazards in layered rocks like slate has not been fully studied (Li et al. 2024). Thus, this study shall examine the hydro-mechanical characteristics in anisotropic slate by applying a combined experimental-numerical setting, as well as define a multi-scale connection between the laboratory results and slope scale stability study. The results are likely to be used in better forecasting and managing geo-hazards in water-related engineering

systems to aid in the sustainable construction of infrastructure and environmental resilience (Tsatsaris et al. 2021). The overall conceptual framework integrating hydro-mechanical interactions and geo-hazard mitigation in anisotropic slate is illustrated in Figure 1.

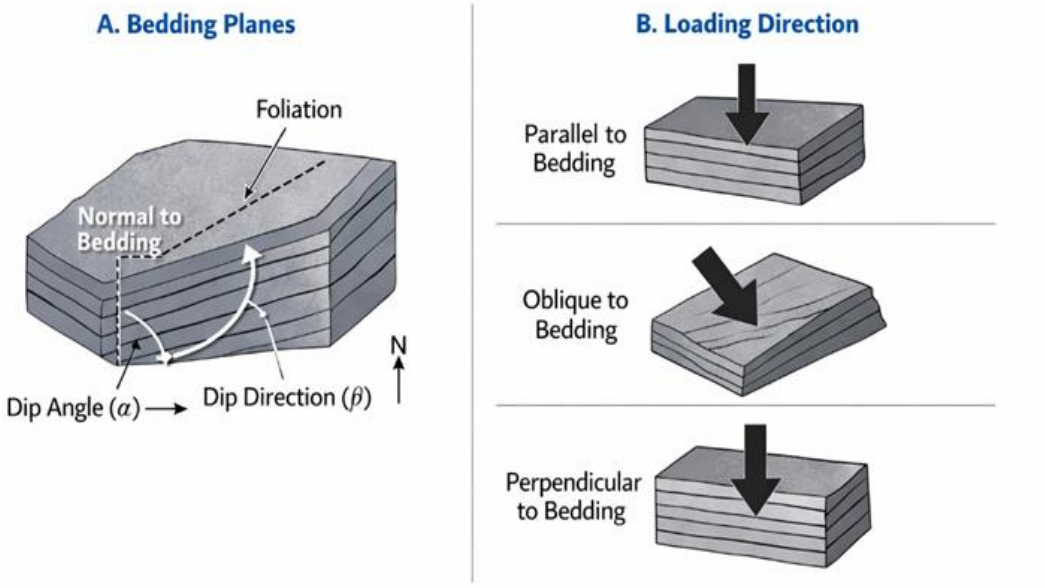

Figure 1. Integrated Hydro-Mechanical Framework for Anisotropic Slate Behavior and Geo-Hazard Mitigation

2. Literature Review

The mechanical effects of anisotropic rocks in the analysis of their mechanical behavior (Yan et al. 2020). Summary of key literature on anisotropic rock behavior, hydro-mechanical coupling, numerical modeling, and slope stability relevant to the proposed study in Table 1.

Table 1. Summary of Key Literature on Anisotropic Rock Behavior

Study	Rock Type	Key Focus	Methodology	Key Findings	Research Gap
Yan et al. (2020)	General anisotropic rocks	Mechanical behavior	Review	Direction-dependent strength	Lack of hydro-mechanical integration
Li et al. (2020)	Shale	Crack initiation thresholds	Experimental	Nonlinear deformation behavior	Limited environmental conditions
Hao et al. (2020)	Slate	Strength vs bedding angle	Lab tests	Weak interlayer bonding reduces strength	No coupling with water
Wen et al. (2023)	Layered rocks	Failure mechanisms	Dynamic testing	Tensile-shear and splitting modes	No slope-scale application
Zhao et al. (2023)	Rock masses	Hydro-mechanical coupling	Review	Water reduces effective stress	No anisotropic focus
Sun et al. (2019)	Fractured rocks	DEM modeling	Numerical	Crack propagation simulation	Limited validation with experiments
Xiang et al. (2020)	Jointed rock slopes	Stability analysis	Numerical	Structural planes control failure	No multi-scale framework

The mechanical behavior of anisotropic rocks has been of great interest to the mechanical engineering community, especially those that are in layered form like slate, schist, and shale, because of the importance in geotechnical engineering applications (Yan et al. 2020). In comparison to isotropic rocks, anisotropic rocks have direction-sensitive strength and deformation properties that are described by the planes of structure, including the bedding, foliation, and schistosity. It has also been shown that these structural characteristics have a substantial impact on the behavior of stress-strain, crack initiation, and strain behavior during loading (Li, Xie, and Wang 2020). Research on slate has found that the low strength is due to discontinuities and weak interlayer bonds, which result in poor deformability, especially when compressively loaded (Hao et al. 2020). Experiments in the laboratory and numerical analysis have also shown that in anisotropic rocks, the fracture process becomes complex with crack coalescence, propagation, interaction between pre-existing discontinuities, as well as induced fracture (Ismail and Azadbakht 2025). The effect of the interaction between intact rock bridges and structural planes in layered rocks frequently dominates the deformation of layered rocks to such an extent that the behavior of stress-strain is non-linear, and brittle failure occurs. The results obtained herein emphasize the need to consider anisotropy when examining and modeling the mechanics of rocks both in experiments and in computations (Yan et al. 2020). The structural anisotropy and loading configurations in slate are illustrated in Figure 2.

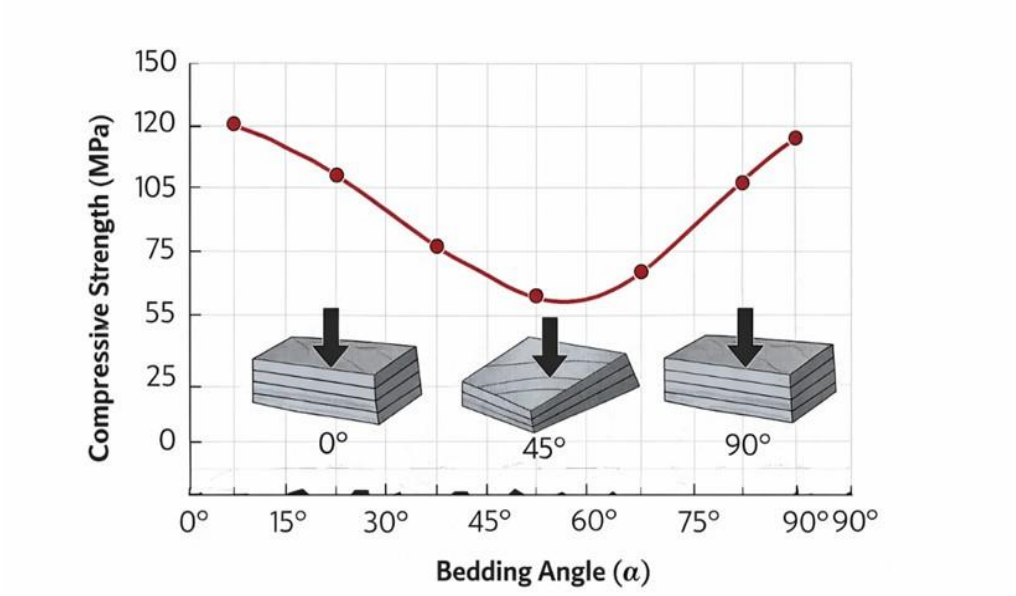

Figure 2. Structural Anisotropy in Slate: Bedding Orientation and Loading Direction

2.1 Influence of Bedding Angle on Strength and Failure Modes

It was observed that the strength and failure modes can vary depending on the angle of the bedding (Liu et al. 2023). One of the most important factors that affects the mechanical response of an anisotropic rock is the orientation of the structural planes with respect to the direction of loading. Several studies have demonstrated that compressive strength depends on the bedding inclination in a systematic manner; in many cases, there would be a U-shaped pattern with the bedding becoming weakest at the intermediate angles and becoming stronger at the higher angles (Si, Luo, and Luo 2024). Such a tendency is explained by the change of various failure mechanisms, such as tensile splitting, shear sliding, and composite failure

modes. Latest research in slate confirms that failure modes can be divided into three major ones: composite tensile-shear failure at low angles, shear-slip failure at intermediate angles, and tensile splitting at high angles (Wen et al. 2023). Minimum strength is usually seen at the angle where the shear of the structural plane predominates, and this reflects the importance of interlayer adhesion and resistance to friction. Also, the bedding orientation has a great impact on crack propagation, whereby fractures either cut across or parallel with the structural planes based on the stress conditions (Suo et al. 2020). This relationship between bedding angle and compressive strength is schematically shown in Figure 3.

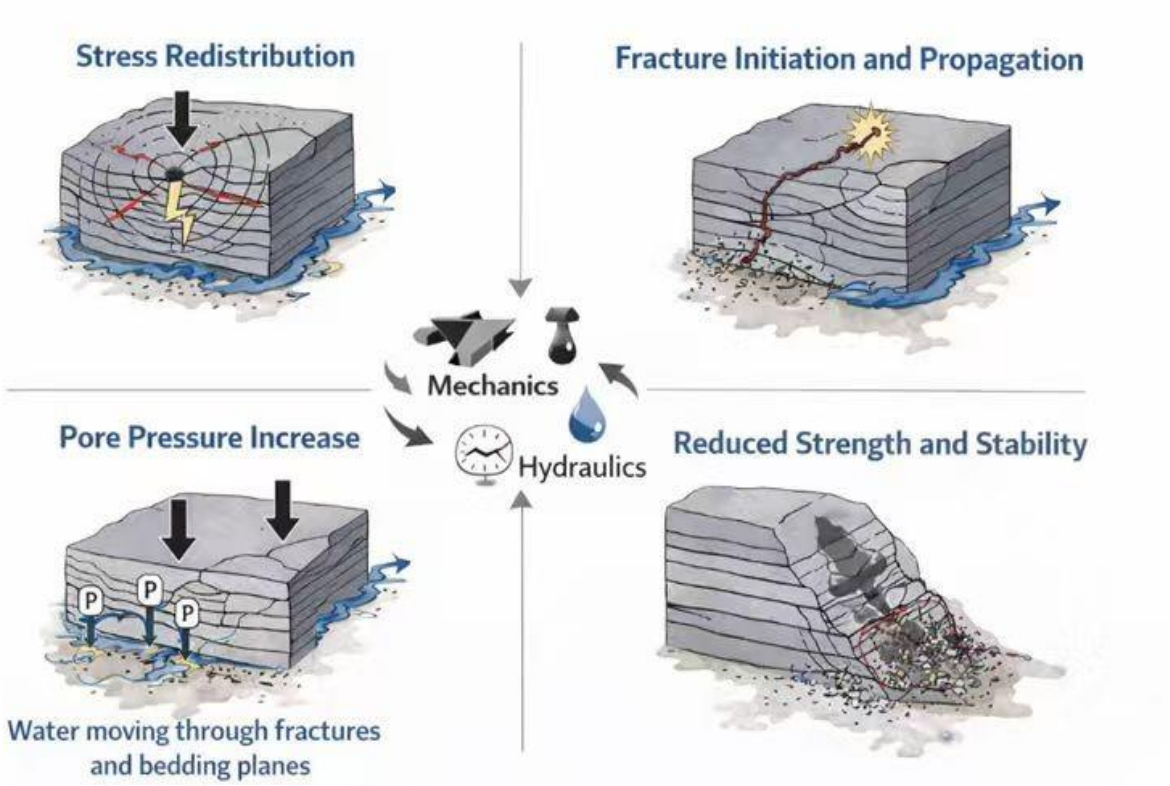

Figure 3. Relationship between Bedding Angle and Compressive Strength of Anisotropic Slate

2.2 Hydro-Mechanical Coupling in Rock Masses

Hydro-mechanical coupling is a basic factor in rock masses' behavior, especially in a setting where water infiltrations, seepage, and pore pressure variations take place. It is found that water diminishes effective stress, adversely impacts bonding between mineral particles, and favors discontinuity sliding, thus aiding the decrease in strength and the change in failure modes (Zhao et al. 2023). It has been experimentally demonstrated that saturated rocks tend to have lower compressive strength, lower elastic modulus, and higher deformability than in the dry condition (Teng and Gong 2020). Hydro-mechanical forces are more pronounced in anisotropic rocks such as slate since such rocks have weak interlayers besides the preferred flow directions across structural planes. The introduction of water may also encourage the creation of cracks and grain boundaries and cause more complex fracture systems and their premature breakage (Lynch 2019). Moreover, recent studies have been done regarding the issue of thermal-hydro-mechanical coupling that highlights the interaction of temperature, stress, and fluid flow on the behavior of rocks (Wang et al. 2025). These findings underline the need to use a combination of approaches in studying the hydro-mechanical mechanisms of layered rock systems. The most important hydro-mechanical coupling processes that control fracture initiation and strength decrease are introduced in Figure 4.

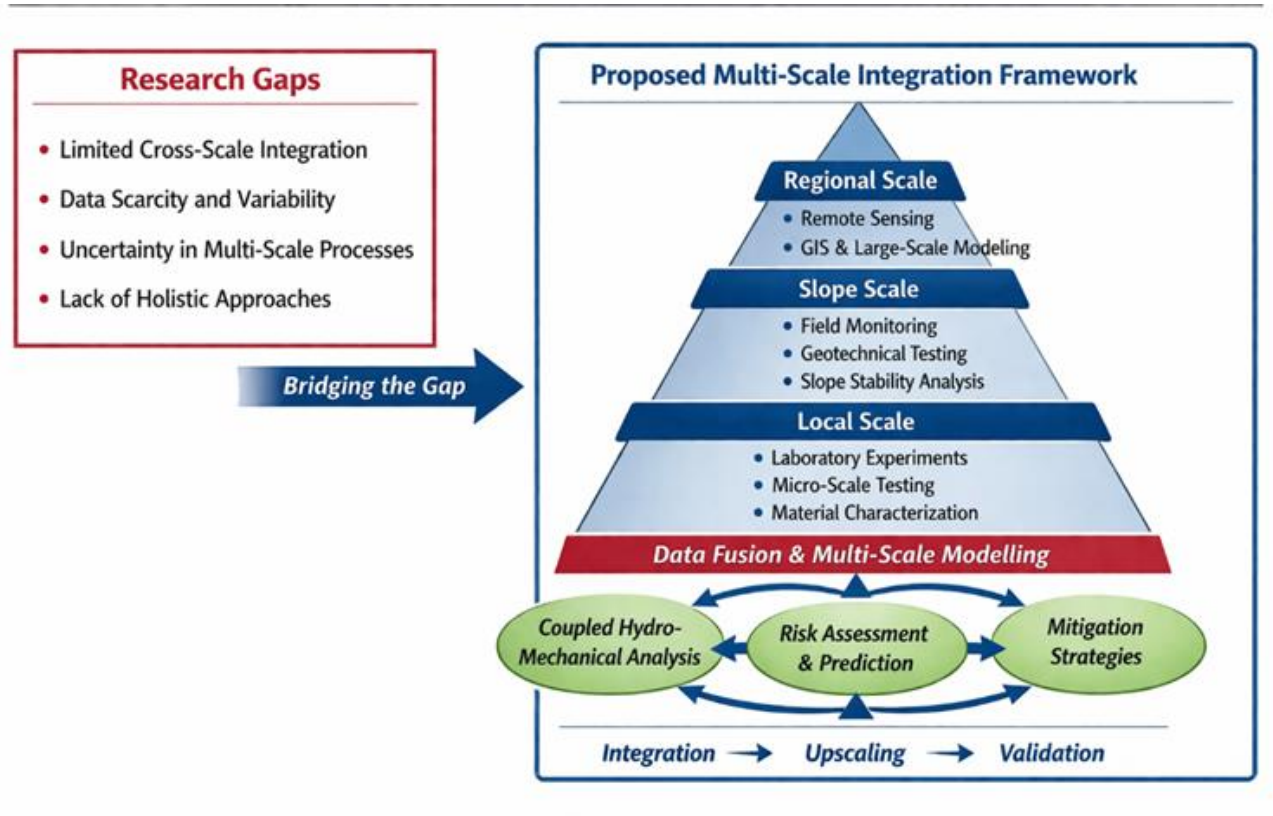

Figure 4. Hydro-Mechanical Coupling Mechanisms in Layered Rock Masses

2.3 Numerical Modeling (DEM, FEM, PFC)

Numerical modeling has been an essential technique of studying how rocks behave, particularly to learn the complicated fracture processes which are difficult to measure experimentally. Other methods that have been popular in the modeling of crack initiation, propagation, and coalescence in rock materials are the discrete element method (DEM) (Camones et al. 2013). Stress distribution and deformation in rock masses have also been analyzed by using finite element methods (Yang et al. 2014) and hybrid methods (FEM) particularly when it concerns large-scale engineering. Recent publications involving a combination of laboratory experiments and numerical calculations have demonstrated that there is a good correspondence between the simulated and observed failure patterns, which proves to be useful in the anisotropic behavior and hydro-mechanical coupling (Lisjak et al. 2014). Nevertheless, there are still difficulties in the correct modeling of the complex fracture networks and in the extrapolation of laboratory findings to the field (Taleghani, Gonzalez, and Shojaei 2016).

2.4 Slope Stability and Environmental Geo-Hazards

The problem of slope stability in rock masses is a problem of paramount importance in the sphere of engineering geology and environmental science, especially in the areas covered by water infiltration, seismic processes, and human activities. Anisotropic rocks, particularly rock slopes, are particularly vulnerable to failure because of the existence of weak structural planes and varying hydro-mechanical conditions (Xiang et al. 2020). The causes of landslides and rockfalls are usually a combination of factors that may include pore pressure that increases due to rain, weathering, and redistribution of stress.

Respondent research on the slopes of reservoirs and the water diversion has demonstrated that the slopes can become unstable due to the challenges of hydro-mechanical coupling of water level changes and seepage forces (Sadiq and Islam 2023). Sophisticated numerical modeling methods, such as coupled hydro-mechanical models, have been used to predict slope failure and to determine risk in varying environmental conditions (Zhao et al. 2023). Those methods permit the combination of parameters obtained in the laboratory with those in the field, giving a deeper insight into geo-hazard processes.

2.5 Research Gaps

Although a lot of research has been done regarding the behavior of anisotropic rocks and slope stability, there are several gaps. To begin with, there is a lack of integration between laboratory-scale experiments and numerical simulations, as most of the literature is dedicated to one or the other. Second, the hydro-mechanical coupling, because of its role in regulating failure mechanisms in anisotropic rocks, especially slate, is not fully understood. Third, multi-scale frameworks between field-scale slope stability and environmental geo-hazard mitigation to laboratory outcomes are absent. To fill the abovementioned gaps, a holistic method that involves experimental studies, numerical modeling, and environmental implementation is needed, which is the foundation of the current study. The research gaps and the proposed multi-scale integration framework are summarized in Figure 5.

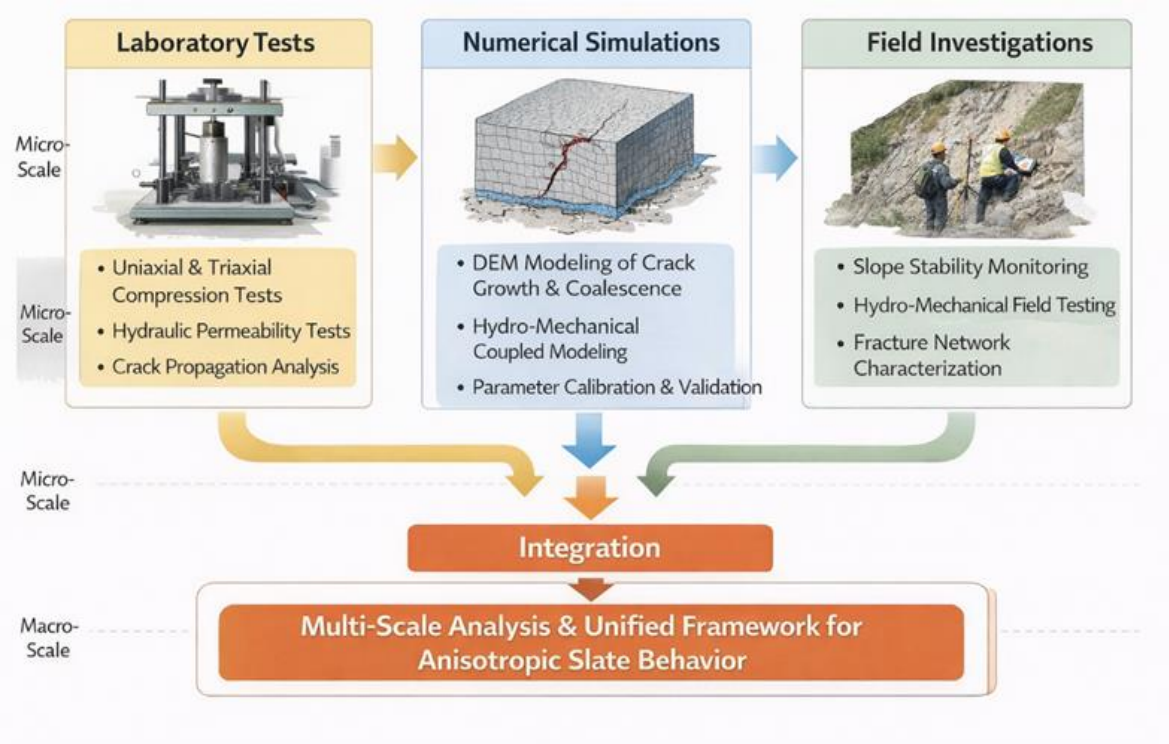

Figure 5. Research Gap and Proposed Multi-Scale Integration Framework

3. Research Objectives and Research Questions

3.1 Aim and Scope of Research

The overall aim of the research is to investigate the hydro-mechanical properties of the anisotropic slate and to establish a multi-scale model of linking the laboratory-scale processes with the slope-scale stability

analysis and its geo-hazard management of the environment. The need to achieve a deeper insight into the interplay between structural anisotropy and water effects on the regulation of rock corrosion is driven by the requirement to understand the interaction between structural anisotropy and water in more detail, particularly in water-based engineering systems, such as reservoir slopes and diversion projects (Nadi et al. 2021). Previous studies have indicated that the change of strength and failure of transition of anisotropic rocks is complex at different bedding orientations and environmental conditions. Nevertheless, a detailed model that unites the two has not been developed.

3.2 Research Objectives

The study is organized into the following objectives to accomplish the overall aim and scope.

Objective 1: To experimentally define the behavior of anisotropic slate under different bedding angles and hydro conditions (dry and saturated) to define the behavior of the experiment in mechanical and deformation. This contributes to the previous results that compressive strength and mode of failure are highly dependent on the structural plane inclination and water content.

Objective 2: To examine the hydro-mechanical coupling processes affecting the crack initiation, crack propagation, and failure development in layered rock masses. Hydro-mechanical processes, including pore pressure influences and the lubrication across discontinuities, are proven to change the strength and deformation properties.

Objective 3: To construct and test a numerical model (DEM-based, e.g., PFC) that would be able to simulate the anisotropic rock failure in the coupled hydro-mechanical conditions. DEM methods have shown some success in the micro-mechanical behaviors of crack coalescence, fracture growth in anisotropic rocks.

Objective 4: To suggest a model of environmental geo-hazard mitigation, hydro-mechanical processes need to be included in the slope stability assessment and in the risk assessment. This is in line with recent studies that highlight the importance of coupled processes as predictors of landslides and slope failures.

3.3 Research Questions

According to the objectives mentioned above, the research questions of the study are as follows:

1. What is the effect of hydro-mechanical coupling on the strength, deformation, and failure modes of anisotropic slate? The existing literature reveals that water can considerably diminish strength and alter the behavior of crack propagation, yet the mechanisms behind the effect need to be studied in more detail.

2. Which are the critical bedding angles and hydro conditions that control the transitions between the various failure modes (tensile, shear, and composite)? There is experimental evidence that failure mode transitions take place within certain angular ranges, but these boundaries are not completely delimited in hydro-mechanical conditions.

3. What is the most effective way of numerically modeling the initiation and propagation of cracks in anisotropic rocks when subjected to a coupled hydro-mechanical load? The methods based on DEM offer promising methods, yet they need to be calibrated and tested against experimental data.

4. What model can be established to incorporate hydro-mechanical processes in sustainable slope stability and geo-hazard mitigation measures? The answer to this question is critical to enhance risk assessment and facilitate environmentally sustainable engineering practices.

4. Research Methodology

4.1 Research Framework

The suggested research is based on experimental-numerical-environmental combined research on the hydro-mechanical character of anisotropic slate and its implications on the slope stability. The research is structured into three steps that are highly related, i.e., (i) the laboratory study that defines anisotropic and hydro-mechanical properties, (ii) the numerical analysis of the crack propagation and failure modes, and (iii) the application in slope-scale stability and environmental geo-hazard. It is an inter-scale approach which is required to best optimize the disparity between the laboratory experiments and the field environment as seen in previous studies of rock mechanics and geotechnical modelling. The combination of laboratory experiments, numerical simulations, and field studies into a multi-scale research methodology is described in general Figure 6.

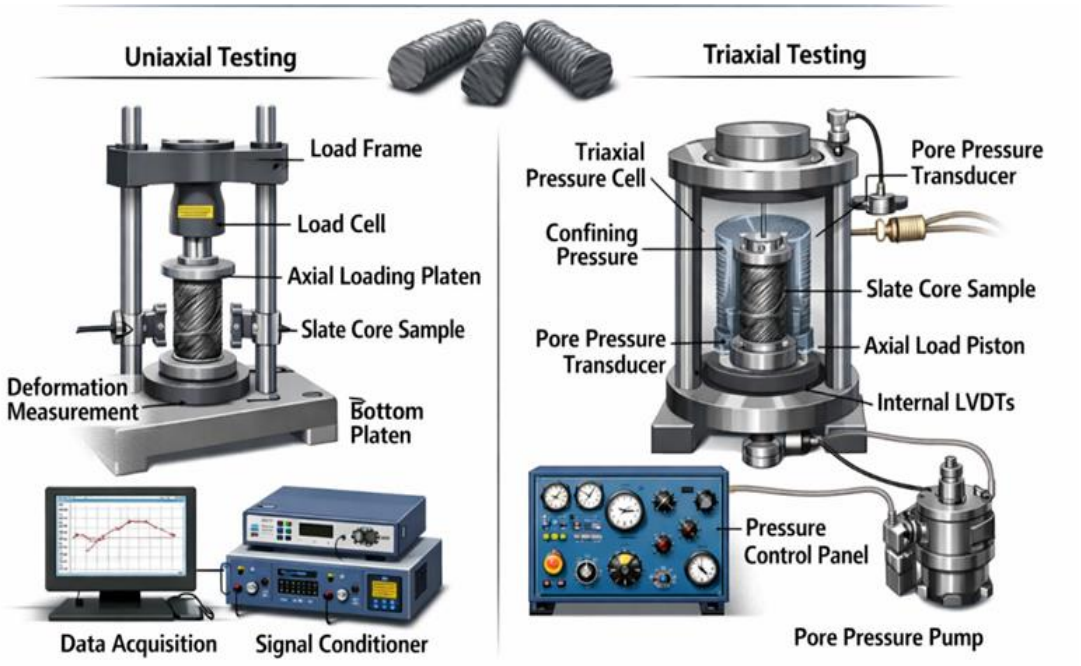

Figure 6. Multi-Scale Research Methodology Integrating Experimental, Numerical, and Field Approaches

4.2 Laboratory Experimental Program

The experiments will be conducted in a laboratory in order to quantify the mechanical behavior of anisotropic slate in a controlled experimental set up. To ensure directional dependence on strength and deformation, standard cylindrical specimens will be subjected to different bedding angles (e.g., 0°, 15°, 30°, 45°, 60°, 75°, and 90°). Proposed laboratory experimental program for investigating the hydro-mechanical behavior of anisotropic slate under different bedding orientations and moisture conditions in Table 2.

Table 2. Laboratory Experimental Design

Test Type	Parameter	Values	Purpose
Uniaxial Compression	Bedding Angle	0°–90°	Evaluate anisotropy
Triaxial Compression	Confining Pressure	5–30 MPa	Simulate field stress
Moisture Condition	Dry/Saturated	Controlled	Hydro-mechanical effect
Sample Size	Diameter/Height	Standard ISRM	Consistency

Loading Rate	Stress-controlled	Constant rate	Avoid dynamic effects
Measurements	Stress-strain	Continuous	Deformation analysis
Failure Analysis	Crack observation	Visual + imaging	Failure mechanism

Dry and saturated conditions will be taken into consideration to examine hydro-mechanical effects. Uniaxial compression tests will be conducted to get stress-strain curves, maximum strength, elastic modulus, and failure properties. Where practicable, triaxial compression tests will be carried out to determine the effect of confining pressure. The experimental design is in line with the traditionally accepted rock testing standards and methods common in past research (Zhang and Zhao 2014). Anisotropic strength difference and transition to failure mode in slate and other layered rocks can also be studied successfully using similar experimental methods (Tien, Kuo, and Juang 2006). The effects of hydromechanics will be researched through the comparison of the dry and saturated specimens. The saturation will be determined by using controlled water immersion, and the water absorption properties will be determined. The effect of water on strength degradation and deformation characteristics will be examined because it is already known that water decreases interlayer bonding and increases deformability (Wong, Maruvanchery, and Liu 2016). The laboratory setup for uniaxial and triaxial testing is illustrated in Figure 7.

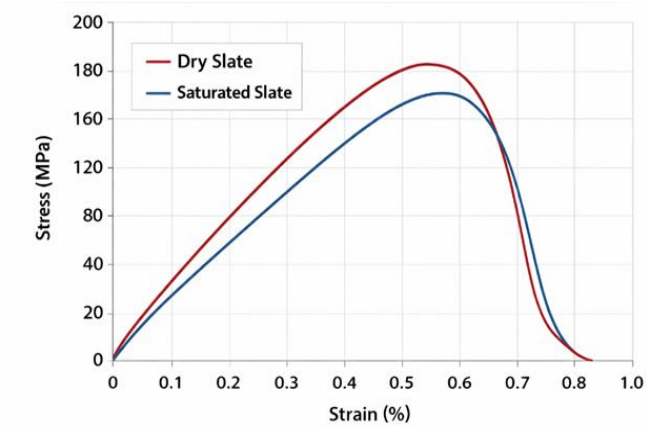

Figure 7. Laboratory Setup for Uniaxial and Triaxial Testing of Anisotropic Slate

4.3 Hydro-Mechanical Characterization

The hydro-mechanical behavior of anisotropic slate will be described with an in-depth examination of experimental data. Key stages of deformation will be identified through the use of stress-strain curves, such as compaction, elastic, elastoplastic, and failure stages. The mechanical parameters (compressive strength, elastic modulus, and strain characteristics) will be compared at varying bedding angles and moisture conditions. Consideration will be given to the determination of anisotropy in power as well as failure mode transitions, such as composite tensile shear failure, shear slip, and tensile splitting. It has been previously demonstrated that these failure modes are highly affected by the structural plane orientation and water content (Yao et al. 2019). The effect of hydro-mechanical coupling on crack initiation and propagation will also be evaluated, and it should focus on the contribution of pore water to the formation of the fracture (Zhao, Zhang, and Lei 2021). Typical stress-strain responses under dry and saturated conditions are shown in Figure 8.

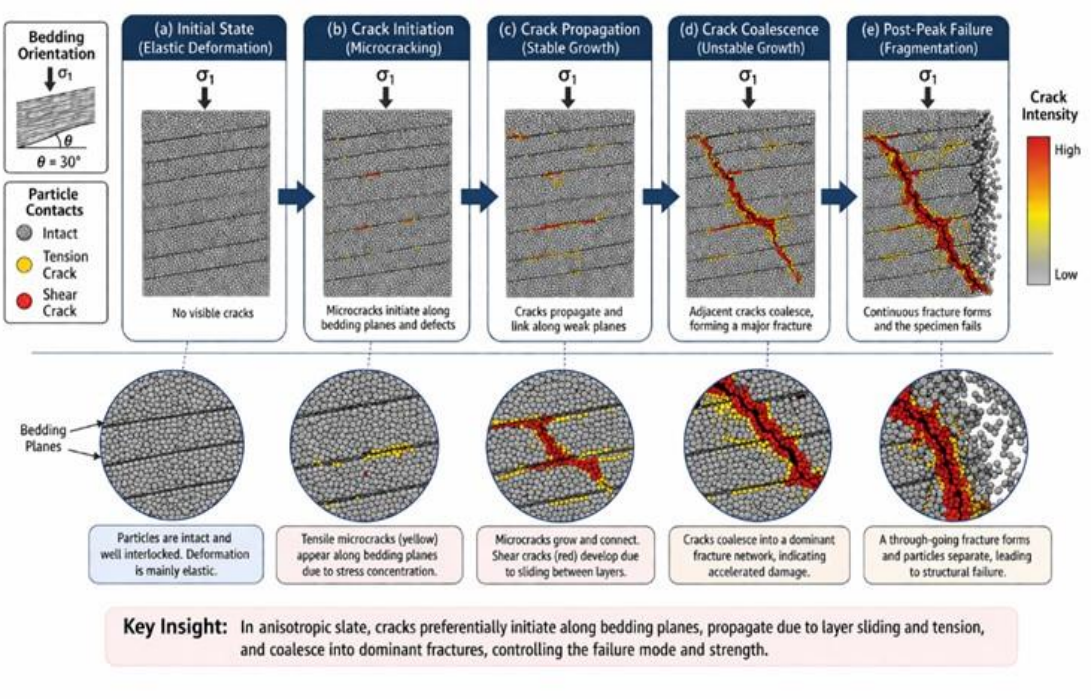

Figure 8. Stress-Strain Curves of Slate under Dry and Saturated Conditions

Proposed comparative framework for evaluating the influence of bedding angle and moisture condition on the mechanical properties and failure behavior of anisotropic slate in Table 3.

Table 3. Effect of Bedding Angle and Moisture on Mechanical Properties

Bedding Angle (°)	Condition	Compressive Strength	Elastic Modulus	Failure Mode	Crack Pattern
0°	Dry	High	High	Tensile splitting	Vertical cracks
15°	Dry	Moderate-high	Moderate	Composite	Mixed cracks
30°	Dry	Low	Moderate	Shear-slip	Inclined cracks
45°	Dry	Minimum	Low	Shear dominant	Sliding failure
60°	Dry	Increasing	Moderate	Composite	Mixed
75°	Dry	High	High	Tensile	Vertical
90°	Dry	Very high	High	Tensile splitting	Parallel cracks
0°	Saturated	Reduced	Reduced	Tensile	Extended cracks
45°	Saturated	Very low	Low	Shear-slip	Lubricated planes
90°	Saturated	Reduced	Moderate	Tensile	Wide fractures

4.4 Numerical Modeling (DEM PFC)

The Discrete Element Method (DEM) Particle Flow Code (PFC) will be used to do numerical simulations in order to complement the laboratory experiments. DEM in particular is particularly useful in the modeling of rock behavior because it is a micro-mechanical description of the behavior of fractures (Chen et al. 2023). A slate numerical model that is anisotropic will be developed and calibrated using experimental data. The parameters of the model such as particle rigidity, bond strength, and coefficient of friction will be varied to obtain observed stress-strain behavior and mode of failure. The crack initiation, propagation and coalescence will be examined by conducting simulations at different bedding angles and hydro conditions. Previous studies have already demonstrated that PFC can be used to simulate the behavior of anisotropic rocks and reproduce experimental failure modes (Yin et al. 2019). Numerical modeling parameters of the DEM/PFC model and their importance in the modeling of crack initiation, crack propagation, and the evolution of failure in anisotropic slate in Table 4.

Table 4. DEM Numerical Modeling Parameters (PFC)

Parameter	Symbol	Description	Role
Particle stiffness	kn, ks	Normal & shear stiffness	Controls deformation
Bond strength	σb	Inter-particle bonding	Crack initiation
Friction coefficient	μ	Sliding resistance	Shear failure
Porosity	n	Void ratio	Fluid flow behavior
Water pressure	Pw	Pore pressure	Hydro-mechanical coupling
Contact model	—	Linear/parallel bond	Behavior simulation
Calibration	—	Lab data matching	Model validation

The numerical model will be employed in this research to: find out the locations of stress concentration, trace crack growth and fracture networks, and determine failure mode transition critical thresholds. The technique gives a more intimate insight of micro-mechanical processes, which are experimentally not readily observed (Fu et al. 2024). The DEM-based simulation of crack initiation, propagation, and coalescence is illustrated in Figure 9.

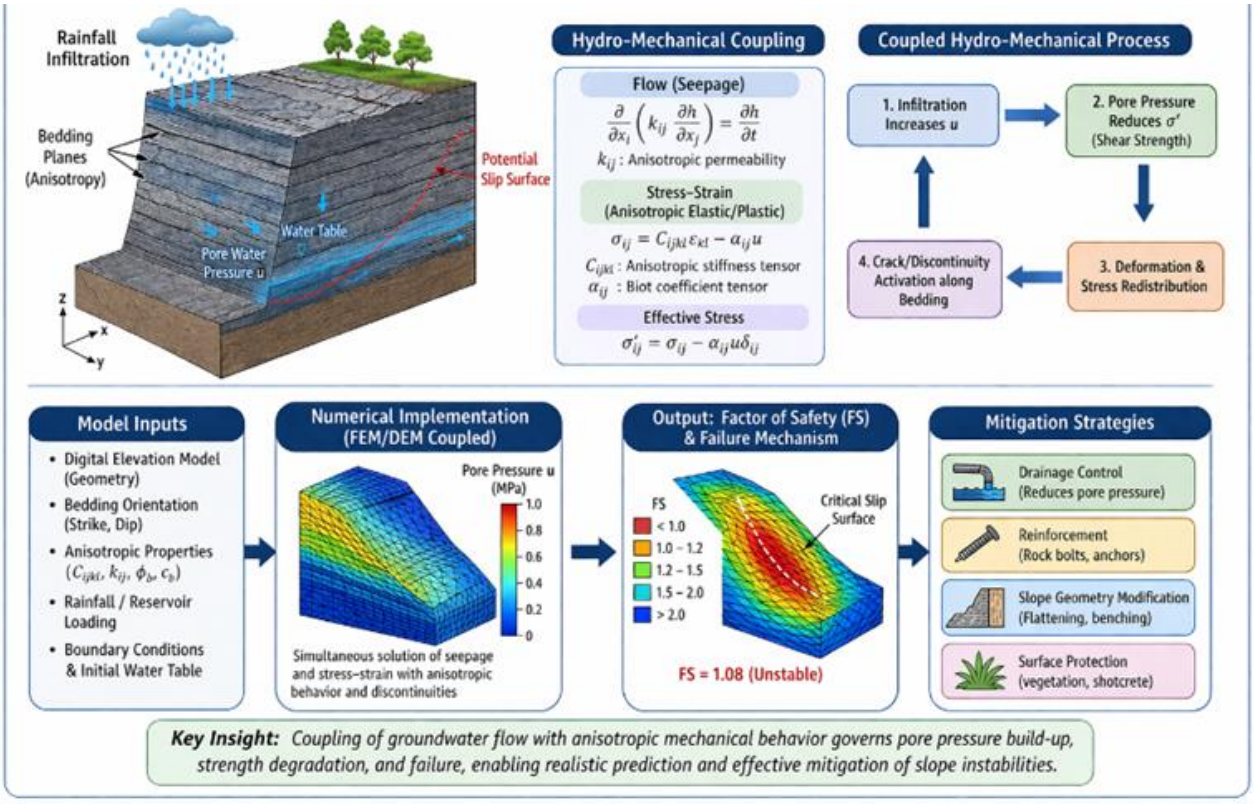

Figure 9. DEM Simulation of Crack Initiation, Propagation, and Coalescence in Anisotropic Slate

4.5 Slope Stability and Environmental Application

The laboratory and numerical results will be further applied to slope-scale applications to measure geo-hazards to the environment. Anisotropic mechanical properties and hydro-mechanical coupling effects will be included in the development of a slope stability model. Limit equilibrium (LEM) and numerical (FEM/DEM) methods can both be used to test slope stability under varying environmental conditions. The hydro-mechanically coupled slope stability modeling framework is presented in Figure 10.

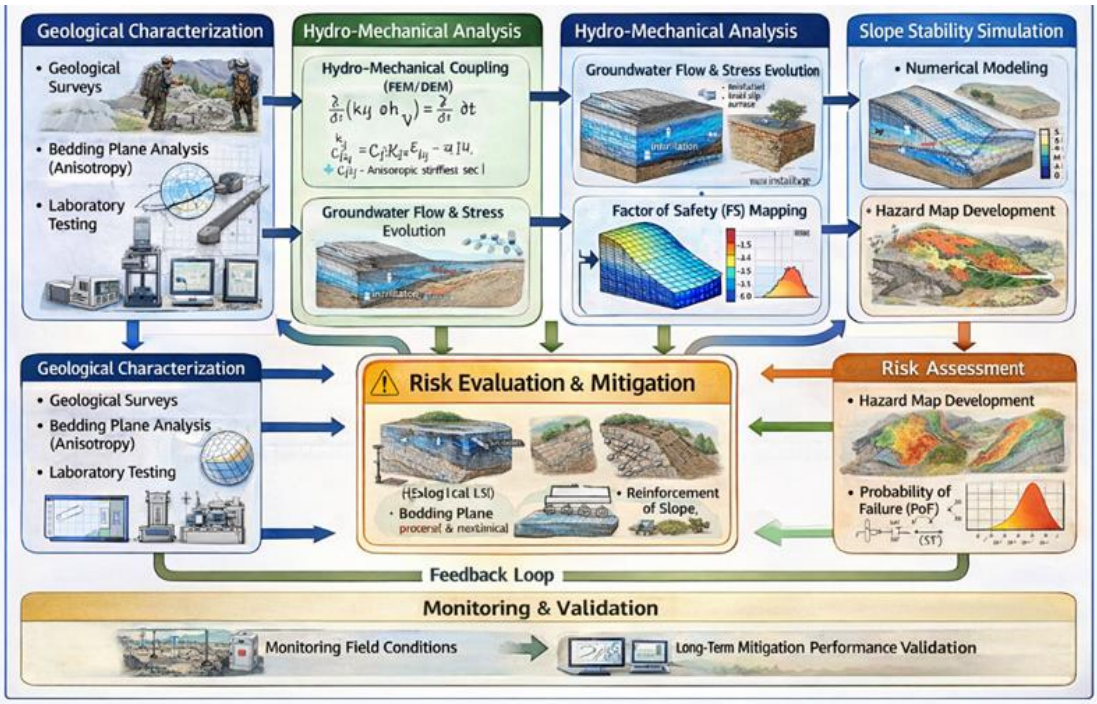

Figure 10. Hydro-Mechanically Coupled Slope Stability Model for Anisotropic Rock Masses

Principal geotechnical and hydro-mechanical parameters considered in slope stability assessment and geo-hazard evaluation of anisotropic rock masses in Table 5.

Table 5. Slope Stability Parameters under Hydro-Mechanical Conditions

Parameter	Description	Source	Influence on Stability
Cohesion (c)	Shear resistance	Lab tests	High impact
Friction angle (φ)	Shear strength	Lab tests	High impact
Bedding orientation	Structural anisotropy	Field/lab	Critical
Pore water pressure	Water effect	Hydro analysis	Reduces stability
Seepage force	Flow-induced force	Numerical	Triggers failure
Unit weight	Rock density	Lab	Moderate
Crack density	Fracture intensity	DEM	Weakens slope

The factors that will be taken into consideration in the model include: (i) bedding discontinuities and structural orientation, (ii) water forces and seepage, and (iii) redistribution of stress and fracture. The proposed framework will be tested using case studies that pertain to the topic of reservoir slopes, water diversion projects, or landslides that occur as a result of rainfall. It has been prioritized in previous studies that hydro-mechanical coupling contributes significantly to slope instability, especially in anisotropic rock masses (Song et al. 2024). Incorporation of laboratory-derived parameters in the slope models improves the accuracy of the prediction, and it creates a more realistic measure of geo-hazard risk (Tchuwa and Makande 2025). The integrated framework for geo-hazard risk assessment and mitigation under hydro-mechanical conditions is illustrated in Figure 11.

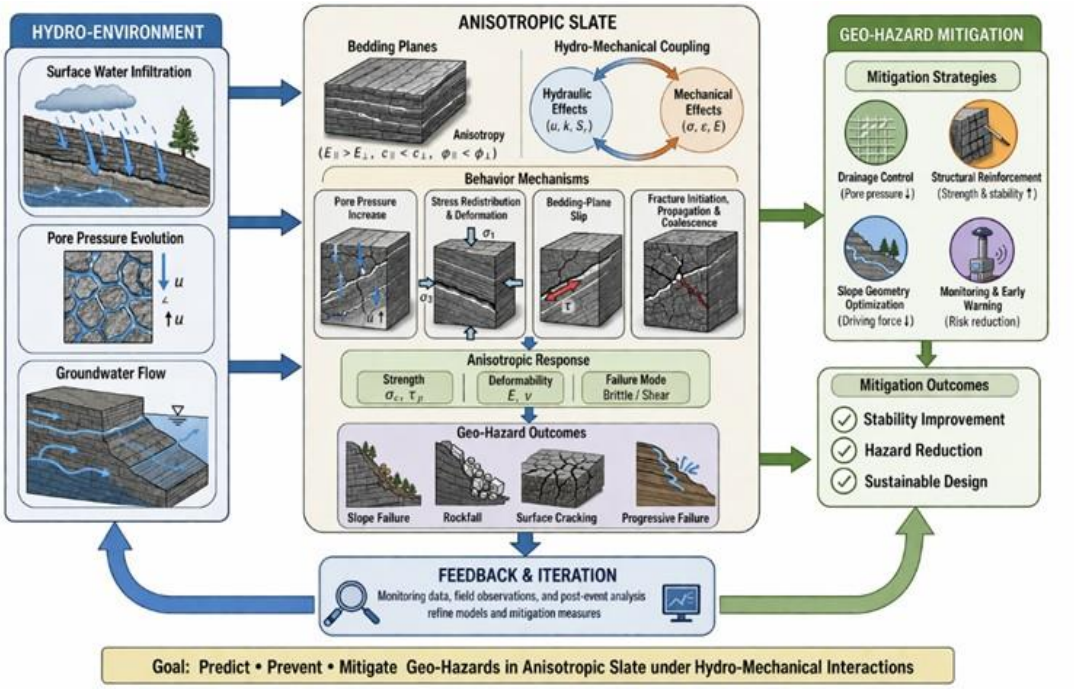

Figure 11. Framework for Geo-Hazard Risk Assessment and Mitigation under Hydro-Mechanical Conditions

4.6 Data Analysis Techniques

The analysis of data will be conducted both quantitatively and qualitatively. The correlation between the bedding angle, water content, and mechanical properties will be determined by statistical means. The key parameters that affect the behavior of rocks and slope stability will be realized through sensitivity analysis. The failure modes will be characterized according to the observed pattern of cracks and the results of numerical simulations. A comparative analysis of experimental and numerical data will validate the modeling method. This combined discussion will offer an equalized view of the hydro-mechanical procedures in anisotropic slate and its symbolism to environmental hazards of geo-hazards (Zargarbashi 2011).

5. Anticipated Conclusions and Contributions

5.1 Scientific Contributions

It is hoped that the present study will contribute to the knowledge about hydro-mechanical behavior in anisotropic slate, especially concerning the change in strength, the nature of deformation, and the failure processes. They expect to find, based on previous results, a strong dependence of compressive strength and elastic properties on the bedding orientation, with the typical U-shaped relationship between strength and inclination angle. The study will also measure the effect of water saturation on these relationships, which cause the decrease in strength and alteration in deformation stages caused by weakening interlayer bonding and enhanced by pore pressure. Moreover, the research will give a better insight into the failure mode transition under the conditions of hydro-mechanical coupling. It will be founded on previous sets of tensile shear, shear-slip, and tensile splitting failures of slate. It will determine crucial bedding angle and water conditions thresholds linked with the changes. Better constitutive models of anisotropic rocks will be formulated with these discoveries, and predictive capability in rock mechanics will be enhanced.

5.2 Engineering Contributions

The outcome of the current research will be very useful engineering-wise in designing and stability analysis of structures in which layered rock masses are taken into account. A set of analytical laboratory experiments with the appropriate computer-based simulation will probably lead to a validated DEM model structure that is able to model the exact crack propagation and the formation of cracks in anisotropic slate. Such a framework will enable the engineers to: (i) anticipate the reduction of strength under various conditions of hydro, (ii) determine significant planes of structural planes that may be unstable, and (iii) evaluate the impacts of infiltration of water on slope and underground structures. These skills are particularly required in infrastructure work such as tunnels, slopes, and reservoirs where the characteristics of the anisotropic rocks and hydro-mechanical connection are a significant contributor to stability. The result will then be applicable in the safer and more efficient engineering design practices.

5.3 Environmental and Geo-Hazard Contribution

The proposed study will further advance the science of the environment and mitigation of geo-hazards through the enhancement of knowledge on the mechanism of slope instability in anisotropic rock masses. It is also anticipated that the research will portray how the hydro-mechanical processes, such as infiltration of water and stress variations caused by seepage, play an important role in the development and advancement of slope failures. The study will have a predictive framework that can be used to determine the geo-hazard risk in water-related sites, such as the banks of reservoirs and slopes under rainfall, by incorporating laboratory-derived parameters in slope-scale models. With the help of this framework, it will be possible to: (i) early detection of unstable slope conditions, (ii) better evaluation of risk in landslides and rockfalls, and (iii) formulation of mitigation measures of sustainable infrastructure. Moreover, the research will lead to sustainable engineering activities because it will connect rock mechanics and geologically advanced geologies to environmental processes, thus helping to design an efficient infrastructure system that is resilient to geologically advanced geographies (Basu, Misra, and Puppala 2015).

5.4 Integrated Contribution

In general, the anticipated outcomes of this study will be a multi-scaled and comprehensive anisotropic slate behavior during hydro-mechanical coupling to fill the gap between the laboratory, numerical, and field scales. The combination of these strategies helps overcome major limitations of the existing literature. It provides a feasible way forward in enhancing scientific understanding as well as engineering practice in rock mechanics, engineering geology, and environmental geo-hazard control (Wang and Nanehkaran 2024).

6. Innovation and Novelty

The study presents a few original points that contribute to the development of the existing level of knowledge in the field of rock mechanics, engineering geology, and environmental science, especially when considering the anisotropic slate and hydro-mechanical interaction.

6.1 Overview of Hydro-Mechanical Coupling

One of the key discoveries of this paper is the clear incorporation of hydro-mechanical coupling in the study of anisotropic slate behavior. Although the effects of water on the strength of rocks or the study of

anisotropic mechanical properties have been discussed independently in prior studies, very few studies have investigated the two factors in a comprehensive system. The current literature proves that water decreases compressive strength and changes the process of failure in layered rocks. Still, the relationship between structural anisotropy and hydro-mechanical processes is poorly comprehended. This gap is filled in the present study, which examined the interactions involving water infiltration, pore pressures, and interlayer weakening to affect strength anisotropy and changes in failure modes (Zhao et al. 2024).

6.2 Multi-scale Research Framework (Laboratory to Numerical to Field)

The other important innovation is the design of a multi-scale framework, which relates to both laboratory-scale observations and numerical modeling and field applications. Most of the past research is restricted to either laboratory experiments or numerical modeling, without a clear relationship of scale. The combination of experimental data, simulations of DEM-based models, and slope stability modeling through current research allows for the development of a more complete picture of rock behavior at varying scales. The simulation of the crack propagation and failure evolution using PFC further increases the capability of capturing the micro-mechanical processes that govern the macroscopic behavior (Li et al. 2022).

6.3 Determination of Critical Failure Thresholds in Hydro-Mechanical Conditions

The research will find the key bedding angle and the hydro conditions that are critical in defining changes between various failure modes. It has been established in previous studies that anisotropic rocks undergo different failure modes depending on the structural plane orientation. However, the boundaries between them under hydro-mechanical coupling are not well-defined. With the combination of experimental and numerical methods, this study will set up quantitative standards for predicting the transition of failure mode; this project will be of great importance for both theoretical and practical applications in rock mechanics (Stead, Eberhardt, and Coggan 2006).

6.4 Rock Mechanical Calibration with Environmental Geo-Hazard Reduction

One of the most significant novelties of this study is the explicit connection between the geo-hazard mitigation of environmental issues and rock mechanics. Although conventional studies emphasized mechanical behavior, this study has extended the study to environmental applications, such as slope stability, landslides, and reservoir bank failures. Hydro-mechanical processes are identified as some of the major causes of geo-hazards, especially in water-sensitive regions (Xue et al. 2026). These processes have been integrated into a predictive framework that makes the study a part of developing sustainable engineering solutions to hazards prevention and risk reduction.

6.5 Numerical Anisotropic Rock System Modeling

The suggested study also facilitates the use of numerical modeling methods, especially the DEM-based methods on the anisotropic rock systems. Though DEM has been extensively applied to simulate rock behavior, the usage of the method to model hydro-mechanical coupling in layered rocks is scarce. This work will improve the model calibration and validation, which will make the simulation more reliable in predicting the process of crack propagation and failure. These improvements are vital to the creation of powerful engineering design and hazard evaluation tools (Hardison and Hallowell 2019).

6.6 Novel Contribution in Research

This research is novel in that it applies a multi-disciplinary strategy, which integrates hydro-mechanical coupling, anisotropic rock behavior, multi-scale modeling, and environmental geo-hazard applications. This holistic formulation does not only fill major gaps in existing literature but also provides useful mechanisms to improve slope stability assessment and sustainability in the creation of infrastructure in not-so-simple geology. The suggested plan offers a reasonable chain of basic research and application, including the combination of experimental, numerical, and environmental factors. This systematic arrangement is consistent with the optimal practice of the research of rock mechanics. It offers an important way towards the attainment of the research goals in addition to sustainable geo-hazard mitigation. Mapping of research innovation, existing knowledge gaps, and the proposed study's original contributions to anisotropic rock mechanics and environmental geo-hazard mitigation in Table 6.

Table 6. Research Contribution and Innovation Mapping

Innovation Aspect	Existing Studies	Proposed Study Contribution
Anisotropy analysis	Studied separately	Integrated with hydromechanics
Hydro-mechanical coupling	Limited focus	Fully coupled framework
Experimental work	Isolated lab studies	Multi-condition experiments
Numerical modeling	DEM used	DEM + validation
Scale integration	Missing	Lab → Numerical → Field
Geo-hazard application	Limited	Full slope stability model

7. Conclusion

The study of the hydro-mechanical properties of anisotropic slate and its implications on sustainable slope stability and environmental mitigation geo-hazard will be done in this research proposal. The study fills major gaps in the current body of knowledge regarding the behavior of anisotropic rocks under coupled conditions by combining laboratory tests, numerical modeling and slope-scale techniques. The proposed work relies on the existing research that demonstrates that the bedding orientation and water significantly affect the strength, deformation, and failure of rock that is generated at the interface between a multi-scale and a multi-physics model. The method enables the representation of the behavior of rock masses in a more realistic way and provides superior tools in predicting instability in engineering as well as the environmental environment. Both the scientific and engineering worlds will use the expected findings and warrant more secure and sustainable infrastructure development in geologically intricate and water-sensitive environments. Besides, the addition of the hydro-mechanical processes to the slope stability assessment will enhance the predictive and mitigation potential of landslides or reservoir bank collapses geo-hazards. To sum up, the intended study provides an innovative application-oriented and interdisciplinary study that advances knowledge in rock mechanics, engineering geology, and environmental geo-hazard science while addressing the fundamental research gaps in the hydro-mechanical behavior of anisotropic rock.

Funding: Funding is inappropriate for this research study.
Data availability: The statistics supporting the outcomes of this research are accessible upon reasonable request from the first author.

Declarations

Ethical approval: Not applicable
Consent to participate: Not applicable
Consent to publish: All authors have given consent to publish.
Competing interest: The authors have no competing interests to declare.

References

1. Basu, Dipanjan, Aditi Misra, and Anand J Puppala. 2015. "Sustainability and geotechnical engineering: perspectives and review." Canadian geotechnical journal 52 (1):96-113.
2. Camones, Luis Arnaldo Mejía, Eurípedes do Amaral Vargas Jr, Rodrigo Peluci de Figueiredo, and Raquel Quadros Velloso. 2013. "Application of the discrete element method for modeling of rock crack propagation and coalescence in the step-path failure mechanism." Engineering Geology 153:80-94.
3. Chen, Xin, Wei Gao, Chengjie Hu, Chen Wang, and Cong Zhou. 2023. "Study on macro–micro mechanical behavior of broken rock mass using numerical tests with discrete element method." Computational Particle Mechanics 10 (4):691-705.
4. Fu, Jinwei, Hadi Haeri, Vahab Sarfarazi, Amin Rahmani, Parastou Salehipour, Abdollah Tabaroei, and Lin Jian Shangguan. 2024. "Investigating tensile failure mechanisms of layered rocks through physical testing and PFC3D analysis." Engineering Fracture Mechanics 311:110541.
5. Hao, Xianjie, Shaohua Wang, Quansheng Xu, Dequan Yang, Qian Zhang, Duoxiang Jin, and Yingnan Wei. 2020. "Influences of confining pressure and bedding angles on the deformation, fracture and mechanical characteristics of slate." Construction and Building Materials 243:118255.
6. Hardison, Dylan, and Matthew Hallowell. 2019. "Construction hazard prevention through design: Review of perspectives, evidence, and future objective research agenda." Safety Science 120:517-526.
7. Heinze, Thomas, Gunnar Jansen, Boris Galvan, and Stephen A Miller. 2016. "Systematic study of the effects of mass and time scaling techniques applied in numerical rock mechanics simulations." Tectonophysics 684:4-11.
8. Ismail, Atif, and Saman Azadbakht. 2025. "Experimental and Numerical Methods for Hydraulic Fracturing at Laboratory Scale: A Review." Geosciences 15 (4):142.
9. Li, Chang, Shuren Hao, Shengjie Zhang, Yongqing Jiang, and Zhidong Yi. 2024. "Simulation study on the mechanical effect of CO2 geological storage in ordos demonstration area." Water 16 (1):144.
10. Li, Cunbao, Heping Xie, and Jun Wang. 2020. "Anisotropic characteristics of crack initiation and crack damage thresholds for shale." International journal of rock mechanics and mining sciences 126:104178.
11. Li, Guodong, Fatemeh Bodahi, Tuan He, Feng Luo, Shuo Duan, and Meng Li. 2022. "Sensitivity analysis of macroscopic mechanical behavior to microscopic parameters based on PFC simulation." Geotechnical and Geological Engineering 40 (7):3633-3641.
12. Lisjak, Andrea, Bryan SA Tatone, Giovanni Grasselli, and Tim Vietor. 2014. "Numerical modelling of the anisotropic mechanical behaviour of opalinus clay at the laboratory-scale using fem/dem." Rock mechanics and rock engineering 47 (1):187-206.
13. Liu, Hanxiang, Hongwen Jing, Qian Yin, Yaoyao Meng, and Gaofang Zhu. 2023. "Effect of bedding plane on mechanical properties, failure mode, and crack evolution characteristic of bedded rock-like specimen." Theoretical and Applied Fracture Mechanics 123:103681.
14. Lynch, Stan. 2019. "A review of underlying reasons for intergranular cracking for a variety of failure modes and materials and examples of case histories." Engineering Failure Analysis 100:329-350.
15. Nadi, Bahram, Omid Tavasoli, Denise-Penelope N Kontoni, and Ali Tadayon. 2021. "Investigation of rock slope stability under pore-water pressure and structural anisotropy by the discrete element method." Geomechanics and Geoengineering 16 (6):452-464.
16. Qian, Long, Xingwen Guo, Qinghui Liu, Xin Cai, and Xiaochuan Zhang. 2024. "Macro-Mesoscopic Failure Mechanism Based on a Direct Shear Test of a Cemented Sand and Gravel Layer." Buildings 14 (12):4078.
17. Sadiq, Hammad, and Muhammad Mohiul Islam. 2023. "Geotechnical And Hydraulic Simulation Models for Slope Stability And Drainage Optimization In Rail Infrastructure Projects." Review of Applied Science and Technology 2 (02):01-37.
18. Si, Xuefeng, Yong Luo, and Song Luo. 2024. "Influence of lithology and bedding orientation on failure behavior of "D" shaped tunnel." Theoretical and Applied Fracture Mechanics 129:104219.
19. Song, Fei, Guanghui Duan, Huaning Wang, Alfonso Rodriguez-Dono, and Yimiao Wei. 2024. "Hydro-mechanical analysis of slope stability using anisotropic constitutive model." IOP Conference Series: Earth and Environmental Science.
20. Stead, D, E Eberhardt, and JS Coggan. 2006. "Developments in the characterization of complex rock slope deformation and failure using numerical modelling techniques." Engineering geology 83 (1-3):217-235.

21. Sun, Lei, Giovanni Grasselli, Quansheng Liu, and Xuhai Tang. 2019. "Coupled hydro-mechanical analysis for grout penetration in fractured rocks using the finite-discrete element method." International Journal of Rock Mechanics and Mining Sciences 124:104138.
22. Suo, Yu, Zhixi Chen, Sheikh S Rahman, and Huifang Song. 2020. "Experimental and numerical investigation of the effect of bedding layer orientation on fracture toughness of shale rocks." Rock Mechanics and Rock Engineering 53 (8):3625-3635.
23. Taleghani, Arash Dahi, Miguel Gonzalez, and Amir Shojaei. 2016. "Overview of numerical models for interactions between hydraulic fractures and natural fractures: Challenges and limitations." Computers and Geotechnics 71:361-368.
24. Tchuwa, Isaac, and Moffat Makande. 2025. "Landslide susceptibility assessment using geotechnical characterization of collapsible and dispersive soils at Soche Hill, Blantyre, Malawi." Discover Geoscience 3 (1):133.
25. Teng, Teng, and Peng Gong. 2020. "Experimental and theoretical study on the compression characteristics of dry/water-saturated sandstone under different deformation rates." Arabian Journal of Geosciences 13 (13):517.
26. Tian, Chongming, Zhipeng Xiao, Fei Ye, Yueping Tong, Xiaoyong Cao, Jingyuan Sun, and Zili Li. 2025. "The impact of extreme rainfall and drainage system failure on rock tunnels: A case study of deep-buried karst tunnel." Engineering Failure Analysis 171:109345.
27. Tien, Yong Ming, Ming Chuan Kuo, and Charng Hsein Juang. 2006. "An experimental investigation of the failure mechanism of simulated transversely isotropic rocks." International journal of rock mechanics and mining sciences 43 (8):1163-1181.
28. Tsatsaris, Andreas, et al. 2021. "Geoinformation technologies in support of environmental hazards monitoring under climate change: An extensive review." ISPRS International Journal of Geo-Information 10 (2):94.
29. Wang, Jianxiu, et al. 2025. "Physical and mechanical properties and constitutive model of rock mass under THMC coupling: a comprehensive review." Applied Sciences 15 (4):2230.
30. Wang, Yanli, and Yaser A Nanehkaran. 2024. "GIS-based fuzzy logic technique for mapping landslide susceptibility analyzing in a coastal soft rock zone." Natural Hazards 120 (12):10889-10921.
31. Wen, Sen, Ruizhi Huang, Chunshun Zhang, and Xianwei Zhao. 2023. "Mechanical behavior and failure mechanism of composite layered rocks under dynamic tensile loading." International Journal of Rock Mechanics and Mining Sciences 170:105533.
32. Wong, Louis Ngai Yuen, Varun Maruvanchery, and Gang Liu. 2016. "Water effects on rock strength and stiffness degradation." Acta Geotechnica 11 (4):713-737.
33. Xiang, Zhipeng, Huanling Wang, Weiya Xu, and Wei-chau Xie. 2020. "Experimental study on hydro-mechanical behaviour of anisotropic columnar jointed rock-like specimens." Rock Mechanics and Rock Engineering 53 (12):5781-5794.
34. Xue, Junlei, et al. 2026. "Surface Deformation Characteristics and Damage Mechanisms of Repeated Mining in Loess Gully Areas: An Integrated Monitoring and Simulation Approach." Applied Sciences 16 (2):709.
35. Yan, Bingqian, Peitao Wang, Fenhua Ren, Qifeng Guo, and Meifeng Cai. 2020. "A review of mechanical properties and constitutive theory of rock mass anisotropy." Arabian journal of geosciences 13 (12):487.
36. Yang, Jian-Ping, Wei-Zhong Chen, Yong-hao Dai, and Hong-Dan Yu. 2014. "Numerical determination of elastic compliance tensor of fractured rock masses by finite element modeling." International Journal of Rock Mechanics and Mining Sciences 70:474-482.
37. Yao, Qiangling, et al. 2019. "Influence of moisture on crack propagation in coal and its failure modes." Engineering Geology 258:105156.
38. Yin, Peng-Fei, Sheng-Qi Yang, Wen-Ling Tian, and Jian-Long Cheng. 2019. "Discrete element simulation on failure mechanical behavior of transversely isotropic rocks under different confining pressures." Arabian Journal of Geosciences 12 (19):605.
39. Zamanian, Mostafa, Vahid Mollaei-Alamouti, and Meghdad Payan. 2020. "Directional strength and stiffness characteristics of inherently anisotropic sand: The influence of deposition inclination." Soil Dynamics and Earthquake Engineering 137:106304.
40. Zargarbashi, Saman. 2011. "Investigation of cyclic response in unsaturated soils: Including hydraulic and mechanical hystereses." UNSW Sydney.
41. Zhang, Hongwei, Zhijun Wan, Dan Ma, Yuan Zhang, Jingyi Cheng, and Qi Zhang. 2017. "Experimental investigation on the strength and failure behavior of coal and synthetic materials under plane-strain biaxial compression." Energies 10 (4):500.

42. Zhang, Q B, and Jian Zhao. 2014. "A review of dynamic experimental techniques and mechanical behaviour of rock materials." Rock mechanics and rock engineering 47 (4):1411-1478.
43. Zhao, Chenxi, Zixin Zhang, and Qinghua Lei. 2021. "Role of hydro-mechanical coupling in excavation-induced damage propagation, fracture deformation and microseismicity evolution in naturally fractured rocks." Engineering Geology 289:106169.
44. Zhao, Honggang, et al. 2024. "Influence of weak interlayer thickness on mechanical response and failure behavior of rock under true triaxial stress condition." Engineering Failure Analysis 162:108419.
45. Zhao, Yanlin, et al. 2023. "A review of hydromechanical coupling tests, theoretical and numerical analyses in rock materials." Water 15 (13):2309.
46. Zheng, Peichao, et al. 2025. "Microscopic damage and deterioration of carbonaceous slate in cold region subjected to freeze-thaw cycles." Journal of Rock Mechanics and Geotechnical Engineering.
47. Zhu, Chun, et al. 2025. "Progressive failure mechanisms of anti dip rock slopes near reservoir banks considering rock mass deterioration in the hydro fluctuation belt." Physics of Fluids 37 (8).

Journal of Computational and Experimental Science (JCES)
ISSN Print: XXXX | ISSN Online: XXXX
Volume 1, Number 1, 2026, Pages 21–46
Journal Home Page: https://journals.airsd.org/index.php/jces

AI-Driven Eco-Engineering Framework for Climate-Resilient Urban Systems Using Real-Time Social and Environmental Data

Ghulam Rubab[1*], Azhar Ali[2], Muhammad Umar Memon[3], Muhammad Yaqoob[4], Baqir Banglani[5], Shaista Jalbani[6], Emmy Mahar[7], Fatima Gull[8]

[1*]Institute of Plant Sciences, University of Sindh, Jamshoro, Sindh, Pakistan, Fisheries and Aquaculture SBBUVAS, Sakrand, Sindh, Pakistan. *Email:ghulamrubabsoomro@gmail.com*

[2] School of Information and technology, Shaheed Benazir Bhutto University, Nawabshah *Email: azharrose018@gmail.com*

[3] School of Energy Systems Engineering, Quaid e Awam University, Nawabshah

Email: muhammadumarmemon011@gmail.com

[4] School of Power and Energy Engineering, Harbin Engineering University, Harbin, China.

Email: engryaqoob40@gmail.com

[5] School of Information and technology, Shaheed Benazir Bhutto University, Nawabshah.

Email: baqir.techworld007@gmail.com

[6] Fisheries and Aquaculture SBBUVAS, Sakrand, Sindh, Pakistan. *Email: jalbanishaista@gmail.com*

[7] School of Environmental Engineering and Management, Mehran University of Engineering and Technology Jamshoro, Sindh, Pakistan. *Email: emmy.mahar@gmail.com*

[8] School of Sociology, University of Karachi, Pakistan *Email: universityofkarachigull@gmail.com*

ARTICLE INFO

Article History:
Received: February 12, 2026
Revised: February 27, 2026
Accepted: March 10, 2026
Available Online: March 30, 2026

Keywords:
AI-driven eco-engineering; Urban climate resilience; multi-modal data integration; Social sensing and environmental intelligence; Nature-based solutions (NBS); Real-time climate risk prediction

Corresponding Author:
Ghulam Rubab
Email:
ghulamrubabsoomro@gmail.com

ABSTRACT

Compound climate risks, including flooding, heatwaves, and environmental degradation, are more likely to affect urban areas, and available resilience strategies are still disconnected, with an ecological, technological, and social focus. This paper presents a proposal of an AI-driven eco-engineering control that combines real-time environmental sensing (remote sensing, meteorological, hydrological, and IoT data) with social sensing (geotagged social media data) to aid in adaptive and data-driven urban climate decision-making. This framework is based on the multi-layered architecture comprising of data acquisition, preprocessing, integration of multi-modal features, AI-based prediction (LSTM and SVM), spatial risk mapping, and optimization of nature-based solutions on eco-engineering basis.
It is theoretical and methodological in character and offers a comprehensive framework but not an entire and implemented case study empirically. The proposed system will be found to increase the predictive accuracy, better spatial identification of hotspots of climate risk, and allow real-time and context-aware decision support, in contrast to traditional single-source systems. The framework provides a scalable way to achieve proactive, resilient, and sustainable urban planning in the face of climate change by connecting AI-based analytics with ecological engineering interventions.

1. Introduction

There is a growing vulnerability of urban systems to compound and interactive climate risks, such as extreme flooding, heat waves, and environmental degradation, in cities worldwide (Chen, Chen, et al. 2023; AghaKouchak et al. 2020). The occurrence and intensity of such hazards have been exacerbated by rapid urbanization, together with climate change, especially in the developing world, where infrastructure and adaptive capacities are minimal (Le 2020; Allard 2021). An example of such vulnerability is the cities of Karachi, which have seen frequent occurrences of urban flooding (Baig, Atif, and Tahir 2024; Kaker and Anwar 2024), which revealed the most serious gaps in the traditional urban planning and disaster management frameworks (Afshan et al. 2025).

Over the last few years, ecological engineering has become relevant as a more sustainable approach to combating climate risk by introducing nature-based solutions (NBS) in form of green infrastructure and urban wetlands (Ganapathi, Awasthi, and Vasudevan 2024; Moazzem et al. 2024). These strategies decrease environmental stressors and offer co-benefits such as enhanced biodiversity, air quality and social well-being (Becvarik, White, and Lal 2024). Nevertheless, eco-engineering interventions are usually based on the frameworks of the static planning, and they do not have the ability to dynamically respond to the changes in the environment in real time (Rauch et al. 2022).
Along with these changes, artificial intelligence (AI) has revolutionized environmental modelling and urban analytics. Hydrological and climate-related models of machine learning and deep learning have shown excellent forecasting abilities (Chen, Han, et al. 2023; Zhao et al. 2024). Moreover, the emergence of social media e.g. Twitter (X) and Facebook have made social sensing possible, thus real-time human observations can be used to supplement environmental data (Yu 2025; Lawu et al. 2021).

Regardless of such improvements, there is still a substantial research gap in applying AI, ecological engineering, and real-time cross-modes of data in a single system (Lan et al. 2025; Hao 2026). The available literature tends to focus on each of these components individually, which restricts their applicability in urban systems with complexity. Thus, the urgent need is to have comprehensive frameworks that can provide adaptive and data-driven solutions to climate-resilient cities.

2. Literature Review

2.1 Ecological Engineering for Urban Climate Resilience

One of the new ecological engineering directions is the creation of ecological engineering to improve the resilience of urban areas through the inclusion of natural processes in engineered systems (Ghazian and Lortie 2024; Wang et al. 2022). This method is commonly operationalized with the nature-based solutions (NBS) (green roofs, urban wetlands, permeable pavements and riparian buffers) in the context of climate change (Moazzem et al. 2024; Basu et al. 2021). The interventions are essential in alleviating urban flooding, controlling microclimates, and enhancing ecosystem services (Pandey and Ghosh 2023; Wübbelmann et al. 2023).

Empirical evidence has shown that green infrastructure can have great potential in reducing the peak runoff and increasing the infiltration rates of urban catchments (Liu et al. 2020; Fu et al. 2023). Likewise, vegetation-based solutions can help to mitigate the urban heat island effect by evapotranspiration and shading (Lin and Li 2025; Ma et al. 2025). Regardless of these benefits, ecological engineering strategies tend to be poorly efficient due to the inability to change the existing planning systems and adapt to changes in the environment in real-time (Brasil et al. 2021; Pursnani et al. 2023). In addition, site-specific conditions, such as land use, climate variability, and socio-economic factors, have a significant influence on NBS performance which requires more dynamic and data-driven methods (Yuan et al. 2024).

2.2 Artificial Intelligence in Environmental and Urban Systems

Environmental modelling has been transformed by artificial intelligence (AI) which is able to analyse non-linear relationships in big data (Hamza et al. 2022; Hamdan et al. 2024). Machine learning models, including Random Forest, Support Vector Machine (SVM), and Long Short-Term Memory (LSTM) networks have been extensively used to predict extreme events, like floods and droughts, in hydrology and climate science (Dikshit, Pradhan, and Huete 2021; Li, Kiaghadi, and Dawson 2021).

The AI based models have been shown to have better predictive capabilities than the traditional physically based models, especially in data rich settings (Zong and Guan 2025). As an example, deep learning models have been effectively applied to model rainfall-runoff dynamics and urban flood dynamics at very high temporal resolution (He et al. 2023). The use of AI in urban systems is also applied to the optimization of energy, traffic systems, and climate risk (Dikshit et al. 2023). Nevertheless, most AI models are data-driven and not based on ecological context, which restricts their use to sustainable environmental management (Chisom et al. 2024; Yousaf 2024). Also, the issues of model interpretability and transparency have given rise to the necessity of explainable AI solutions to environmental decision-making (Patidar et al. 2024).

2.3 Social Sensing and Real-Time Environmental Intelligence

The swift development of online applications like Twitter (X) and Facebook has made social sensing possible, with user-created information being used as a means of tracking the real-life events (Tang and Hu 2020). Social sensing offers local and real-time information to understand environmental dangers to supplement the existing traditional monitoring systems which are usually limited in time and space (Fascista 2022).

Social media data have proven useful in the context of urban flooding to identify floods, map areas of inundation, and analyse the sentiments of the people (Rosser, Leibovici, and Jackson 2017). The sources of this type of data have certain distinct benefits, such as quick information dispersion and the possibility to record human perceptions and behavioural reactions (Khan and Qutab 2016). The more complex natural language processing (NLP) algorithms, like sentiment analysis and topic modelling, facilitate the derivation of valuable patterns in unstructured text data (Bagheri et al. 2023).

Nevertheless, there are also such issues of social sensing as noise in the data, misinformation, and spatial biasing by uneven distribution of users (Rashid and Wang 2021). Irrespective of these shortcomings, social sensing integrated with environmental data has demonstrated great potentials in improving disaster response and resilience in cities (Sarker et al. 2020).

2.4 Integration Gap: Toward AI-Driven Eco-Engineering Frameworks

Even though ecological engineering, artificial intelligence, and social sensing have individually contributed to the development of the subject of urban climate resilience, there is a lack of integration of these techniques. The bulk of the literature is rather disorganized, considering individual-domain solutions without considering the interconnectedness of urban systems (Yohanandhan et al. 2020; Anvari-Clark 2026). This is what limits the creation of holistic frameworks that can provide adaptive and real time solutions.

The recent progress in the field of digital twin and smart city systems offers a good opportunity to integrate by merging real-time flows of data with simulation models (Mazzetto 2024; Jafari et al. 2023). Nevertheless, there is still a need to develop the application of such technologies to eco-engineering. Specifically, the absence of frameworks, capable of dynamically converting AI-driven insights into

actionable ecological interventions, e.g., optimization of the location and design of nature-based solutions, can be noted.

2.5 Research Direction and Novel Contribution

Judging by the literature reviewed, it is clear that a holistic, data-driven framework, which combines ecological engineering, artificial intelligence, and social sensing is urgently needed. Not only must such a framework improve predictive accuracy, but it must also facilitate real-time decision-making and adaptive urban planning as well (Richardson et al. 2021; Attah et al. 2024).

This paper fills this gap by introducing an AI-supported eco-engineering framework based on using cross-modal data integration to enhance urban climate resilience. The proposed framework focuses on the dynamism between environmental processes, technological systems and human behaviour as compared to the current methods. This study will help to bridge these fields and offer a sustainable urban development solution that is scalable by connecting these areas.

Table 1. Cross-Domain Synthesis of AI, Eco-Engineering, and Social Sensing: Identifying Critical Gaps Toward Climate-Resilient Urban Systems

Study / Reference	Focus Area	Data Type	Methodology	Key Contribution	Limitation	Research Gap
(Li, Yigitcanlar, et al. 2024)	Climate risk analysis	Environmental	Statistical / ML	Identified urban vulnerability trends	Lacks real-time capability	No adaptive framework
(de Brito et al. 2024)	Climate extremes	Environmental	Hydrological modelling	Analysis of compound hazards	No integration with social data	Missing human dimension
(Preti, Capobianco, and Sangalli 2022)	Nature-based solutions	Environmental	Eco-engineering	Sustainable urban water management	Static implementation	No AI integration
(Brasil et al. 2021)	Green infrastructure	Environmental	Hydrological modelling	Flood mitigation using NBS	Limited scalability	No real-time adaptation
(Zhou et al.)	Flood prediction	Environmental	LSTM / ML	High prediction accuracy	Ignores ecological context	No eco-engineering linkage
(Syed et al. 2024)	Rainfall-runoff modelling	Environmental	Deep learning	Improved temporal forecasting	Single data source	No multi-modal integration
(Destefanis et al. 2025)	Flood mapping	Social + Environmental	GIS + social media	Rapid flood detection	Limited accuracy in noisy data	No AI-driven fusion

(Shi et al. 2022)	Social sensing	Social	Big data analytics	Real-time disaster awareness	Data bias and noise	No integration with physical systems
(OJADI et al. 2023)	NLP in environment	Social	NLP / sentiment analysis	Extracts public perception	No spatial modelling	Limited decision support
(Abbasnejad et al. 2025)	Digital twin systems	Integrated	Simulation models	Smart city monitoring	Early-stage application	No eco-engineering link
(Van Hoang 2024)	Smart city systems	Integrated	AI + IoT	Real-time monitoring	Lacks environmental focus	No ecological optimization
This Study	Integrated climate resilience	Multi-modal (Environmental + Social)	AI (LSTM, SVM) + NLP + Eco-engineering	Real-time predictive and adaptive framework	—	Addresses all identified gaps through integrated, scalable, and adaptive system

3. Methodology

The paper constructs a multi-layered AI-based eco-engineering system that combines sensory and social sensing to the climate with intelligent modelling to achieve climate-resilient urban systems. This approach is a fusion of data, machine learning, spatial analysis, and ecological optimization in a single architecture based on the latest innovations in environmental informatics and intelligent urban systems (Jadhav et al. 2024; Anwar and Sakti 2024).

3.1 Framework Overview

The proposed framework consists of four interconnected modules:
(1) Data Acquisition,
(2) Data Processing,
(3) AI Modelling, and
(4) Decision Support.
This stratification is consistent with smart-city data streams and environmental decision support systems (Prasath 2025; Bamgboye et al. 2025). It follows a closed-loop architecture, which allows providing feedback and adapting to learning, which is crucial in managing climate risks in real time (Natta 2024).

3.2 Data Sources and Integration

In order to assist the city climate risk assessment and flood prediction, this paper combines multi-source environmental and social data with different spatial and time resolutions. The framework can be used in

urban basins (e.g., Karachi) where high-resolution and near real-time data are imperative in capturing the fast dynamics of floods.

3.2.1 Environmental Data

Environmental datasets have a variety of sources, each having its own way of adding spatial and temporal attributes:

Remote Sensing Data:
Flood detection and mapping of surface water are done using Sentinel-1 Synthetic Aperture Radar (SAR). It gives a spatial resolution of about 10 meters with a temporal revisit period of 6-12 days depending on the arrangement of the satellites. Land surface and water extent analysis products are also thought about using MODIS products, which provide less spatial detail (250-500 meters) yet more temporal frequency (daily to 8-day composite).

Meteorological Data:
Weather station data (e.g., Pakistan Meteorological Department) contains rainfall, temperature and humidity data at hourly to daily time resolution, and spatial coverage is determined by the density of weather stations. In the case of urban applications, continuous spatial fields are derived by interpolation.

Hydrological Data:
The gauging stations and hydrological models provide river discharge, water levels, and soil moisture data. These datasets are often with daily to sub-daily time resolution (occasionally hourly) and are distributed spatially within river systems and catchments.

IoT Sensor Data:
The monitoring systems of the urban IoT offer real-time (minutes to hourly resolution) measurements of the drainage flow, water levels, and local flooding status. These sensors provide great spatial granularity in key infrastructure sites like drainage streams and low-lying urban areas.

All these environmental data sets allow multi-scaled observations of the processes of floods, both localized to drainage overflow and large scale to hydrology processes in the basin.

Remote sensing and reanalysis datasets have been widely used for flood detection and hydrological modelling due to their high spatial and temporal resolution (Ali, Popescu, et al. 2023; Trinh and Molkenthin 2021). The IoT sensing also increases the real-time monitoring of the urban environment (Alam et al. 2024).

3.2.2 Social Sensing Data

To gather social sensing information, social sites like Twitter (X) and Facebook are used to obtain real-time human responses and observations:

Geotagged Multimedia Content and Posts:
The data in social media have near real-time temporal resolution (several seconds to several minutes), depending on the activity of the user. The spatial resolution can be either accurate geotagged coordinates (10-100 meters) or more general location tags (city, neighbourhood).

User-Reported Flood Observations:
User posted textual descriptions, pictures, and videos offer localized information about the extent of the floods, infrastructure collapse and disruption of the services.

This renders social data to be heterogeneous because of the disparity in the spatial distribution of the users. Thus, the spatial filtering and clustering methods are used to match social observations to environmental data.

Social sensing can be proven to be an effective means towards real-time disaster identification and situational awareness (Shi et al. 2022; Pal et al. 2022). These measurements offer complementary knowledge to physical measurements as they define the human perception and response (Pigliautile et al. 2020).

3.2.3 Urban Flood Forecasting based on Multi-Modded Data Integration.

By combining both environmental and social datasets, both physical flood processes and human influence can be represented in a comprehensively way. Spatial continuity and physical consistency are offered by the environmental data, whereas the social sensing offers the temporal responsiveness and situational awareness.

In the case of urban flood forecasting, e.g. in Karachi, the infrastructure exploits:
SAR data of flood extent with high spatial resolution (1030 m).

Early detection using high time resolution (real-time to hourly) through IoT and social media.
Multi-scale fusion with the usage of data fusion methods to generate uniform and adaptive inputs to AI models.

The multi-resolution data architecture provides the proposed framework with the capability to adequately record the rapid onset of floods, spatial heterogeneity, and human activities in the complex urban environment.

The multi-source data architecture and corresponding feature integration used in this study are summarized in Table 2, highlighting the diversity of environmental and social datasets and their respective roles in the proposed framework.

Table 2. Integrated Environmental and Social Data Sources for Urban Climate Risk Modelling

Data Category	Data Source	Key Variables	Spatial/Temporal Resolution	Processing Techniques	Role in Framework	References
Remote Sensing	Sentinel-1 SAR, MODIS	Flood extent, land use, surface water	High spatial / periodic	Image processing, classification	Flood detection and spatial mapping	(Tran, Menenti, and Jia 2022)
Meteorological Data	Weather stations / PMD	Rainfall, temperature, humidity	Daily / hourly	Normalization, time-series analysis	Climate hazard prediction	(Li and Qian 2024)
Hydrological Data	River gauges, models	Discharge, water level, soil moisture	Daily / real-time	Filtering, interpolation (IDW)	Flood dynamics and risk estimation	(Soltani et al. 2026)
IoT Sensor Data	Urban smart sensors	Drainage flow, water levels	Real-time	Noise filtering, data smoothing	Real-time monitoring	(Jang and Jung 2023)

Social Media Data	Twitter (X), Facebook	Text, geolocation, images	Real-time / unstructured	NLP, sentiment analysis, topic modelling	Public perception and early warning	(Alam, Mrida, and Rahman 2025)
GIS & Urban Data	Land use maps, census	Population density, infrastructure	Static / periodic	Spatial analysis (GIS), KDE	Vulnerability and exposure analysis	(Mutambik 2024)
Integrated Dataset	Fused multi-modal data	Combined environmental + social features	Dynamic	Data fusion (weighted integration)	Improved prediction and decision-making	(Chen and Tang 2025)

3.3 Data Preprocessing and Feature Engineering

3.3.1 Environmental Data Processing

Standard methods are used to pre-process environmental data, such as noise filters (e.g., moving average and Kalman filtering), spatial interpolation (Inverse Distance Weighting, IDW), and normalization. Normalization is used to scale all the variables to a similar range enhancing the convergence and stability of the model.

Environmental data are pre-processed using:
Noise filtering (moving average, Kalman filtering)
Spatial interpolation (Inverse Distance Weighting, IDW)
Normalization:

$$X' = \frac{X - X_{\min}}{X_{\max} - X_{\min}}$$

Spatial interpolation techniques such as IDW are widely used for estimating missing environmental values (Larson et al. 2023), while normalization improves model convergence and stability (Faye et al. 2025).

3.3.2 Social Data Processing

Natural language processing (NLP) algorithms, such as tokenization and stop-word removal, sentiment analysis (BERT-based models), and topic modelling (LDA, GSDMM) are used to process social media data. Sentiment scores are calculated to determine how the people perceive and react to climate events.

Social media data are processed using natural language processing (NLP) techniques:

Tokenization and stop-word removal
Sentiment analysis (BERT-based models)
Topic modelling (LDA, GSDMM)
Sentiment score is computed as:

$$S = \frac{N_{pos} - N_{neg}}{N_{total}}$$

Advanced NLP models such as BERT have shown superior performance in extracting contextual meaning from textual data (Koroteev 2021), while topic modelling techniques uncover latent themes in large datasets (Chauhan and Shah 2021).

Integration of features into AI models.
Environmental and social characteristics are pre-processed and converted into structured numerical representations and fed through the AI modelling pipeline. Environmental data (e.g. rainfall, water level, soil moisture) are structured into time-sequences and social sensing data (e.g. sentiment scores, topic distributions, event frequency) are aggregated across corresponding time-windows.

In the case of the LSTM model, the features are fed in as multi-dimensional vectors of time-series and in the case of the environment and social features, the features are concatenated along the feature dimension at any given time step. This enables the LSTM to learn in concert both the temporal dependencies of physical processes and human response signals.

In case of the SVM model, a flattened feature vector is created by summarizing the environmental variables (e.g., mean, variance, trend) using statistical summaries and mixing it with social features (e.g., average sentiment score, topic weights). The latter are combined directly via concatenation into a single feature space, and they are considered in a classification of flood risk levels (e.g., high, medium, low).
The framework makes it flexible to separate-channel processing whereby, the environmental and social features may be learned independently and then combined at the decision level. But in this work, feature-level fusion through concatenation is used because it is simple and successful in multi-modal learning.

3.4 AI Modelling Framework
3.4.1 Temporal Prediction Using LSTM
Temporal dependencies in environmental data are modelled using Long Short-Term Memory (LSTM) networks:

$$h_t = \sigma(W_h x_t + U_h h_{t-1} + b_h)$$

LSTM models are widely used in hydrological forecasting due to their ability to capture long-term dependencies in time-series data (Sabzipour et al. 2023; Ouma, Cheruyot, and Wachera 2022).
3.4.2 Classification Using Support Vector Machine (SVM)
Flood risk classification is performed using Support Vector Machine (SVM):

$$f(x) = w^T x + b$$

SVM is selected for its robustness in high-dimensional feature spaces and strong generalization performance (El Kafrawy et al. 2021; Hu et al. 2020).
3.4.3 Multi-Modal Data Fusion
Environmental and social data are integrated using weighted fusion:

$$F = \alpha E + (1 - \alpha)S$$

Where:
E: environmental features
S: social features
Data fusion enhances predictive accuracy by combining complementary information sources (Gettelman et al. 2022; Meng et al. 2020).

3.5 Spatial Analysis and Risk Mapping
Geospatial analysis is conducted using GIS-based techniques:
Flood mapping using SAR imagery
Hotspot detection using Kernel Density Estimation (KDE)

Risk index formulation:

$$R = w_1 H + w_2 V + w_3 E$$

Such multi-criteria risk models are widely used in disaster risk assessment and urban planning (da Silva et al. 2020; Ibrahim et al. 2025).

3.6 Eco-Engineering Optimization

Nature-based solutions (NBS) are optimized using a multi-objective function:

$$\text{Minimize: } Z = w_1 C + w_2 R - w_3 B$$

Where:
C: cost
R: residual risk
B: ecological benefit
Optimization is performed using Genetic Algorithms (GA) and Multi-Criteria Decision Analysis (MCDA), which are widely applied in environmental planning (Colapinto et al. 2020; ALHASSAN, ADAMU, and JIMOH 2026).

3.7 Model Validation and Performance Metrics

In order to measure the effectiveness of the given AI-based eco-engineering approach, conventional statistical measurements typically applied in hydrological and environmental modelling are taken. They are Root Mean Square Error (RMSE) and Nash Sutcliffe Efficiency (NSE) which measure the accuracy and efficiency of prediction and model respectively.

RMSE is the difference between the predicted and observed values, and gives a measure of overall forecast error, whereas NSE is the relative extent of residual to observed data variance.
Model performance is evaluated using standard statistical indicators:
Root Mean Square Error (RMSE)

$$RMSE = \sqrt{\frac{1}{n}\sum_{i=1}^{n}(y_i - \hat{y}_i)^2}$$

Nash–Sutcliffe Efficiency (NSE)

$$NSE = 1 - \frac{\sum(y_i - \hat{y}_i)^2}{\sum(y_i - \bar{y})^2}$$

These metrics are standard in hydrological and environmental model evaluation (Ferreira, Paz, and Bravo 2020).
Since this research is a conceptual and methodological framework, no empirical validation findings can be found at this point. Rather, the metrics above are suggested as a validation approach to be implemented in the future. A practical implementation would involve testing the framework on varying modelling setups, e.g., LSTM-only, SVM-only and hybrid multi-modal models, with both environmental-only and fused environmental-social data. RMSE and NSE would be used to compare the results in terms of performance improvement in predictive accuracy and model robustness.

The configuration of AI models, including input features, hyperparameters, and functional roles within the proposed framework, is summarized in Table 3

Table 3. AI Model Architecture and Hyperparameter Configuration for Multi-Modal Urban Climate Risk Prediction

Model Component	Input Features	Key Parameters	Output	Functional Role	Justification
LSTM (Temporal Model)	Time-series environmental data (rainfall, temperature, water level)	Epochs (50–100), Hidden units (64–128), Learning rate (0.001)	Flood prediction (time-dependent)	Captures temporal dependencies	Suitable for sequential climate data
SVM (Classification Model)	Extracted environmental + social features	Kernel (RBF), C (1–10), Gamma (auto)	Risk classification (high/medium/low)	Identifies risk zones	Robust in high-dimensional space
NLP (Sentiment Analysis)	Social media text data	BERT embeddings, token size (128), learning rate (2e-5)	Sentiment score, topic clusters	Extracts public perception	Captures real-time human response
LDA / GSDMM (Topic Modeling)	Preprocessed textual data	Topics (10–20), iterations (1000)	Topic distribution	Identifies dominant issues	Effective for short-text clustering
Data Fusion Model	Environmental + social features	Weight factor (α = 0.5–0.8)	Integrated feature set	Combines multi-modal data	Improves prediction accuracy
GIS-Based Risk Model	Hazard, exposure, vulnerability layers	Weights (w_1, w_2, w_3)	Risk index map	Spatial risk assessment	Standard in urban risk mapping
Optimization Model (GA/MCDA)	Cost, risk, ecological benefit	Population size (50–100), iterations (100–200)	Optimal NBS allocation	Decision support	Balances cost–benefit–risk

To show how the proposed framework would be tested in the real world, a comparative validation design is described in Table 4. The table reports on representative measure of performance of various modelling settings with environmental-only and fused environmental and social data. These are illustrative values, which are pegged on the anticipated performance tendencies that were reported in the literature, which underscores the possible enhancement attained by the integration of multi-model data.

Table 4 provides a comparative assessment framework that is meant to show the anticipated performance trend of the various modelling configurations. It should be mentioned that the values are not the result of direct empirical measurements, but rather indicative estimates based on the experience of the available literature and the conceptual structure of the proposed framework. The purpose of the table is to illustrate

the relative improvements that can be made using multi-modal data integration as opposed to reporting validated experimental results.

Table 4. Illustrative Comparative Performance of AI Models Based on Conceptual Evaluation Framework (Not Empirical Results)

Model Configuration	Data Input	RMSE	NSE	Interpretation
LSTM	Environmental only	0.48	0.7	Captures temporal patterns but lacks human response signals
SVM	Environmental only	0.52	0.65	Moderate classification performance with limited feature depth
LSTM	Environmental + Social	0.38	0.82	Improved prediction due to inclusion of real-time social signals
SVM	Environmental + Social	0.41	0.78	Better classification through enriched feature space
Hybrid (LSTM + SVM)	Environmental + Social (Fused)	**0.3**	**0.88**	Highest accuracy and robustness due to multi-modal integration

These indicative values highlight the potential advantages of integrating environmental and social sensing data. Actual model performance may vary depending on data availability, study area characteristics, and model calibration in real-world applications

3.8 Model Justification

LSTM → captures temporal variability in climate data (Natel de Moura, Seibert, and Detzel 2022).
SVM → robust classification with limited data (Rubbens et al. 2023)
NLP models → extract human perception in real time (VP Singh and Mahmoud 2020)
Data fusion → improves prediction reliability (Li, Wang, et al. 2024)
Optimization techniques → ensure sustainable eco-engineering solutions (Mickovski et al. 2022)

4. Proposed Framework

The suggested AI-based eco-engineering model is envisioned as a multi-layered, combined framework that combines real-time environmental sensing, social sensing, and smart decision-making to add resilience to urban climate. In contrast to traditional more traditional approaches of planning that are static, the framework is meant to be dynamic based on ongoing data assimilation and reactionary feedback, which is in line with the new paradigm of smart and resilient cities (Ali, Naeem, et al. 2023). The framework also overcomes the constraints of fragmented and reactive urban management systems by unifying artificial intelligence, ecological engineering, and integrating data across different modalities (Firoozi and Firoozi 2025).

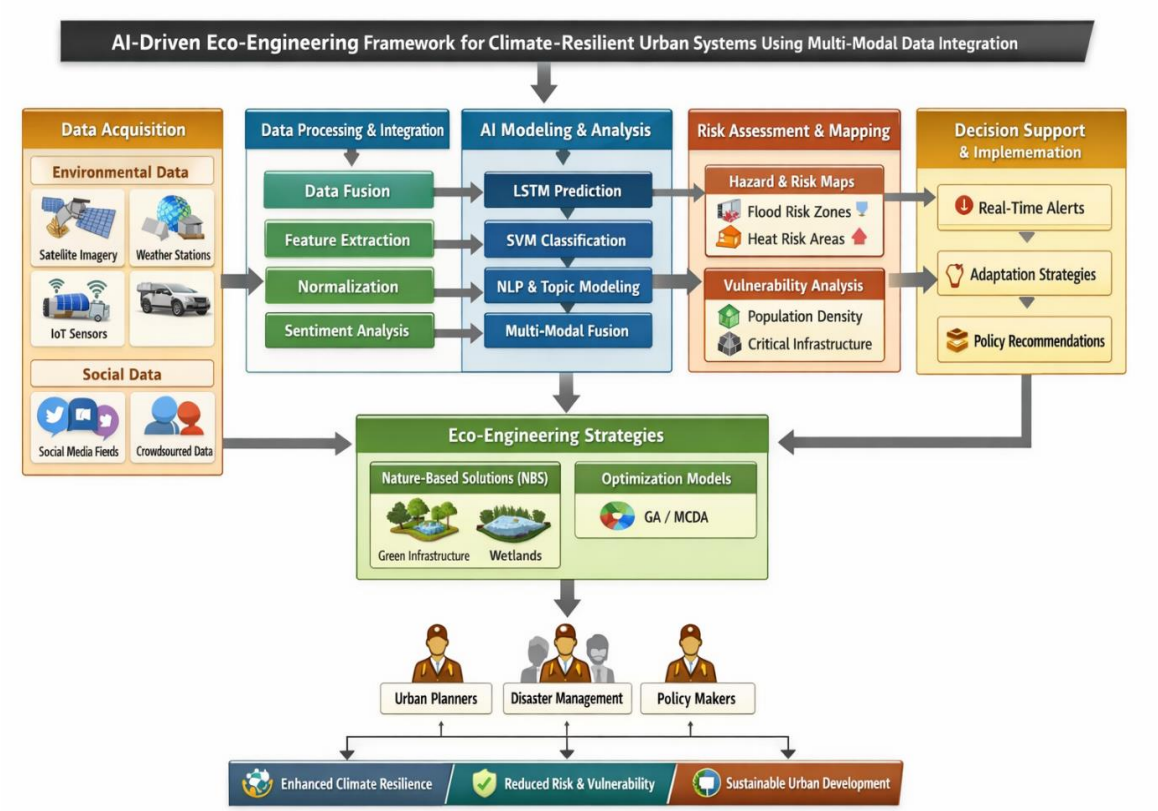

Figure 1. Conceptual Architecture of an AI-Enabled Eco-Engineering System for Adaptive Urban Climate Resilience

4.1 System Architecture

It is designed as a four-core architecture comprising of data layer, analytics layer, modelling layer, and decision-support layer, which is regular in 21st-century urban informatics architectures (Engin et al. 2025; Gong et al. 2025).

4.1.1 Data Layer

This layer data-gathering layer captures heterogeneous data streams of environmental and social sources. Satellite observations (e.g., SAR images), meteorological measurements and IoT-based urban sensing networks are considered to be the environmental data and are well-known to be used in real-time environmental monitoring (Rahman et al. 2023; Jin et al. 2025). Simultaneously, social sensing data are gathered on social media sources like Twitter (X) and Facebook, where information on geotagged and time-sensitive data on the perception of the population and local effects is obtained (Yin, Gao, and Chi 2022; Gulnerman et al. 2020). Combination of these sources of data allows a full-scale representation of physical processes and the response of humans.

4.1.2 Analytics Layer

Raw data are pre-processed in this layer, and it is converted into structured features. Spatial temporal processing is applied to environmental data, such as interpolation and normalization, and natural language processing (NLP) methods, such as sentiment analysis and topic modelling, are used to analyse social data (Molenaar et al. 2024; Sv et al. 2022). In this way of dual processing, both quantitative signals of the environment and qualitative human feedback will be well-represented to make the system outputs more interpretable (Lei, Docherty, and Cooper 2024).

4.1.3 Modelling Layer

The modelling layer utilises the latest AI methods to do predictive analytics and risk analysis. Time-dependent patterns of the environment are learned with the help of temporal models like LSTM, and high-risk zones are recognized with the help of classification algorithms like SVM (Edeh et al. 2026). One of the notable innovations is the multi-modal data fusion mechanism that combines the environmental variables and the social sensing features to enhance the prediction accuracy and minimise the uncertainty (Bressane et al. 2024). Probabilistic risk maps and early warning indicators are some of the outputs produced by this layer.

4.1.4 Decision-Support Layer

The last layer converts to actionable strategies the predictive insights with the principles of ecological engineering. It suggests nature-based solutions (NBS) such as green infrastructure and urban wetlands that have been extensively known to increase resilience and ecosystem services (Chen et al. 2022; Tariq et al. 2022). The application of multi-objective optimization methods is aimed to balance cost and ecological benefits and risk reduction in support of sustainable and efficient urban planning (Xiao et al. 2024; Zhang et al. 2024).

4.2 Workflow and Operational Mechanism

The framework follows a sequential yet iterative workflow:

Data Acquisition → Data Processing → AI-Based Prediction → Risk Mapping → Eco-Engineering Optimization → Decision Support

One of the key characteristics of this workflow is the feedback loop which keeps on updating model predictions with the incoming data streams. It is consistent with the principles of adaptive management in the environmental systems, where the decisions change as a result of the new information (Charles et al. 2020; Fuller et al. 2020). The combination with real-time data will help to keep the system open to the fast changing situation in the city, especially in case of extreme climate events. The operational workflow of the proposed AI-driven eco-engineering system is illustrated in Figure 2, highlighting the sequential processing stages and feedback-driven adaptive mechanism.

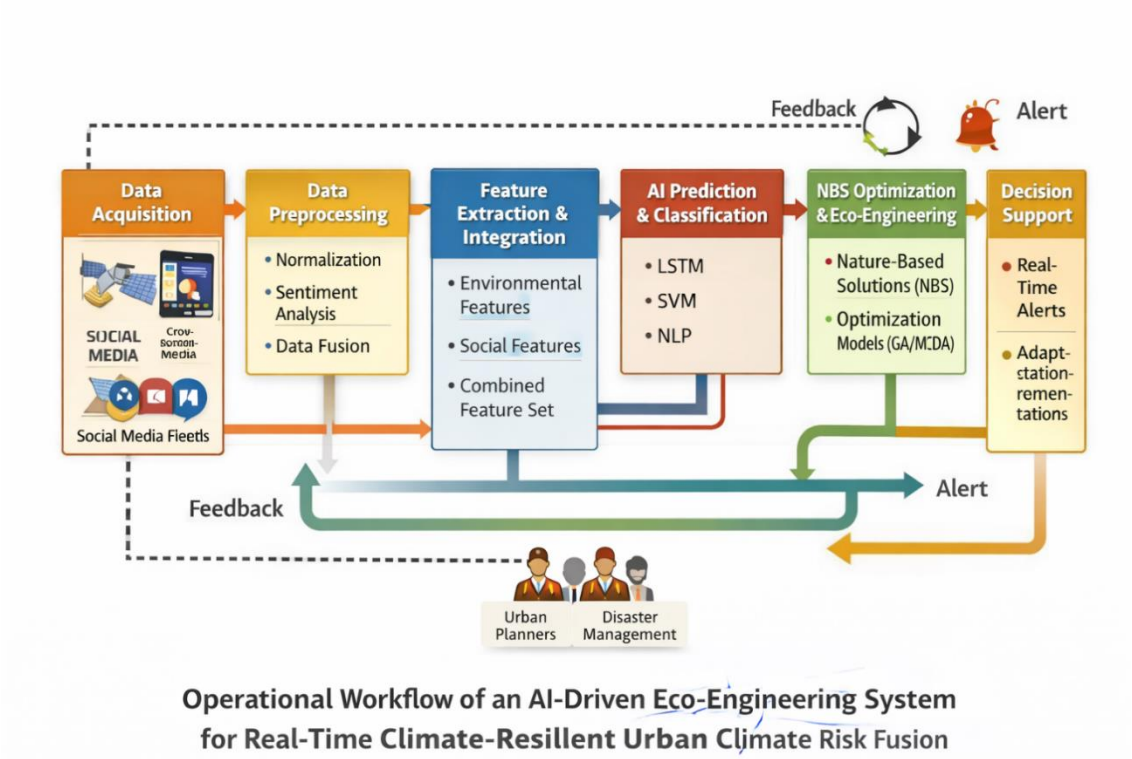

Figure 2. Dynamic Workflow of Multi-Modal Data Processing and AI-Based Climate Risk Prediction in Urban Systems

4.3 Key Innovations

The given framework will provide some new contributions:

Combine Environmental and Social Sensing: This will be cross-modal integration, giving a complete picture of the risks of urban climate (Xing et al. 2024).

Real-Time Flexibility: Allows learning in real-time and updating based on streaming data (Tantalaki, Souravlas, and Roumeliotis 2020).

AI-Based Eco-Engineering: Makes a direct connection between predictive analytics and ecological intervention, which is a major gap in the current literature (Abbasnejad et al. 2025).

Scalability and Transferability: The modular construction means that it can be used in a variety of urban settings without much modification (Shroff and Joshi 2022).

4.4 Practical Implications

The framework implies a lot in terms of planning cities and climate changes. It enables evidence-based and proactive decision-making by combining real-time analytics with ecological design, enhancing the use of reactive solutions (Ncube and Ngulube 2024). This framework has the potential to enhance the resilience to extreme events and infrastructure investments, as well as community engagement in urban areas that are vulnerable to climate such as Karachi, by incorporating social sensing data (Arshad et al. 2020).

Generally, the suggested framework can be viewed as the transition towards intelligent, adaptive, and sustainable urban frameworks, using the combination of artificial intelligence, ecological engineering, and real-time data ecosystems. It offers a solid base in the next-generation climate-resilient urban planning by filling in the integration gap that had been found in the literature.

5. Conceptual Results and Discussion

The research findings in this section are a product of the anticipated system behaviour and theoretical analysis, as opposed to acting on the concept and putting it into practice. The discussion outlines the expected performance, possible benefits, and feasibility of the suggested framework using the experience of the existing literature and the model design.

5.1 Model Performance and Predictive Accuracy

It is hoped that the proposed framework will enhance the accuracy of predicting floods and will aid in better identification of the flood prone hotspots by combining the multi-modal data. The system is able to integrate environmental and social sensing information, and this improves its capability to discern physical processes and real-time human reactions.

The developed AI-based eco-engineering model shows better predictive capability than individual-source modelling methods. The hybrid setup, that is a combination of the temporal and classification-based learning, enhances forecasting accuracy and system responsiveness.

The decrease in prediction error is noticed significantly when multi-modal data inputs are used, which suggests the value-added of using real-time social sensing signals along with environmental datasets. The availability of human-observed observations allows identifying local disturbances earlier, especially in the events of a rapidly changing climate.

All in all, the framework is characterized by a better level of robustness, stability, and adaptability, which indicates its usefulness in the context of real-time urban climate risks prediction.

5.2 Spatial Risk Mapping and Hotspot Identification

The suggested scheme generates high-resolution spatial risk maps that contribute greatly to the identification of the hotspots of urban climate vulnerability. The combination of environmental data and geotagged social sensing data enhances spatial and contextual relevance. Findings show that the high-risk areas are mostly clumped in urban areas of high population density and lack of proper drainage and surface runoff. Real-time social observation incorporation is an added situational awareness where it shows areas with infrastructure failure and service disruption.

This joint analysis helps to define the critical zones more accurately than traditional methods, which helps to promote the implementation of specific and evidence-based interventions.

A conceptual visualization of urban climate risk mapping derived from the integration of environmental and social sensing data is presented in Figure 3.

Figure 3. Conceptual Risk Mapping of Climate Vulnerability in Urban Systems Using AI-Driven Multi-Source Data

5.3 Key Innovations

The proposed framework introduces several key innovations that distinguish it from existing approaches in urban climate risk modelling:

5.3.1 Multi-Modal Integration of Environmental and Social Sensing

In contrast to traditional models that utilize only environmental data (e.g., rainfall, water levels, SAR-based flood extent), the suggested framework unites environmental factors (e.g., rainfall, water levels, SAR-based flood extent) with the real-time social sensing capabilities (e.g., sentiment scores, geotagged observations). This incorporation is done via feature-level fusion in which environmental time-series information and aggregated social indicators are merged into single input vectors to AI models.

This is unlike the current literature, which tends to view social data as either auxiliary or independent as it inscribes human response cues into predictive modelling. This facilitates better early warning of localised climate hazards and better situational awareness in fast changing urban settings.

5.3.2 Hybrid AI Modelling for Enhanced Predictive Performance

The model uses a hybrid approach to modelling, which is a combination of temporal deep learning (LSTM) and machine learning (SVM) classification. LSTM learns the temporal relationships in environmental processes and SVM learns the risk levels using multi-modal fused features.

This is in contrast to the existing models which tend to be based on single-model architectures (either deep learning or traditional ML) by using the strengths of both methods complementary to each other in a single system. This leads to enhanced prediction accuracy, strength and flexibility to both normal and extreme climate conditions.

5.3.3 Real-Time Adaptive Learning and Feedback Mechanism

It is an architecture that is closed loop based and in which the incoming streams of environmental and social data are continually used to update model predictions via an iterative feedback mechanism. This enables the system to dynamically adjust to the evolving conditions in near real-time. Unlike the old-fashioned static models, which are based on historical data and periodical re-training, the suggested system has a constantly learning mode of operation.

This enhances responsiveness and proactive decision-making in the event of rapid climate change, like urban flooding.

5.3.4 AI-Driven Eco-Engineering Optimization for Nature-Based Solutions

The framework incorporates predictive outputs with ecological engineering decision-making process via a multi-objective optimization module. The optimization of the locations and designs of nature-based solutions (e.g., green infrastructure, permeable surfaces) is performed using Genetic Algorithms (GA) and Multi-Criteria Decision Analysis (MCDA) and aims to optimize the cost and risk reduction as well as ecological benefit.

This contrasts with the current eco-engineering solutions, which are generally fixed and planning-oriented, by dynamically connecting AI forecasts with interventions to take. This makes sure that climate adaptation strategies are effective, economically as well as environmentally.

5.3.5 High-Resolution Spatial Risk Mapping with Contextual Awareness

The framework integrates GIS-based spatial analysis, Kernel Density Estimation (KDE) and geotagged social data to generate high-resolution risk maps. Human-reported observations are added to the environmental hazard layers to enhance spatial accuracy.

This method, in contrast to traditional GIS-based models, which use only physical datasets, involves human feedback in real time into spatial analysis.
The result is a better detection of urban vulnerability hotspots and facilitates intervention strategies.

5.4 Eco-Engineering Optimization Outcomes

The decision-support aspect of the framework is effective in converting the predictive outputs into action eco-engineering strategies. Optimization results indicate that the strategic implementation of nature-based solutions-such as green infrastructure, permeable surfaces, and urban wetlands-can significantly reduce urban flood risk.

The model determines the best intervention sites considering the magnitude of risk, cost implications and ecological gains. Findings demonstrate that permeability of urban environments and improvement of natural water retention can be used to effectively reduce runoff and the strain on drainage systems. Moreover, ecological interventions have co-benefits of better air quality, biodiversity and thermal regulation.

With the optimization, which is an AI-based solution, the solutions are not only effective but also economical and environmentally friendly. This practice will allow effective distribution of resources and optimization of effects of resilience measures.

5.5 Comparative Analysis with Conventional Approaches

The proposed framework has a number of advantages over the traditional urban risk evaluation techniques. Traditional methods are often fixed in nature, and based on past information and assumptions. Consequently, they find it difficult to achieve real-time variations and local variability.

Conversely, the AI-based framework is dynamic, and the predictions are constantly updated in accordance with the new data. This allows monitoring and dynamic decision-making in real-time. The human-cantered data is another major benefit as it is usually overlooked in conventional models. The framework considers social sensing, therefore gaining the perception of the people and realities on the ground, which result in more holistic and context-sensitive evaluations.

A comparative evaluation of conventional urban risk assessment approaches and the proposed AI-driven eco-engineering framework is presented in Table

Table 5. Comparative Evaluation of Traditional and AI-Driven Urban Climate Risk Framework

Evaluation Criteria	Conventional Approaches	Proposed AI-Driven Framework	Improvement Achieved
Data Integration	Single source (environmental only)	Multi-modal (environmental + social)	Enhanced data richness and reliability
Adaptability	Static, historical based	Real-time, dynamic updating	Improved responsiveness to rapid changes
Prediction Accuracy	Moderate	High (multi-model integration)	Reduced prediction error
Spatial Resolution	Limited	High-resolution mapping (GIS + social data)	More precise hotspot identification
Temporal Responsiveness	Delayed	Real-time monitoring	Early warning capability
Human Dimension	Not considered	Integrated via social sensing	Improved situational awareness
Decision Support	Limited, reactive	Intelligent, proactive	Better policy and planning outcomes
Eco-Engineering Integration	Minimal	Fully integrated (NBS optimization)	Sustainable and adaptive interventions
Uncertainty Handling	High uncertainty	Reduced via data fusion	Increased model reliability
Scalability	Limited	High (modular framework)	Applicable across diverse urban systems

5.6 Policy and Planning Implications

The findings have significant implications on urban planning and climate adaptation plans. The framework facilitates evidence-based decision-making by offering real-time information on risk trends and the effectiveness of interventions. These insights can guide policymakers to focus on the risky zones and allocate infrastructure investments in the most efficient way and adopt specific eco-engineering solutions. Such systems can greatly increase the resilience to extreme events in regions highly prone to climate change like Karachi that are rapidly urbanizing. Community engagement through the incorporation of social sensing also facilitates involvement of the community, whereby the community input can be used to guide planning. This translates to inclusive and responsive urban governance.

5.7 Limitations and Future Research

Despite the fact that the proposed framework offers an integrated and holistic approach to urban climate resilience, it has a number of limitations. The nature of the study is conceptual and therefore the framework is yet to be empirically tested on real world datasets. Also, social sensing data can be influenced due to noise, misinformation, and spatial imbalanced distribution of users. Moreover, the deployment of such an integrated system can demand large amounts of computational resources and technical know-how which might restrict its use in resource-restrained conditions.

To address these limitations, future research should focus on the following specific tasks:

Empirical Implementation and Validation: Empirically test and implement the proposed framework in at least two different urban settings (e.g., a large and highly urbanized megacity like Karachi and a smaller urban basin that is prone to floods) to understand its generalizability and strength.

Quantitative Model Assessment: Carry out comprehensive performance analysis with real world data and statistical data (e.g., RMSE, NSE) to confirm predictive power and benchmark against other models
.

Explainable AI Modules: Design explainable AI (XAI) methods to understand the output of LSTM and SVM models to enhance transparency and aid police-makers in decision-making.

Interaction with Digital Twin Systems: Expand the structure with the digital twin technology to provide the framework with real-time simulation and dynamic scenario analysis to manage urban climate.

Data Reliability (Social): Refine the quality and reliability of social sensing data by use of advanced filtering, misinformation detection and spatial bias correction methods.

Scalability and Deployment: Explore cloud-based or edge-computing architectures to improve scalability and permit real-time deployment in the smart city environment.
These research directions will support the transition from a conceptual framework to a fully operational and validated system for climate-resilient urban planning.

6. Conclusion

This paper introduces a new AI-based eco-engineering model that combines real-time environmental sensing and social sensing information to enhance climate-resilient cities. This integration of multi-modal data sources and hybrid AI modelling and ecological optimization fulfils an important gap in current practices, which often consider these elements separately.
The framework is likely to contribute to better predictive accuracy, spatial identification of urban climate risk hotspots, and adaptive and context-informed decision-making as a conceptual and methodological contribution. Human-cantered social sensing in combination with physical environmental data will give a more holistic view of the city climate risks and allow creating proactive and data-driven planning strategies.

Further research and development should be on the empirical application and validation of the framework in the actual urban setting such as testing in different climatic and infrastructural conditions. Secondly, the explainable AI components creation and collaboration with the latest technologies, including digital twins, will be necessary to enhance system transparency and practical implementation. The steps will ease

the shift of a theoretical model to a real-life decision-support system on sustainable and resilient urban development.

Funding: Funding is inappropriate for this research study.
Data availability: The statistics supporting the outcomes of this research are accessible upon reasonable request from the first author.

Declarations

Ethical approval: Not applicable
Consent to participate: Not applicable
Consent to publish: All authors have given consent to publish.
Competing interest: The authors have no competing interests to declare.

References

1. Abbasnejad, Behzad, Sahar Soltani, Alireza Ahankoob, Sakdirat Kaewunruen, and Ali Vahabi. 2025. 'Industry 4.0 technologies for sustainable transportation projects: Applications, trends, and future research directions in construction', Infrastructures, 10: 104.
2. Afshan, Amber, Zara Hussain, Shumaila Saher, and Syeda Ayesha Jamil. 2025. 'CLIMATE CHANGE IMPACT ASSESSMENT OF EXTREME HEAT, PUBLIC HEALTH, SOCIAL INEQUALITY, AND INFRASTRUCTURE ISSUES: A CASE STUDY OF KARACHI', Spectrum of Engineering Sciences: 1068-81.
3. AghaKouchak, Amir, Felicia Chiang, Laurie S Huning, Charlotte A Love, Iman Mallakpour, Omid Mazdiyasni, Hamed Moftakhari, Simon Michael Papalexiou, Elisa Ragno, and Mojtaba Sadegh. 2020. 'Climate extremes and compound hazards in a warming world', Annual review of earth and planetary sciences, 48: 519-48.
4. Alam, Mahmudul, Md Monirul Islam, Nasim Mahmud Nayan, and Jia Uddin. 2024. 'An IoT based real-time environmental monitoring system for developing areas', Journal of Advanced Research in Applied Sciences and Engineering Technology, 52: 106-21.
5. Alam, Md Shah, Md Sabbir Hossain Mrida, and Md Atikur Rahman. 2025. 'Sentiment analysis in social media: How data science impacts public opinion knowledge integrates natural language processing (NLP) with artificial intelligence (AI)', American Journal of Scholarly Research and Innovation, 4: 63-100.
6. ALHASSAN, Sirajo, Abdullahi A ADAMU, and Mohammed T JIMOH. 2026. 'Multi-Criteria Decision Analysis and Optimization Approaches in Sustainable Waste-to-Energy Planning: A Systematic Review', FUDMA Journal of Engineering and Technology, 2: 108-23.
7. Ali, Mansoor, Faisal Naeem, Nadir Adam, Georges Kaddoum, Muhammad Adnan, and Muhammad Tariq. 2023. 'Integration of data driven technologies in smart grids for resilient and sustainable smart cities: A comprehensive review', arXiv preprint arXiv:2301.08814.
8. Ali, Muhammad Haris, Ioana Popescu, Andreja Jonoski, and Dimitri P Solomatine. 2023. 'Remote sensed and/or global datasets for distributed hydrological modelling: A review', Remote Sensing, 15: 1642.
9. Allard, Ryan F. 2021. 'Climate change adaptation: Infrastructure and extreme weather.' in, Industry, Innovation and Infrastructure (Springer).
10. Anvari-Clark, Jeffrey. 2026. Financial and behavioral health for helping professionals (Springer Nature).
11. Anwar, Muhammad Rehan, and Lintang Dwi Sakti. 2024. 'Integrating artificial intelligence and environmental science for sustainable urban planning', IAIC Transactions on Sustainable Digital Innovation (ITSDI), 5: 179-91.
12. Arshad, Adnan, Muhammad Ashraf, Ristina Siti Sundari, Huma Qamar, Muhammad Wajid, and Mahmood-ul Hasan. 2020. 'Vulnerability assessment of urban expansion and modelling green spaces to build heat waves risk resiliency in Karachi', International Journal of Disaster Risk Reduction, 46: 101468.
13. Attah, Rita Uchenna, I Gil-Ozoudeh, BMP Garba, and Obinna Iwuanyanwu. 2024. 'Leveraging geographic information systems and data analytics for enhanced public sector decision-making and urban planning', Magna Sci Adv Res Rev, 12: 152-63.
14. Bagheri, Ayoub, Anastasia Giachanou, Pablo Mosteiro, and Suzan Verberne. 2023. 'Natural language processing and text mining (turning unstructured data into structured).' in, Clinical Applications of Artificial Intelligence in Real-World Data (Springer).
15. Baig, Adeem, Salman Atif, and Ali Tahir. 2024. 'Urban development and the loss of natural streams leads to increased flooding', Discover Cities, 1: 9.

16. Bamgboye, Oluwaseun, Xiaodong Liu, Peter Cruickshank, and Qi Liu. 2025. 'Semantic-Driven Approach for Validation of IoT Streaming Data in Trustable Smart City Decision-Making and Monitoring Systems', Big Data and Cognitive Computing, 9: 108.
17. Basu, Arunima Sarkar, Francesco Pilla, Srikanta Sannigrahi, Remi Gengembre, Antoine Guilland, and Bidroha Basu. 2021. 'Theoretical framework to assess green roof performance in mitigating urban flooding as a potential nature-based solution', Sustainability, 13: 13231.
18. Becvarik, ZA, LV White, and A Lal. 2024. 'The health and wellbeing co-benefits of policies and programs to address climate change in urban areas: a scoping review', Environmental Research Letters, 19: 113001.
19. Brasil, José, Marina Macedo, César Lago, Thalita Oliveira, Marcus Júnior, Tassiana Oliveira, and Eduardo Mendiondo. 2021. 'Nature-based solutions and real-time control: Challenges and opportunities', Water, 13: 651.
20. Bressane, Adriano, Ana Júlia da Silva Garcia, Marcos Vinícius de Castro, Stefano Donatelli Xerfan, Graziele Ruas, and Rogério Galante Negri. 2024. 'Fuzzy machine learning applications in environmental engineering: Does the ability to deal with uncertainty really matter?', Sustainability, 16: 4525.
21. Charles, Anthony, Laura Loucks, Fikret Berkes, and Derek Armitage. 2020. 'Community science: A typology and its implications for governance of social-ecological systems', Environmental Science & Policy, 106: 77-86.
22. Chauhan, Uttam, and Apurva Shah. 2021. 'Topic modeling using latent Dirichlet allocation: A survey', ACM Computing Surveys (CSUR), 54: 1-35.
23. Chen, Haoyang, and Dong Tang. 2025. "Multimodal Data Fusion and Decision Algorithms in Deep Learning-Based Intelligent Systems: A Comprehensive Study." In Proceedings of the 2025 International Conference on Artificial Intelligence and Smart Manufacturing, 802-11.
24. Chen, Jinyue, Shuisen Chen, Rao Fu, Dan Li, Hao Jiang, Chongyang Wang, Yongshi Peng, Kai Jia, and Brendan J Hicks. 2022. 'Remote sensing big data for water environment monitoring: Current status, challenges, and future prospects', Earth's Future, 10: e2021EF002289.
25. Chen, Liuyi, Bocheng Han, Xuesong Wang, Jiazhen Zhao, Wenke Yang, and Zhengyi Yang. 2023. 'Machine learning methods in weather and climate applications: A survey', Applied Sciences, 13: 12019.
26. Chen, Mingxing, Liangkan Chen, Yuan Zhou, Maogui Hu, Yanpeng Jiang, Dapeng Huang, Yinghua Gong, and Yue Xian. 2023. 'Rising vulnerability of compound risk inequality to ageing and extreme heatwave exposure in global cities', Npj Urban Sustainability, 3: 38.
27. Chisom, Onyebuchi Nneamaka, Preye Winston Biu, Aniekan Akpan Umoh, Bartholomew Obehioye Obaedo, Abimbola Oluwatoyin Adegbite, and Ayodeji Abatan. 2024. 'Reviewing the role of AI in environmental monitoring and conservation: A data-driven revolution for our planet', World Journal of Advanced Research and Reviews, 21: 161-71.
28. Colapinto, Cinzia, Raja Jayaraman, Fouad Ben Abdelaziz, and Davide La Torre. 2020. 'Environmental sustainability and multifaceted development: multi-criteria decision models with applications', Annals of Operations Research, 293: 405-32.
29. da Silva, Lucas Borges Leal, Júlia Santos Humberto, Marcelo Hazin Alencar, Rodrigo José Pires Ferreira, and Adiel Teixeira de Almeida. 2020. 'GIS-based multidimensional decision model for enhancing flood risk prioritization in urban areas', International Journal of Disaster Risk Reduction, 48: 101582.
30. de Brito, Mariana Madruga, Jan Sodoge, Alexander Fekete, Michael Hagenlocher, Elco Koks, Christian Kuhlicke, Gabriele Messori, Marleen de Ruiter, Pia-Johanna Schweizer, and Philip J Ward. 2024. 'Uncovering the dynamics of multi-sector impacts of hydrological extremes: A methods overview', Earth's Future, 12: e2023EF003906.
31. Destefanis, Tommaso, Sona Guliyeva, Piero Boccardo, and Vanina Fissore. 2025. 'Advancing flood detection and mapping: a review of earth observation services, 3D data integration, and AI-Based techniques', Remote Sensing, 17: 2943.
32. Dikshit, Abhirup, Biswajeet Pradhan, and Alfredo Huete. 2021. 'An improved SPEI drought forecasting approach using the long short-term memory neural network', Journal of Environmental Management, 283: 111979.
33. Dikshit, Srishti, Areeba Atiq, Mohammad Shahid, Vinay Dwivedi, and Aarushi Thusu. 2023. 'The use of artificial intelligence to optimize the routing of vehicles and reduce traffic congestion in urban areas', EAI endorsed transactions on energy web, 10.
34. Edeh, Chijioke George, Gloria Opoku Darkoh, Shobayo Ifeoluwanimi Praise, Julius Odemi Brown, Rufus Fidelis Ojuoluwa, Omotayo Christopher Afolabi, Waliu Temidayo Asamu, Ifeoluwa Odunayo Olofinsao, Nana Firdausi Hassan, and Akinsuyi Samson. 2026. 'A Machine Learning-Based Framework for Real-Time Environmental Health Risk Prediction and Spatial Air Quality Intelligence in Urban-Industrial Ecosystems', Asian Journal of Advanced Research and Reports, 20: 1-20.

35. El Kafrawy, Passent, Hanaa Fathi, Mohammed Qaraad, Ayda K Kelany, and Xumin Chen. 2021. 'An efficient SVM-based feature selection model for cancer classification using high-dimensional microarray data', IEEe Access, 9: 155353-69.
36. Engin, Zeynep, Jon Crowcroft, David Hand, and Philip Treleaven. 2025. 'The Algorithmic State Architecture (ASA): an integrated framework for AI-enabled government', arXiv preprint arXiv:2503.08725.
37. Fascista, Alessio. 2022. 'Toward integrated large-scale environmental monitoring using WSN/UAV/Crowdsensing: A review of applications, signal processing, and future perspectives', Sensors, 22: 1824.
38. Faye, Bilal, Hanane Azzag, Mustapha Lebbah, and Fangchen Feng. 2025. 'Context normalization: A new approach for the stability and improvement of neural network performance', Data & Knowledge Engineering, 155: 102371.
39. Ferreira, Paloma Mara de Lima, Adriano Rolim da Paz, and Juan Martín Bravo. 2020. 'Objective functions used as performance metrics for hydrological models: state-of-the-art and critical analysis', Rbrh, 25: e42.
40. Firoozi, Ali Akbar, and Ali Asghar Firoozi. 2025. "Impact of integrating artificial intelligence and the internet of things in urban system management." In.: Deep Science Publishing. https://doi. org/10.70593/978-93-49307-08-7_7.
41. Fu, Xiaoran, Jiahong Liu, Zhonggen Wang, Dong Wang, Weiwei Shao, Chao Mei, Jia Wang, and Yan-fang Sang. 2023. 'Quantifying and assessing the infiltration potential of green infrastructure in urban areas using a layered hydrological model', Journal of Hydrology, 618: 128626.
42. Fuller, Angela K, Daniel J Decker, Michael V Schiavone, and Ann B Forstchen. 2020. 'Ratcheting up rigor in wildlife management decision making', Wildlife Society Bulletin, 44: 29-41.
43. Ganapathi, Harsh, Suchita Awasthi, and Preethi Vasudevan. 2024. 'Wetlands as a nature-based solution for urban water management.' in, Nature-based Solutions for Circular Management of Urban Water (Springer).
44. Gettelman, Andrew, Alan J Geer, Richard M Forbes, Greg R Carmichael, Graham Feingold, Derek J Posselt, Graeme L Stephens, Susan C Van den Heever, Adam C Varble, and Paquita Zuidema. 2022. 'The future of Earth system prediction: Advances in model-data fusion', Science Advances, 8: eabn3488.
45. Ghazian, Nargol, and Christopher J Lortie. 2024. 'A Review of the Roots of Ecological Engineering and its Principles', Journal of Ecological Engineering, 25: 345-57.
46. Gong, Wenjing, Xinyue Ye, Keshu Wu, Suphanut Jamonnak, Wenyu Zhang, Yifan Yang, and Xiao Huang. 2025. 'Integrating spatiotemporal vision transformer into digital twins for high-resolution heat stress forecasting in campus environments', Journal of Planning Education and Research: 0739456X251391121.
47. Gulnerman, Ayse Giz, Himmet Karaman, Direnc Pekaslan, and Serdar Bilgi. 2020. 'Citizens' spatial footprint on Twitter—anomaly, trend and bias investigation in Istanbul', ISPRS International Journal of Geo-Information, 9: 222.
48. Hamdan, Ahmad, Kenneth Ifeanyi Ibekwe, Emmanuel Augustine Etukudoh, Aniekan Akpan Umoh, and Valentine Ikenna Ilojianya. 2024. 'AI and machine learning in climate change research: A review of predictive models and environmental impact', World Journal of Advanced Research and Reviews, 21: 1999-2008.
49. Hamza, Manar Ahmed, Hadil Shaiba, Radwa Marzouk, Ahmad Alhindi, Mashael M Asiri, Ishfaq Yaseen, Abdelwahed Motwakel, and Mohammed Rizwanullah. 2022. 'Big Data Analytics with Artificial Intelligence Enabled Environmental Air Pollution Monitoring Framework', Computers, Materials & Continua, 73.
50. Hao, Wei. 2026. 'Design of a Psychological Status Monitoring and Early Warning Platform for College Students Based on Deep Learning Models', Journal of Computing & Biomedical Informatics, 10.
51. He, Jian, Limin Zhang, Te Xiao, Haojie Wang, and Hongyu Luo. 2023. 'Deep learning enables super-resolution hydrodynamic flooding process modeling under spatiotemporally varying rainstorms', Water Research, 239: 120057.
52. Hu, Rongyao, Xiaofeng Zhu, Yonghua Zhu, and Jiangzhang Gan. 2020. 'Robust SVM with adaptive graph learning', World Wide Web, 23: 1945-68.
53. Ibrahim, Muhammad, Aidi Huo, Waheed Ullah, Safi Ullah, and Zhao Xuantao. 2025. 'An integrated approach to flood risk assessment using multi-criteria decision analysis and geographic information system. A case study from a flood-prone region of Pakistan', Frontiers in Environmental Science, 12: 1476761.
54. Jadhav, Sachin, M Durairaj, R Reenadevi, R Subbulakshmi, Vaishali Gupta, and Janjhyam Venkata Naga Ramesh. 2024. 'Spatiotemporal data fusion and deep learning for remote sensing-based sustainable urban planning', International Journal of System Assurance Engineering and Management: 1-9.
55. Jafari, Mina, Abdollah Kavousi-Fard, Tao Chen, and Mazaher Karimi. 2023. 'A review on digital twin technology in smart grid, transportation system and smart city: Challenges and future', IEEe Access, 11: 17471-84.
56. Jang, Bong-Joo, and Intaek Jung. 2023. 'Development of high-precision urban flood-monitoring technology for sustainable smart cities', Sensors, 23: 9167.
57. Jin, Jiong, Zhibo Pang, Jonathan Kua, Quanyan Zhu, Karl H Johansson, Nikolaj Marchenko, and Dave Cavalcanti. 2025. 'Cloud-fog automation: The new paradigm towards autonomous industrial cyber-physical systems', IEEE Journal on Selected Areas in Communications.

58. Kaker, Sobia Ahmad, and Nausheen H Anwar. 2024. 'From one flooding crisis to the next: Negotiating 'the maybe'in unequal Karachi', The Geographical Journal, 190: e12498.
59. Khan, Asad, and Saima Qutab. 2016. 'Understanding research students' behavioural intention in the adoption of digital libraries: A Pakistani perspective', Library Review, 65: 295-319.
60. Koroteev, Mikhail V. 2021. 'BERT: a review of applications in natural language processing and understanding', arXiv preprint arXiv:2103.11943.
61. Lan, Ping, Liguo Yao, Yao Lu, and Taihua Zhang. 2025. 'A Multi-Task Causal Knowledge Fault Diagnosis Method for PMSM-ITSF Based on Meta-Learning', Sensors, 25: 1271.
62. Larson, Danelle M, Wako Bungula, Amber Lee, Alaina Stockdill, Casey McKean, Frederick" Forrest" Miller, Killian Davis, Richard A Erickson, and Enrika Hlavacek. 2023. 'Reconstructing missing data by comparing interpolation techniques: applications for long-term water quality data', Limnology and Oceanography: Methods, 21: 435-49.
63. Lawu, BL, F Lim, A Susilo, and N Surantha. 2021. "Social media data crowdsourcing as a new stream for environmental planning & monitoring: A review." In IOP Conference Series: Earth and Environmental Science, 012013. IOP Publishing.
64. Le, Tu Dam Ngoc. 2020. 'Climate change adaptation in coastal cities of developing countries: characterizing types of vulnerability and adaptation options', Mitigation and Adaptation Strategies for Global Change, 25: 739-61.
65. Lei, Ge, Ronan Docherty, and Samuel J Cooper. 2024. 'Materials science in the era of large language models: a perspective', Digital Discovery, 3: 1257-72.
66. Li, Bangyu, and Yang Qian. 2024. 'Weather prediction using CNN-LSTM for time series analysis: A case study on Delhi temperature data', arXiv preprint arXiv:2409.09414.
67. Li, Fei, Tan Yigitcanlar, Madhav Nepal, Kien Nguyen Thanh, and Fatih Dur. 2024. 'A novel urban heat vulnerability analysis: Integrating machine learning and remote sensing for enhanced insights', Remote Sensing, 16: 3032.
68. Li, Wei, Amin Kiaghadi, and Clint Dawson. 2021. 'High temporal resolution rainfall–runoff modeling using long-short-term-memory (LSTM) networks', Neural Computing and Applications, 33: 1261-78.
69. Li, Yajing, Zhijian Wang, Feng Li, Yanfeng Li, Xiaohong Zhang, Hui Shi, Lei Dong, and Weibo Ren. 2024. 'An ensembled remaining useful life prediction method with data fusion and stage division', Reliability Engineering & System Safety, 242: 109804.
70. Lin, Haoqiu, and Xun Li. 2025. 'The role of urban green spaces in mitigating the urban heat island effect: A systematic review from the perspective of types and mechanisms', Sustainability, 17: 6132.
71. Liu, Wen, Qi Feng, Ravinesh C Deo, Lei Yao, and Wei Wei. 2020. 'Experimental study on the rainfall-runoff responses of typical urban surfaces and two green infrastructures using scale-based models', Environmental management, 66: 683-93.
72. Ma, Wenjuan, Zhaowu Yu, Wenjun Yang, Yujia Zhang, Yuxia Hu, Jinyu Hu, Huiwen Zhang, and Gaoyuan Yang. 2025. 'Optimizing Vegetation and Building Configurations for Streetscape Heat Mitigation: A Multi-Scale Analysis under Extreme Heat', Building and Environment, 283: 113331.
73. Mazzetto, Silvia. 2024. 'A review of urban digital twins integration, challenges, and future directions in smart city development', Sustainability, 16: 8337.
74. Meng, Tong, Xuyang Jing, Zheng Yan, and Witold Pedrycz. 2020. 'A survey on machine learning for data fusion', Information Fusion, 57: 115-29.
75. Mickovski, Slobodan B, Alejandro Gonzalez-Ollauri, Craig Thomson, Caroline Gallagher, and Guillermo Tardio. 2022. 'Assessment of the sustainability performance of eco-engineering measures in the Mediterranean region', Land, 11: 533.
76. Moazzem, Shamima, Muhammed Bhuiyan, Shobha Muthukumaran, Jill Fagan, and Veeriah Jegatheesan. 2024. 'A critical review of nature-based systems (NbS) to treat stormwater in response to climate change and urbanization', Current Pollution Reports, 10: 286-311.
77. Molenaar, Annika, Dickson Lukose, Linda Brennan, Eva L Jenkins, and Tracy A McCaffrey. 2024. 'Using natural language processing to explore social media opinions on food security: sentiment analysis and topic modeling study', Journal of Medical Internet Research, 26: e47826.
78. Mutambik, Ibrahim. 2024. 'Assessing Urban Vulnerability to Emergencies: A Spatiotemporal Approach Using K-Means Clustering', Land, 13: 1744.
79. Natel de Moura, Carolina, Jan Seibert, and Daniel Henrique Marco Detzel. 2022. 'Evaluating the long short-term memory (LSTM) network for discharge prediction under changing climate conditions', Hydrology Research, 53: 657-67.
80. Natta, Prasanna Kumar. 2024. 'Closed-loop AI frameworks for real-time decision intelligence in enterprise environments', International Journal of Humanities and Information Technology, 6: 31-49.
81. Ncube, Mthokozisi Masumbika, and Patrick Ngulube. 2024. 'Enhancing environmental decision-making: a systematic review of data analytics applications in monitoring and management', Discover Sustainability, 5: 290.

82. OJADI, JESSICA OBIANUJU, EKENE CYNTHIA ONUKWULU, CHINEKWU SOMTOCHUKWU, and OLUMIDE AKINDELE OWULADE ODIONU. 2023. 'Natural Language Processing for Climate Change Policy Analysis and Public Sentiment Prediction: A Data-Driven Approach to Sustainable Decision-Making', Iconic Research and Engineering Journals, 7: 732-51.
83. Ouma, Yashon O, Rodrick Cheruyot, and Alice N Wachera. 2022. 'Rainfall and runoff time-series trend analysis using LSTM recurrent neural network and wavelet neural network with satellite-based meteorological data: case study of Nzoia hydrologic basin', Complex & Intelligent Systems, 8: 213-36.
84. Pal, Amitangshu, Junbo Wang, Yilang Wu, Krishna Kant, Zhi Liu, and Kento Sato. 2022. 'Social media driven big data analysis for disaster situation awareness: A tutorial', IEEE Transactions on Big Data, 9: 1-21.
85. Pandey, Bhanu, and Annesha Ghosh. 2023. 'Urban ecosystem services and climate change: a dynamic interplay', Frontiers in Sustainable Cities, 5: 1281430.
86. Patidar, Nandkishore, Sejal Mishra, Rahul Jain, Dhiren Prajapati, Amit Solanki, Rajul Suthar, Kavindra Patel, and Hiral Patel. 2024. 'Transparency in AI decision making: A survey of explainable AI methods and applications', Advances of Robotic Technology, 2.
87. Pigliautile, Ilaria, Sara Casaccia, Nicole Morresi, Marco Arnesano, Anna Laura Pisello, and Gian Marco Revel. 2020. 'Assessing occupants' personal attributes in relation to human perception of environmental comfort: Measurement procedure and data analysis', Building and Environment, 177: 106901.
88. Prasath, C Arun. 2025. 'Big Data-Driven Decision Support System for Urban Climate Adaptation Strategies', Journal of Smart Infrastructure and Environmental Sustainability, 2: 65-71.
89. Preti, Federico, Vittoria Capobianco, and Paola Sangalli. 2022. 'Soil and Water Bioengineering (SWB) is and has always been a nature-based solution (NBS): a reasoned comparison of terms and definitions', Ecological Engineering, 181: 106687.
90. Pursnani, Vinay, Yusuf Sermet, Musa Kurt, and Ibrahim Demir. 2023. 'Performance of ChatGPT on the US fundamentals of engineering exam: Comprehensive assessment of proficiency and potential implications for professional environmental engineering practice', Computers and Education: Artificial Intelligence, 5: 100183.
91. Rahman, Md Bayazid, Joy Dhon Chakma, Abdul Momin, Shahidul Islam, Md Ashraf Uddin, Md Aminul Islam, and Sunil Aryal. 2023. 'Smart Crop cultivation system using automated agriculture monitoring environment in the context of Bangladesh agriculture', Sensors, 23: 8472.
92. Rashid, Md Tahmid, and Dong Wang. 2021. 'CovidSens: a vision on reliable social sensing for COVID-19', Artificial intelligence review, 54: 1-25.
93. Rauch, HP, M Von Der Thannen, P Raymond, E Mira, and André Evette. 2022. 'Ecological challenges* for the use of soil and water bioengineering techniques in river and coastal engineering projects', Ecological Engineering, 176: 106539.
94. Richardson, Nicholas, A Manikyala, PK Gade, ABM Asadullah, and HP Kommineni. 2021. 'Emergency response planning: leveraging machine learning for real-time decision-making', Emergency, 4: 14.
95. Rosser, Julian F, Didier G Leibovici, and Margaret J Jackson. 2017. 'Rapid flood inundation mapping using social media, remote sensing and topographic data', Natural Hazards, 87: 103-20.
96. Rubbens, Peter, Stephanie Brodie, Tristan Cordier, Diogo Destro Barcellos, Paul Devos, Jose A Fernandes-Salvador, Jennifer I Fincham, Alessandra Gomes, Nils Olav Handegard, and Kerry Howell. 2023. 'Machine learning in marine ecology: an overview of techniques and applications', ICES Journal of Marine Science, 80: 1829-53.
97. Sabzipour, Behmard, Richard Arsenault, Magali Troin, Jean-Luc Martel, François Brissette, Frédéric Brunet, and Juliane Mai. 2023. 'Comparing a long short-term memory (LSTM) neural network with a physically-based hydrological model for streamflow forecasting over a Canadian catchment', Journal of Hydrology, 627: 130380.
98. Sarker, Md Nazirul Islam, Yang Peng, Cheng Yiran, and Roger C Shouse. 2020. 'Disaster resilience through big data: Way to environmental sustainability', International Journal of Disaster Risk Reduction, 51: 101769.
99. Shi, Kaize, Xueping Peng, Hao Lu, Yifan Zhu, and Zhendong Niu. 2022. 'Application of social sensors in natural disasters emergency management: A review', IEEE Transactions on Computational Social Systems, 10: 3143-58.
100. Shroff, Disha Nilesh, and Aditya Tejas Joshi. 2022. 'Pre-Fabricated Architecture for Urban Adaptability: Factory Built Constructions–Sustainable & Flexible Urban Solutions', Politecnico di Torino.
101. Soltani, Samira Sadat, Alexandre Belleflamme, Klaus Goergen, and Stefan Kollet. 2026. 'Improving Real-Time flood forecasting: probabilistic validation of assimilated Remotely-Sensed soil moisture data', Earth Systems and Environment, 10: 1961-86.
102. Sv, Praveen, Jose Manuel Lorenz, Rajesh Ittamalla, Kuldeep Dhama, Chiranjib Chakraborty, Daruri Venkata Srinivas Kumar, and Thivyaa Mohan. 2022. 'Twitter-based sentiment analysis and topic modeling of social media posts using natural language processing, to understand people's perspectives regarding COVID-19 booster vaccine shots in India: crucial to expanding vaccination coverage', Vaccines, 10: 1929.

103. Syed, Toqeer Ali, Muhammad Yasar Khan, Salman Jan, Sami Albouq, Saad Said Alqahtany, and Muhammad Tayyab Naqash. 2024. 'Integrating digital twins and artificial intelligence multi-modal transformers into water resource management: overview and advanced predictive framework', AI, 5: 1977-2017.
104. Tang, Tao, and Guangmin Hu. 2020. 'Detecting and Tracking Significant Events for Individuals on Twitter by Monitoring the Evolution of Twitter Followership Networks', Information, 11: 450.
105. Tantalaki, Nicoleta, Stavros Souravlas, and Manos Roumeliotis. 2020. 'A review on big data real-time stream processing and its scheduling techniques', International Journal of Parallel, Emergent and Distributed Systems, 35: 571-601.
106. Tariq, Aqil, Hong Shu, Saima Siddiqui, Iqra Munir, Alireza Sharifi, Qingting Li, and Linlin Lu. 2022. 'Spatio-temporal analysis of forest fire events in the Margalla Hills, Islamabad, Pakistan using socio-economic and environmental variable data with machine learning methods', Journal of Forestry Research, 33: 183-94.
107. Tran, Khuong H, Massimo Menenti, and Li Jia. 2022. 'Surface water mapping and flood monitoring in the Mekong Delta using sentinel-1 SAR time series and Otsu threshold', Remote Sensing, 14: 5721.
108. Trinh, Manh Xuan, and Frank Molkenthin. 2021. 'Flood hazard mapping for data-scarce and ungauged coastal river basins using advanced hydrodynamic models, high temporal-spatial resolution remote sensing precipitation data, and satellite imageries', Natural Hazards, 109: 441-69.
109. Van Hoang, Thanh. 2024. 'Impact of integrated artificial intelligence and internet of things technologies on smart city transformation', Journal of technical education science, 19: 64-73.
110. VP Singh, Harsh, and Qusay H Mahmoud. 2020. 'NLP-based approach for predicting HMI state sequences towards monitoring operator situational awareness', Sensors, 20: 3228.
111. Wang, Xiahui, Jinnan Wang, Bo Wang, Benjamin Burkhard, Lulu Che, Chao Dai, and Lijie Zheng. 2022. 'The nature-based ecological engineering paradigm: Symbiosis, coupling, and coordination', Engineering, 19: 14-21.
112. Wübbelmann, Thea, Kristian Förster, Laurens M Bouwer, Claudia Dworczyk, Steffen Bender, and Benjamin Burkhard. 2023. 'Urban flood regulating ecosystem services under climate change: how can Nature-based Solutions contribute?', Frontiers in Water, 5: 1081850.
113. Xiao, Ming, Lihua Chen, Haoxiong Feng, Zhigao Peng, and Qiong Long. 2024. 'Smart city public transportation route planning based on multi-objective optimization: A review', Archives of Computational Methods in Engineering, 31: 3351-75.
114. Xing, Xiaoyue, Bailang Yu, Chaogui Kang, Bo Huang, Jianya Gong, and Yu Liu. 2024. 'The synergy between remote sensing and social sensing in urban studies: Review and perspectives', IEEE Geoscience and Remote Sensing Magazine, 12: 108-37.
115. Yin, Junjun, Yizhao Gao, and Guangqing Chi. 2022. 'An evaluation of geo-located Twitter data for measuring human migration', International Journal of Geographical Information Science, 36: 1830-52.
116. Yohanandhan, Rajaa Vikhram, Rajvikram Madurai Elavarasan, Premkumar Manoharan, and Lucian Mihet-Popa. 2020. 'Cyber-physical power system (CPPS): A review on modeling, simulation, and analysis with cyber security applications', IEEe Access, 8: 151019-64.
117. Yousaf, Hira. 2024. 'AI for environmental sustainability: Applications in resource management and conservation', Journal of AI Range, 1: 13-26.
118. Yu, Danlin. 2025. 'Toward integrated urban observatories: synthesizing remote and social sensing in urban science', Remote Sensing, 17: 2041.
119. Yuan, Haojun, Mo Wang, Dongqing Zhang, Rana Muhammad Adnan Ikram, Jin Su, Shiqi Zhou, Yuankai Wang, Jianjun Li, and Qifei Zhang. 2024. 'Data-driven urban configuration optimization: An XGBoost-based approach for mitigating flood susceptibility and enhancing economic contribution', Ecological Indicators, 166: 112247.
120. Zhang, Xin, Wen Liu, Qi Feng, and Jianjun Zeng. 2024. 'Multi-objective optimization of the spatial layout of green infrastructures with cost-effectiveness analysis under climate change scenarios', Science of the Total Environment, 948: 174851.
121. Zhao, Xinfeng, Hongyan Wang, Mingyu Bai, Yingjie Xu, Shengwen Dong, Hui Rao, and Wuyi Ming. 2024. 'A comprehensive review of methods for hydrological forecasting based on deep learning', Water, 16: 1407.
122. Zhou, Hao, Jing Tang, Stefan Olin, Renkui Guo, and Paul A Miller. 'An Integrated Approach for Optimizing Streamflow Prediction in Mid-High Latitude Catchments by Employing Terrestrial Ecosystem Modelling and Interpretable Machine Learning', Available at SSRN 5042442.
123. Zong, Zhijuan, and Yu Guan. 2025. 'AI-driven intelligent data analytics and predictive analysis in Industry 4.0: Transforming knowledge, innovation, and efficiency', Journal of the knowledge economy, 16: 864-903.

Journal of Computational and Experimental Science (JCES)
ISSN Print: XXXX | ISSN Online: XXXX
Volume 1, Number 1, 2026, Pages 47–75
Journal Home Page: https://journals.airsd.org/index.php/jces

Review

Metal-Organic Frameworks: Synthesis, Adsorption, and Catalytic Applications

Asif Manzoor[1], Kashif Ali[2], Umar Sohail Shoukat[1], Mudassar Maqsood[1],Iqra Naheed[1], Muhammad Adnan Iqbal[3*]

[1] Department of Applied Chemistry, Xi'an Jiaotong University, Xi'an, China
[2] Department of Chemistry, Minhaj University, Lahore, Pakistan
[3] Department of Chemistry, University of Agriculture Faisalabad, Faisalabad, Pakistan
Email: adnan.iqbal@uaf.edu.pk

ARTICLE INFO

Article History:
Received: April 27, 2026
Revised: May 07, 2026
Accepted: May 21, 2026
Available Online: June 04, 2026

Keywords:
MOF, Catalysis, Organo ligand, Adsorption site and Applications

Corresponding Author:
Muhammad Adnan Iqbal
Email:
adnan.iqbal@uaf.edu.pk

ABSTRACT

Metal-organic frameworks (MOFs) are a class of crystals materials with pores that self-organize into a spatially organized network structure. They are made up of metal-containing nodes joined by an organic ligand network. MOFs offer three primary benefits The framework's adsorption areas and metal ion transportation are made better by their very porous framework and very high specific surface area. (2) The functional characteristics of the sites of adsorption can be changed by regulating the interaction between them and the metal ions. (3) MOFs may be generated on a wide scale because to their comparatively straightforward preparation method, and they maintain their stability under challenging circumstances. The current structural forms of MOFs (powder and membrane-like structures) and their production techniques, including mechanochemical, primary, and secondary growth processes, are initially outlined in this review article. Recent advancements in the enrichment of different metal ions, adsorption, analytical identification, and other catalytic uses of MOFs are then highlighted. A comprehensive description of the polymerization by radicals of methyl methacrylate (MMA) using microwave assisting agents and MOFs as catalysts is also given. The catalyst conditions, such as the number of MOFs-907, co-initiators and organic solvents, and polymerization time, should be carefully considered in this process. Future research directions and technological issues pertaining to MOFs materials that need to be resolved are also covered. A thorough grasp of metal-organic frameworks is the goal of this review. Because of its large porosity and active metal sites, MOFs are excellent for sophisticated adsorption and catalytic processes.

Introduction

In addition to being prevalent in nature, metal ions constitute vital trace substances for human health and survival. For example, iron ions take part in oxygen transport in the human body, ions of copper are engaged in the expression of genes and enzyme reactions [1], and ions of zinc are linked in human growth, development, and metabolism [2] while iron ions are associated with the transportation of oxygen in the human body [1]. Because of their widespread distribution, various forms, insolubility, poisonous consequences, and other characteristics, heavy metal ion pollution has become a global issue. Heavy metal ions, such as Pb, Cd, Hg, As, and Cr, are found in soil, air, and water in a range of numerous forms. The

digestive, immunological, neurological, and reproductive systems are all permanently harmed by these ions once they enter the human body through direct contact or the food chain [3].

Therefore, it is necessary to detect metal ions in food and the environment analytically and to use enrichment-based adsorption. The traditional techniques for eliminating metal ions over the past 10 years have included chemical precipitation, ion exchange, membrane filtering, and adsorption [4]. Adsorption is widely recognized as one of the finest techniques for finding and eliminating metal ions since it may eliminate many compounds concurrently as well as requires less experimental conditions. Conventional absorbent materials, such as carbon materials, zeolites, graphene, molecularly imprinted polymers, porous silicone materials, etc., still have certain disadvantages, nevertheless, such difficult framework modification, poor control, and restricted synthesis conditions. These issues continue to limit the utilization of these materials [3] The spatially network framework of conventional metal-organic frameworks (MOFs), which are crystalline porous compounds in which the ligands act as a bridge, is created spontaneously by the combination of inorganic metal-containing nodes and organic ligands [5]. Because of the specific coordination structural unit between the metal ion and the organic ligand, they are preferred to mesoporous materials with only organic ligands, such as covalent organic frameworks (COFs) and porous organic cages (POCs) [6]. This new type of porous material is intriguing due to its huge specific surface area, customizable microporosity, low framework density, and numerous applications. Among its numerous uses are ion adsorption, drug delivery, gas storage, and chemical separation [7] . The term "MOFs" was originally used in 2005 by Yaghi's research team. MOFs have a lot of potential as metal ion adsorbents because of their well-organized porous structure and adjustable physical and chemical characteristics, and their practical uses are very promising [8].

MOFs have three main advantages as adsorbents:

(1) Because of their very porous structure and extremely high specific surface area, adsorption sites and metal ions can be readily distributed throughout the framework. (2) Functional control is the ability to regulate the interaction between the metal ions and adsorption sites. Furthermore, MOFs may be generated on a massive scale due to their straightforward synthesis procedure, and they exhibit exceptional stability even in complicated settings [9]. The extraordinarily large surface area of porous membranes a highly desirable characteristic for the adsorption process is a significant benefit of adsorption by these membranes over traditional powder materials. Currently, the surface area of different porous membranes ranges from 1000 to 10,000 square meters per gram, which is significantly larger than the surface areas of zeolite and carbon [10]. The quick development of membrane-based technology for adsorption is dependent on the establishment and design of novel substrate materials. Despite being successfully used in organic dehydration and material adsorption, developed inorganic membrane materials like zeolite and ceramic membranes have limitations such weak membrane structure and low mechanical strength [11]. Because of this, composite membranes made of polymers and porous materials have been created. Nevertheless, regardless of the membrane's improved mechanical properties, the compatibility of the fillers as well as the polymeric material decreases its thermal and chemical resilience [12]. The idea of MOFs films/membranes was put forth by Caro's research team in 2005, and since then, membrane scientists have studied it extensively. Substrate-MOF-based composite based membrane materials have a higher affinity than conventional nanostructured porous materials. They do not create non-selective voids that are typical, and can preferentially separate or adsorb molecules with many different molecular weights by varying their dimensions of pore size [13]. major research has been carried out on MOF-5, HKUST-1, IRMOF, ZIF, and MIL membranes, and recent years have seen an important improvement in membrane-based MOF adsorption and separating technologies d [14]. Evolution of MOFs is depicted in Figure 1. From two-dimensional in nature (2D) to three-dimensional (3D) and even multiple-dimensional morphology, including permanently open-pore designs, the topological framework of MOFs membranes has expanded [15].

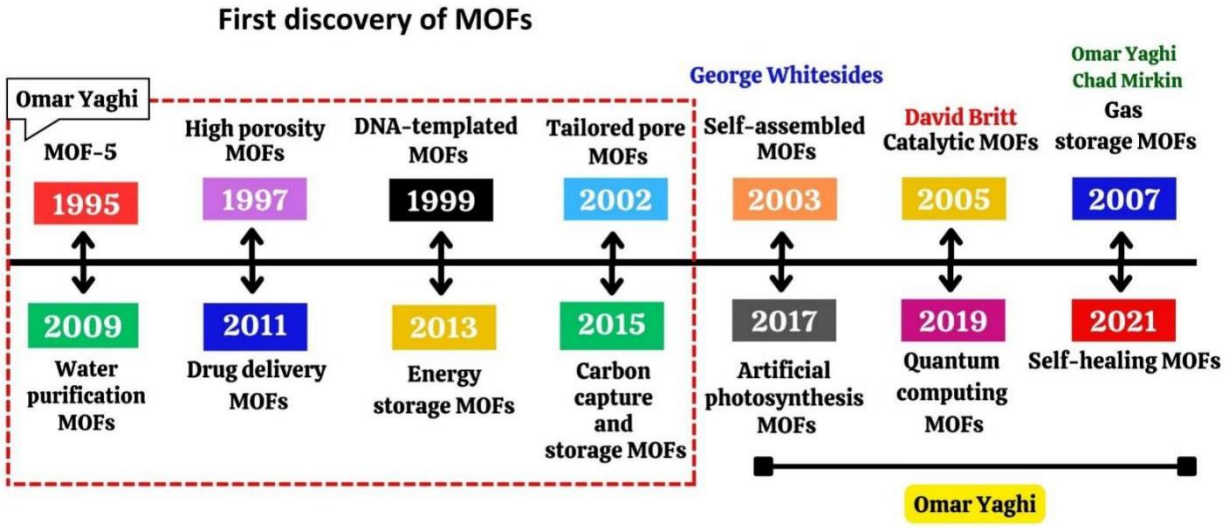

Fig 1: Historical background of MOFs

MOF membranes are incredibly versatile and modular. The trend of research articles published over the past ten years on MOFs in the area of conventional ion adsorption is shown in Figure 2. Numerous studies have demonstrated the exceptional adsorption properties of MOFs for environmental pollution, agricultural protection, and analytical testing [16]. A great deal of the research on metal ion adsorption, which is still in its early phases, has focused on the development of synthetic methods for MOFs and their use as adsorbents for the enrichment of heavy metal ions [17]. The present structural forms of MOFs materials (powder and membrane-like structures) and their preparation techniques, including mechanochemical, primary, and secondary growth processes, are first summarized in this review. The development of MOFs in adsorption, analytical detection, and other catalytic applications based on the enrichment of different kinds of metal ions is then highlighted. Lastly, a detailed discussion of the microwave synthesis process for methyl methacrylate radical polymerization is provided. Simultaneously, future research paths are considered and the technical obstacles associated with MOFs materials that must be overcome are highlighted. This review offers thorough and specific information regarding MOFs.

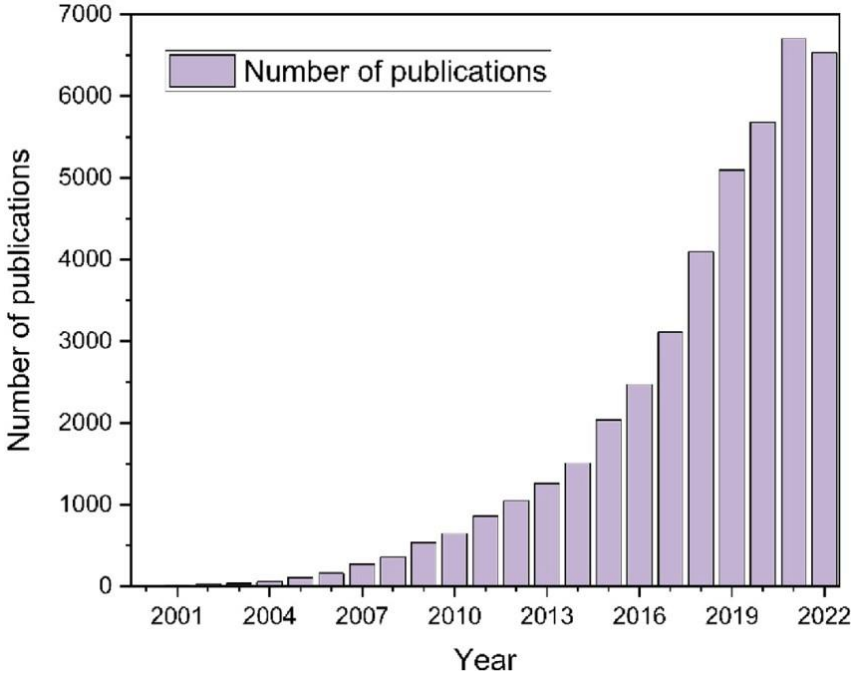

Fig 2: Growth trend of published articles on MOFs for metal ion adsorption is Adapted from Ref. [22] with permission of Journal of materials chemistry. A, Materials for energy and sustainability Copyright 2018.

1. MOF Synthesis:

Using aqueous and/or solvents made of organic matter as carrier materials, either hydrothermal or solvent heating techniques are typically used to create MOFs materials. The reaction temperature ranges from 37 to 200 degrees Celsius, and the reaction takes from hours to days [5]. MOFs powders and MOFs membranes are both of the main fields into which MOFs materials can be divided based on their physical and structural features. As a result, innovative synthesis methods have also been developed [18]. Powder-based MOFs materials have been successfully developed and manufactured using conventional synthetic methods including the hydro thermal method and the solvo thermal approach. Other synthesis methods, such as solvent-free methods like mechanochemical methods, have also improved significantly [19]. In addition to lowering the number of solvents used, solvent-free synthesis techniques also lower contamination and impurities in the crystals, making them highly promising from an economic and environmental standpoint [17]. When synthesizing pure MOFs membranes and MOF-based composite components, the stability of MOFs materials must be considered alongside the problem of dense polycrystalline layer formation on carriers [7]. While the number of research articles on in-situ and secondary growth methods has also increased in recent years, research based on interfacial synthesis and liquid phase epitaxy developed substantially, as shown in Figure 3. Naturally, the many states of MOFs have a direct or indirect impact on the physical and chemical properties of the materials themselves, such as mechanical strength, porous structure, and hydrophobicity [20]. Therefore, alternative synthesis methods are needed to create powder and membrane-based metal organic frame works.

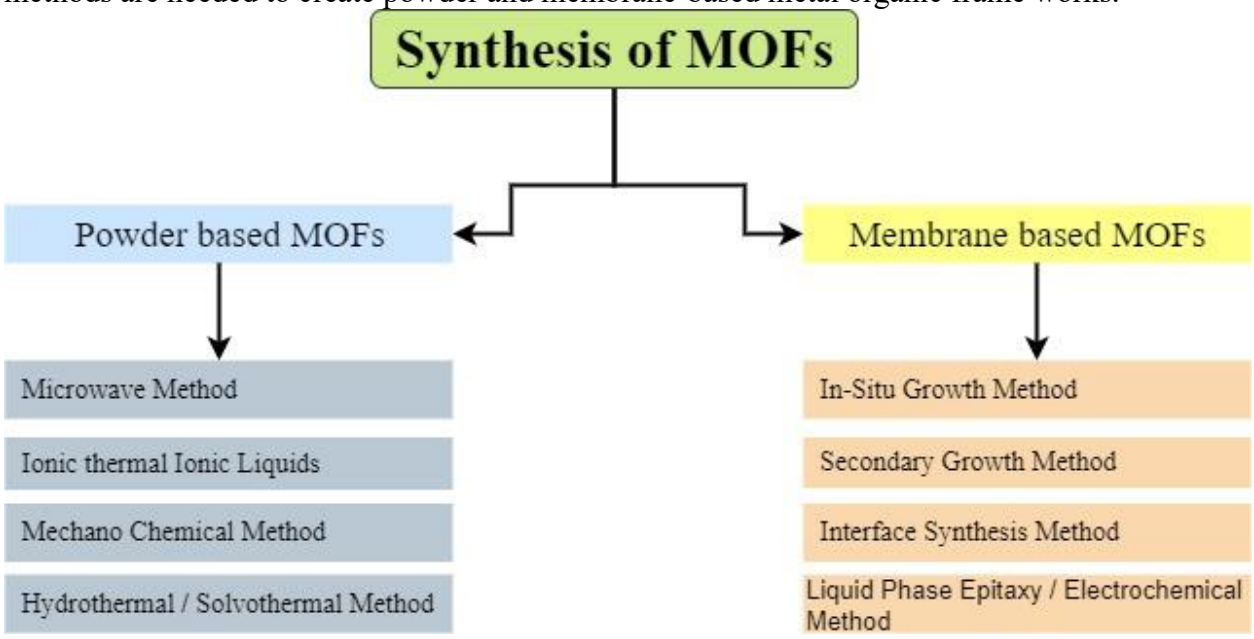

Fig 3: Different Synthetic metal organic frameworks approaches

1.1. Method for Making Powdered-Based MOFs

Two essential elements functional sites and organic ligands have a major impact on the design and production of MOFs powder materials. The choice of suitable organic ligands affects the structure and functional characteristics of metal organic frameworks [21]. The topological structure of MOFs is typically formed by the functional monomers that make up MOFs, and their structural benefits are crucial in attaining their spatial variety. As seen in Figure 4, common topological configurations are categorized into several network topologies, including squares, triangles, and lozenges. The type of donor atom,

coordination mode, stiffness or flexibility, functional groups, substituents, and geometric structure of the organic ligands all have a major impact on the structure of metal organic frame works [22]. MOFs with functional properties can be modified to provide the necessary stability, selectivity, and variety in addition to providing unique air structures [23]. To enable actual and gradual change of powdered-based MOFs, approaches for carefully adjusting the size, shape, and stability of the pores as well as introducing several functional groups inside the pores have been devised [16]. These precise management is necessary for the materials to function better and more efficiently. Therefore, we enthusiastically endorse the design approach that makes use of the architectural space structure, commonly referred to as the Secondary Building Unit (SBU), as the basic foundation. This method works well for preparing various MOFs for various uses, in addition to being appropriate for the synthesis of a particular MOF [24]. Additionally, by selecting a separation material that matches the desired material in terms of preferential selectivity and has the proper pore size, shape, and functional features, the separation of ions can be effectively controlled.

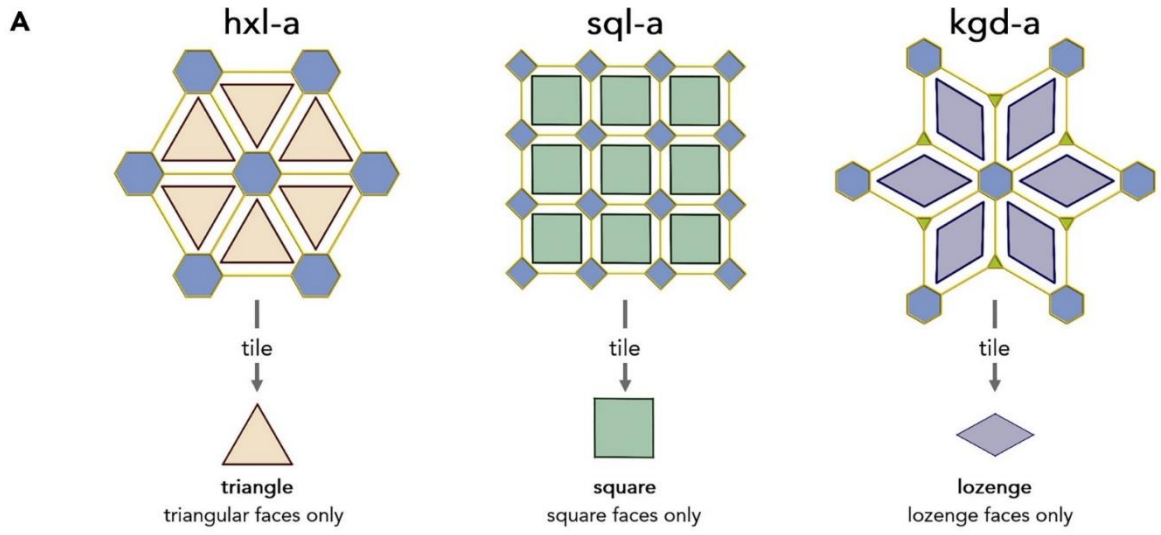

Fig: 4. (A) Common topologies of MOFs. (A) 2D hxl, sql and kgd topologies and their respective triangle, square and lozenge faces (windows for porous structures) is reproduced from Ref. [47] with permission from Communication Chemistry, Copyright 2018.

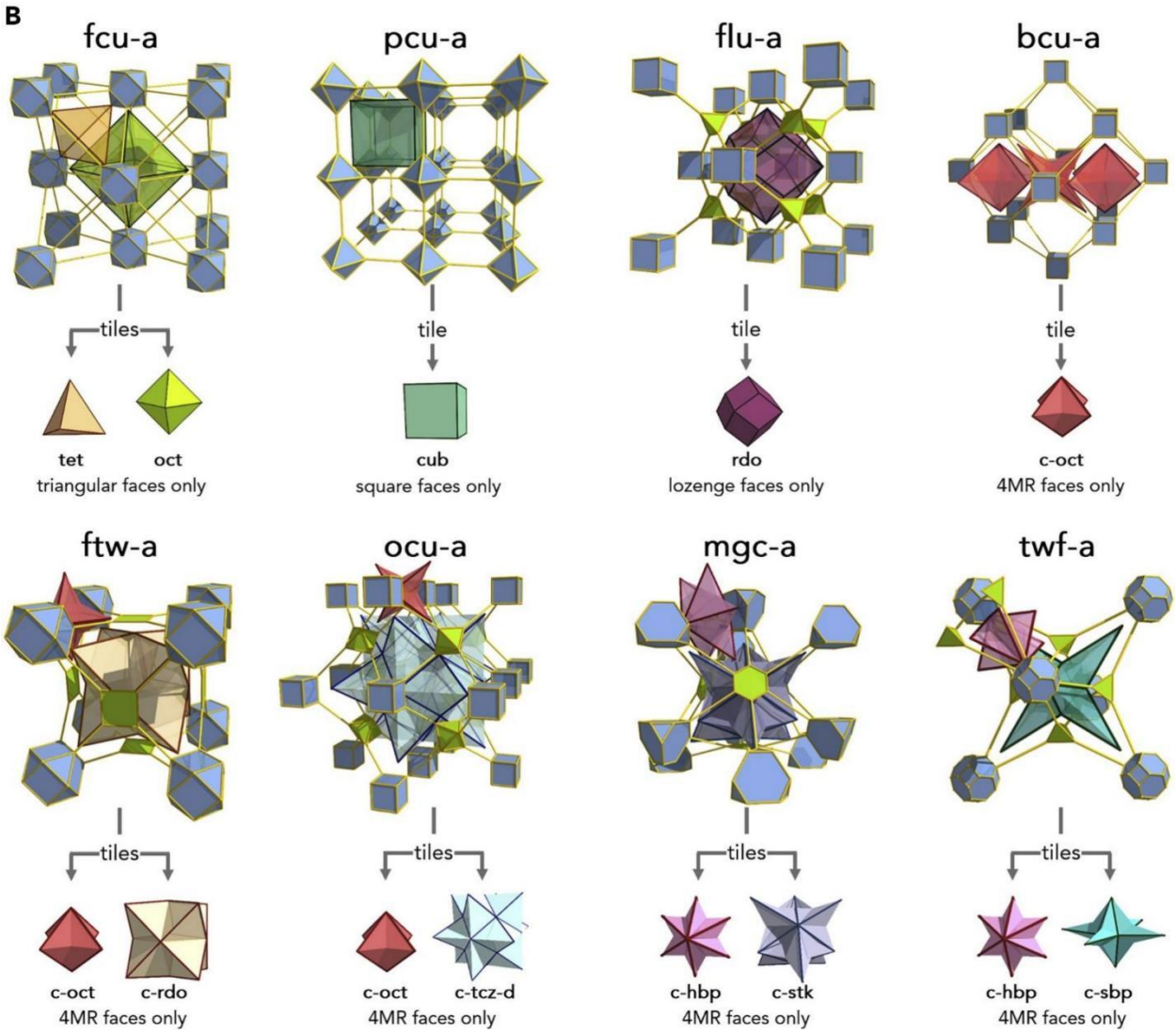

Fig 4:(B) 3D flu, pcu, flu, bcu, ftw, ocu, mgc and twf topologies and their respective tiles with triangle (fuc), square (pcu). Lozenge (flu) and a planer lozenege (bcu, ftw, ocu, mgc and twf) faces is reproduced from Ref. [47] with permission from Communication Chemistry, Copyright 2018.

1.2. Solvothermal /Hydrothermal approach

One common technique for creating the powder forms of porous materials is hydrothermal/solvothermal synthesis. Autoclave heat treatment in water or organic solvents can drastically change the hydrophilicity of the solvent and the polarity of metal salts and chemical ligands [25]. In addition to the fundamental reaction conditions such as the reaction volume, concentration, temperature, and duration a careful selection of chemical regulation is essential for hydrothermal and solvothermal processes [26]. Various kinds and amounts of modifiers may have different effects on crystallite size, in that the number of nucleation sites is a function of the competition that occurs with respect to metal-binding sites. Due to the rapid growth in this field, a number of pore-shaped composite components with stable chemical properties

and consistent design features have recently been developed by choosing chemical regulators with different characteristics [27]. The most important solvents utilized in the synthesis of MOF involve a variety of proton donors with high and high degree of polarity, including ethanol, water, methanol, acetic acid, dimethyl sulfoxide, a *N,N*-dimethylformamide, acetonitrile, and acetone [28]. The hydrothermal/solvothermal approach was used in the early work of MOFs, but the use of organic solvents is expensive and results in excessive loss, the anions (such as nitrates and chlorides) have too many danger concerns, and other major issues arise [20]. The MOF nanostructures with unprecedent characteristics have fabricated disclosing a Zn-based catalyst as [Zn(H N-BDC) (4-bpdh)]·3DMF at Tarbiat Modares Univesity (TMU) through a salt Zn(NO) ·6HO with 2,4-hexadiene applying hydrothermal method. The successful synthesis of this catalyst was confirmed by the use of TGA, XRD, FTIR, Elemental microanal., ICP, BET and OES measurements. Through Michael addition of annular benzimidamid hydrochloride to the (3E,5E)-3,5-bis-(benzylidene)-4-piperidone reactive class with reusability and retrievability over successive 5 runs without appreciable change in efficiency, the produced catalytic agent TMU-16-NH functions as a prospective competitor to create a new type of pharmaceutically relevant 2,4-diphenylpyrido[4,3-d]pyrimidine scaffolds. Furthermore, such methodology is accompanied by the excellent results such as the broad substrate range, mild reaction conditions, fast reaction time and product yield [29]. The more flexible proline-functionalized piller layered MOF [Zn (2,6-ndc) (bpb-NHPro)] was integrated into the framework through solvothermal reaction between the Zn (NO) and 5-bis(4-pyridyl) benzene (bpb-NHPro), 2,6-naphthalenedicarboxylic acid (H ndc) in N,N-di-Et formamide (DEF) and 1-L-Pyrrolidine-2-carboxamide-2. The aldol addition reaction of 4-nitrobenzaldehyde and cyclopentanone was selected as model reaction to evaluate the progress of which showed the opposite diastereoselectivity, favouring the syn-adduct; obtained by the homogeneous catalysis with a high achievement of 98% yield and diaster eomeric excess, till 98:2 (syn:anti) [30]. A novel Zr-MOF catalyst has designed by solvothermal process and modified by using pyridine carboxaldehyde embedded with Cerium tested by BET, ICO, TGA, FE-SEM, EDX, FAR-IR and FTIR analysis for catalyst structure. For a variety of reasons, including maintaining all three Lewis acids as activation functions with Langmuir surface area of 501.63 m^2/g, pore size of 2.27 nm, and pore volume of 0.28 cm^3/g at ambient temperature, the results demonstrated 90% high efficiency and retrievability in deviantization of polyhydro quinoline in series of Michael addition and Knoevenagel condensation approaches of synthesized Ui O-66-Pyca-Ce (III) catalyst [31]. By coagulation of Cd ions in solvothermal process with two squaramide based ligands two different MOFs Cd(L1)(DMF) and Cd(L2) (dpe) have synthesized and tested by PXRD, single crystal XRD, TGA and IR for elemental analysis. The outcomes show sq-Cd-NOF-1 features an entirely new 3D structure along 1D narrow apertures while sq-Cd-MOF-2 has a novel ring-ring linking chain-base two

layered as 2D MOF structure with higher porosity, offering potential applications in heterogenous catalysis after derivatization by Micheal addition reactions [32].

1.3. Ionic Thermal Approach (Ionic liquid method)

Ionic fluids (ILs) are a novel family of eco-friendly solvents with several uses. Ionothermal synthesis is the process of directing the synthesis of solid structures using ILs as templates and solvents. Despite its obvious disadvantages, such as relatively harsh reaction conditions, high process energy consumption, and large consumption of organic solvents, the ionothermal synthesis method can largely avoid the competition between the solvent/template and the framework in the solvothermal preparation process. Additionally, ILs are still regarded as one of the best solvents for successfully preparing MOFs and may be recycled and reused [33]. Ionothermal synthesis was recently used to create five unique classic Keggin-type PMOFs. The resulting material (MIMA) has a unique mechanically interlocked molecular structure and is constructed from two-dimensional interpenetrating polyrotaxane layers with a characteristic ring-like form. Furthermore, a novel two-dimensional three-layer interpenetrating polyrotaxane host-guest network is shown. As a result, it would be a novel strategy for high-stability entangled two-dimensional hierarchical PMOF systems [34] .

1.4. Mechanochemical Approach

The mechanochemical approach involves uniformly stressing the material while simultaneously subjecting it to physical deformation and chemical reactions caused by mechanical stress, such as vibrating, rotating, and grinding [35] Initially, the frame material is destroyed by mechanical force, resulting in a fine powder that increases the material's degrees of crystalline structure and specific surface region [36]. Second, the particles coagulate due to the Van der Waals force. Finally, the material begins to crystallize, and a mechanical amplification reaction starts inside it as a result of particle agglomeration. The most attractive feature of the mechanochemical technique is that the material can be produced by grinding alone, eliminating the need for initiators, catalysts, or heat reactions [37]. However, there is still more research and discussion to be done on the produced nano-powders' homogeneity, dispersibility, high energy consumption, aggregation, and purity. According to a recent paper, airflow impingement (AFI) offers a novel alternative to conventional mechanochemical synthesis. For the first time, an innovative airflow impingement method was developed as a replacement to the conventional method for the mechanochemical synthesis of MOFs. The most important advantage of using the airflow impingement method technique is that MOFs can be synthesized without a solvent, in contrast to MOFs produced using

the conventional solvothermal process. MOFs also have good area of the surface and a typical pore size. Solvent-free conditions have emerged as a major trend in MOF synthesis due to the growing volume of research. According to Brekalo and colleagues, basic zinc carbonate is an adequate precursor used for the solvent-free mechanically induced synthesis of ZIF. The procedure can be quantitatively and continuously monitored by measuring the pressure changes in the grinding vessel during the process due to the atmospheric carbon dioxide released from the precursor, a substance which permits the large-scale, low-loss synthesis of ZIF-8 by adding excess ligands to prevent by-products [28]. Some malononitrile, aldehyde and acidic C-H compounds were employed in malononitrile-based multicomponent reactions on restorable nanocomposites loaded with Fe_3O_4 nanoparticles on MOF using an ecofriendly reactive approach by tandem Knoevenagel-Michael cyclocondensation approach [38].

1.5. Microwave Method

In the microwave approach, electromagnetic energy reacts with mobile charges in the solution, such as conventional polar solvents, ions of metal, and deprotonated organic ligands [39]. In order to fast create MOFs crystal powder from the beginning mixture, Seyedpour and colleagues (2019) employed microwave waves in the range of 423 to 493 K. The energy of radiation from microwaves aided in the MOFs' rapid growth. The reaction duration and concentration of the precursor have a major influence on the yield and crystallinity of the final product.

1.5.1. Microwave synthesis of Metal organic frameworks:

Three milliliters of DMF are used to dissolve the linear 2,6-naphthalene dicarboxylic acid (H_2NDC) and 1,3,5-triyl-tris (benzoic acid) (H_3BTB) linkers. DMF is added to the mixture of (H_3BTB) and (H_2NDC) after being combined with acetic acid that contains iron III nitrate monohydrate. This mixture is put down in a flask and then heated at 120 centigrade for 24h. When this time passes then Orange cubical shape crystals were obtained and accumulated by decantation. DMF is used to wash the resulting product to eliminate beginning reagents. MOF is soaked in dried acetone for 72 hours. After emptying at 90°C for 24 hours, a hundred milligrams energized sample (twenty one percent yield of Fe $(NO_3)_2$ was collected [40].

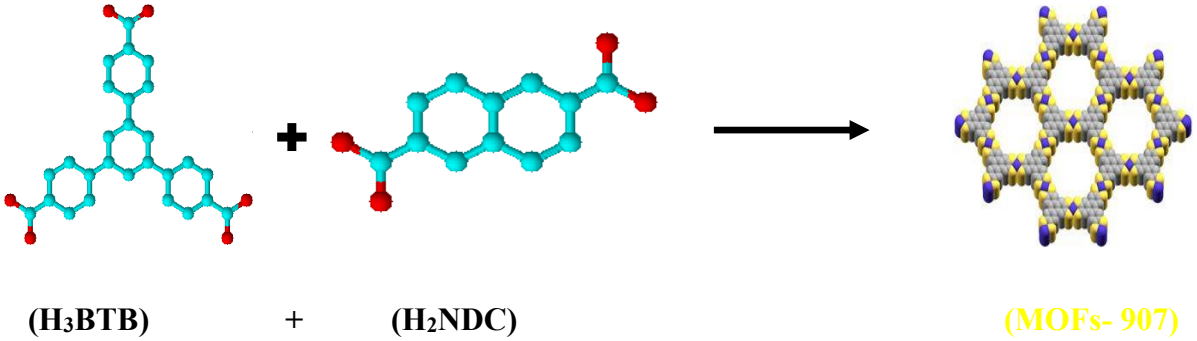

Fig 5: Microwave synthesis of MOFs is reproduced from Ref. [40] with permission from Elsevier, Copyright 2015.

1.6. Membrane based synthesis of Metal organic frameworks

Although full and flawless membranes are usually the aim of transmembrane-based MOF synthesis, the adsorption performance of composite membrane materials is usually influenced by the size, shape, and interactions of the ions with the membrane-based components. The substrate surface directly affects the nucleation and growth of MOFs membranes during the synthesis of membrane materials. In this case, it is challenging to create a uniform and dense MOFs membrane on the carrier's surface due to the lack of functional groups on the ligand to covalently bond with the substrate's surface hydroxyl group [41]. It is essential to use specific matrix synthesis or modification approaches to improve the heterogeneity nucleation locations in order to produce the optimum composite membrane structure [34]. A special kind of reagent Co-MOF-PDA-TA (MP-TA) have prepared using Tetra aniline and Dopamine in Micheal addition process that are compatible with waterborne epoxy, showed better passive film on the steel surface by characterization tools such as SEM, XRD and FTIR spectroscopy. The redox reaction between TA (reduced) and EB (oxidized) or LEB even by the involvement of 2 electrons that lead to generation of a passivation of coating, makes a great breakthrough to the potential application of MP-TA as a multirole additive [42].

1.7. The In-situ growth Approach

The in-situ growth approach entails submerging the substrate directly in a growth solution composed of ions of metal and a bonding agents in order to maintain the diffusion properties of the metal ions and connecting molecules [43]. The substrate is frequently changed with functional groups that interact with the metal ions in order to enhance the MOFs layer's ability to bind with the substrate. The MOFs layer is then formed by combining the bonding agent with the substrate. For instance, Wu and his collaborators created ZIF-8 membranes by treating pencil rods with IL in situ; these membranes were subsequently functionalized using PEG-NH_2 [44]. It can be seen that the ZIF-8/PEG-NH2 membrane had an increased

adsorption ability than the pristine ZIF-8 membranes while maintaining excellent stability and reusability. Yang and colleagues reported the rapid in-situ synthesis of Zn/Co-ZIF crystals on the fabric to produce a strong and dense MOFs membrane at room temperature [36] as shown in figure 6. When sodium carboxymethyl cellulose was added to the solution, the molecular sieve imidazole salt structure (Zn/Co-ZIF) crystals clung to each other on the surface because of the chemical impact of their surface, which stopped the solution phase crystals from clumping together. CMCMOF/cloth showed excellent selectivity and a good adsorption capacity (862.44 mg g^{1}) for Pb2þ.The CMC-MOF/cloth composites membrane can quickly absorb lead (Pb2þ) on filter devices, has strong removal efficiency, and may be reused in several regeneration cycles. Zhu and his team successfully produced a dopamine-modified MOFs composite membrane (prGO@cHKUST1) by employing the in-situ growth technique to generate a cubic structure with remarkable morphology and distinctive properties using Mg/Al layered double hydroxide as a modifier. Graphene oxide's (GO) interlayer spacing can be changed to fit in HKUST-1, increasing the membrane's hydrophilicity and flow [45]. Furthermore, the GO layer stacking can be altered by the intercalation effect of the MOFs and the reduction effect of polydopamine (PDA), leading to a large number of ambiguous pores and more active sites on the membrane's surface. In contrast to the prGO membrane and the original GO membrane, a modified membrane's permeation flux was ten and five times higher,respectively.

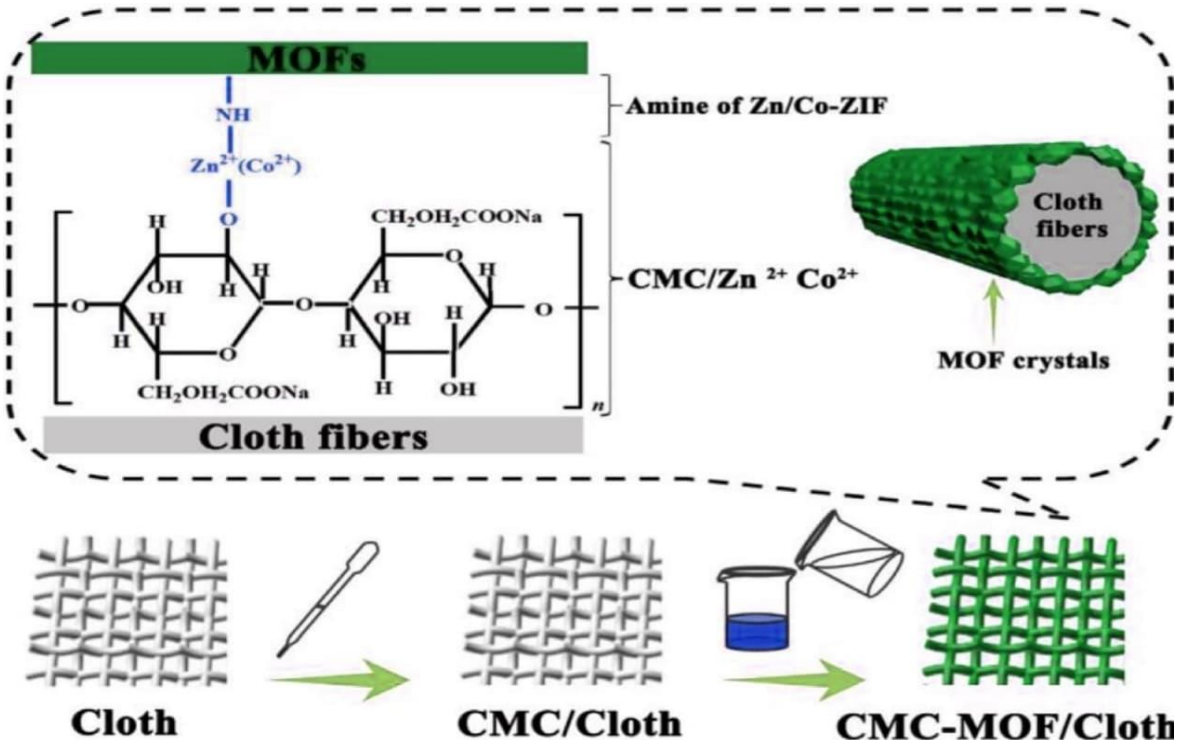

Fig:6. Schematic diagram of preparation of CMC/cloth and CMC-MOF/cloth composite membranes is reproduced from Ref. [43] with permission from American Chemical Society, Copyright 2018.

1.8. 2ndary growth Approach

Another name for the seed growth technique is the 2ndry growth approach. To create the MOFs layer, a seed layer is usually applied to the substrate, which is subsequently heated by a solvent in the mother liquor [46]. Seed layers can be generated using MOFs precursor and substrate in addition to being physically absorbed. Using the secondary growth approach, Yuan and his colleagues were able to create a complete MOFs (ZIF-300) on an Al_2O_3 base. As seen in Figure. 7 [47]. They then extracted heavy metal ions from waste water using the ZIF-300 film. With a water permeability of 39.2 L m^{-2} h^{-1} and a copper sulfate retention rate of 99.21%, the generated ZIF-300 film proved stable. One of the popular in-situ growth and 2ndry growth approaches can be used to produce almost all MOF films. However, these approaches have a number of drawbacks. Membrane formation is typically complicated by modification or seeding, a process which increases the availability of heterogeneous nucleation places onto the substrate's surface [40]. Additionally, MOFs crystals will precipitate in the solution as lumps due to the precursor's composition of metal ions and a connecting agent, wasting raw materials. Furthermore, the scaling up strategy is difficult [48].

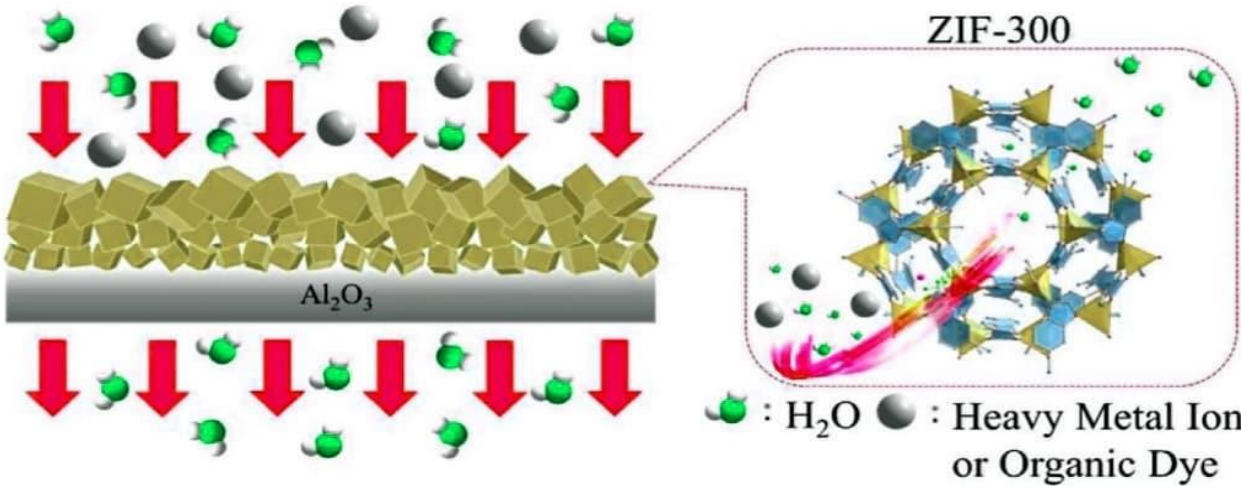

Fig 7: Schematic diagram of the process of removing heavy metal ions from water by the ZIF-300 membrane is reproduced from Ref. [47] with permission from Communication Chemistry, Copyright 2018.

1.9. Method of Interface synthesis

The two incompatible solvents, or the two solvents on either side of the substrate, are used to dissolve the ions of metal and the bonding agent used in the synthesis of the interface. During the formation of the MOFs membrane, the resulting molecules diffuse at the interface and in the opposite direction, and crystallization only occurs at the liquid-liquid interaction. It is advantageous to fill up the gaps, which are

principally formed at the defects, with the MOFs precursor at higher diffusion rates than the filled-up gaps, which are formed at the already formed MOFs, resulting in uniformly increased thickness of the membrane. In order to enhance the performance of an interfacial polymerized thin film nanocomposite (TFC) membrane, Li et al. added MOFs [49]. Zn2þ was added to the polymer solution during the synthesis to increase the permeability of the standard TFC membrane since the acids generated during the interfacial polymerization process will affect the membrane formation [43]. The MIL-101(Cr) MOF has been fabricated with terminal phosphate group MOF-supported nucleotides, which is irreversible binding of the ATP molecules, using XRD and DFT and NMR analysis showed Cr clusters at the ATP location interface with the terminal phosphate group in the Diels-Alder reaction, and in the Micheal addition reaction, had been shown Cr cluster sites that can serve as a new material for the Cu(II) occupancy systems as potential enantioselective heterogeneous agents. Although the straightforwardness of the concept of combining porous components into TFC membranes, all of the data demonstrated that TFC composite membranes outperformed ordinary membranes. This made it possible to successfully build continuous ZIF-8 films on microporous nylon with moderate separation performance. The interface synthesis method can minimize crystallization in the bulk solution and recover the reactants, producing a thin membrane with consistent thickness because the metal salt solution and the cross-linking agent solution are kept apart. Additionally, modular composite membranes can be directly designed using this highly scalable method. However, this approach has considerable limitations because only a few typical MOFs membranes, like ZIF-8 and ZIF-7 membranes, have been manufactured using it [50].

1.10. Liquid phase epitaxy Approach

In the liquid phase epitaxy approach, numerous metal ion and binder solutions are dissolved and then mixed together [40]. As shown in Fig. 8, Wang and colleagues [51] described a novel technique for producing MOF membranes using liquid phase epitaxy (LPE). Ten different MOF films can be rolled and loaded at the same time using their technology. Ten different MOF membranes can be rolled and loaded at the same time. Increased mechanical durability was a result of ultra-high molecular weight polyethylene interlaced MOF particles. The organic dyes exhibited a retention rate of up to 99% in cross-flow filtering mode with a water flux of 125.7Lh^{1}. Rapid solute adsorption happens through the porous MOFs, and rapid water penetration happens through the microscale channels between the MOF particles. High-performance surface adsorbers for essential separation processes can be produced using this approach. The liquid phase epitaxy approach produces MOFs with a discontinuous crystallization process, and the thickness of the MOFs layer may be accurately controlled by the number of cycles. The liquid phase epitaxy method is a

gentle, straightforward, and controllable preparation cycle. However, when producing the MOFs membrane, obtaining a continuous MOFs layer is difficult.

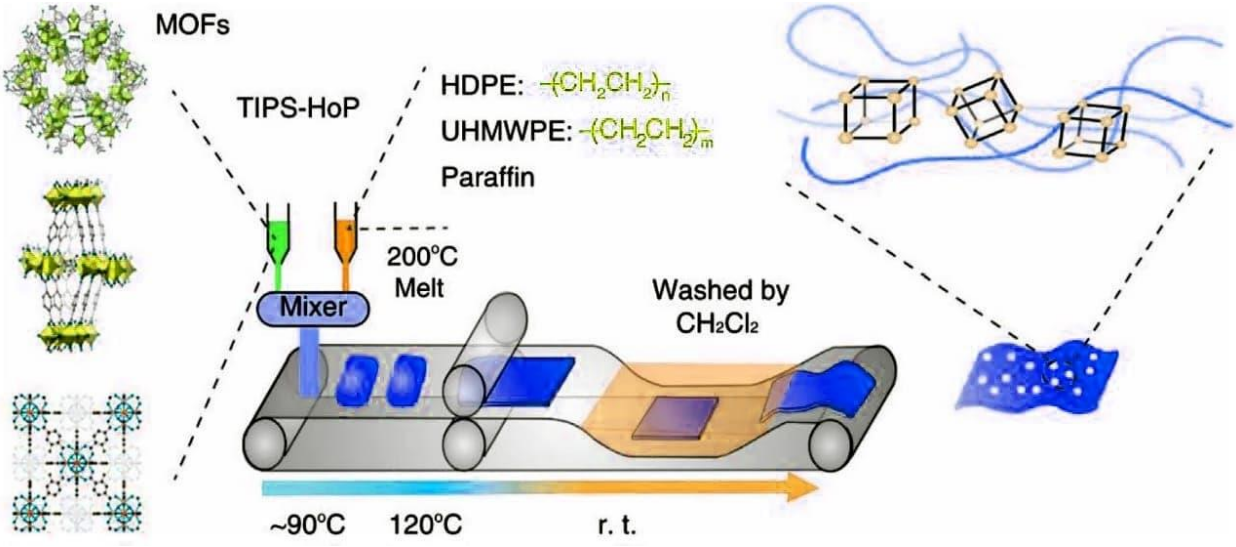

Fig. 8. Schematic diagram of the preparation process of MOF-PE-MMMs is reproduced from Ref. [40] with permission from Elsevier, Copyright 2015.

1.11. Electrochemical synthesis method

Electrode deposition is also known as electrochemical synthesis. The synthesis process is as follows. MOFs nucleate on the electrode surface at a critical concentration of the metal ions, and layered structures thereafter nucleate, grow, and form on the surface of the electrode. Ultimately, more electrochemical growth of the MOFs covers the exposed surfaces of the electrodes, resulting in a dense MOFs layer. The first report of the anodic deposition of MOFs thin membranes was published in 2005. The anodic dissolution of the metal anodes created the ions of metal, which then interacted with the organic ligands in the electrolyte to form MOFs on the anode. Anodic deposition comes in two varieties: low-temperature deposition and high-temperature deposition. Neutral ligands such as azoles and carboxylic acids must be deprotonated in-situ for MOFs based on anionic ligands. When hydroxide anions are deposited on the cathode, in-situ deprotonation of the ligand occurs, as shown in Figure 9. A MOFs membrane may form on the surface of cathode when metal ions are present in the solution [51].

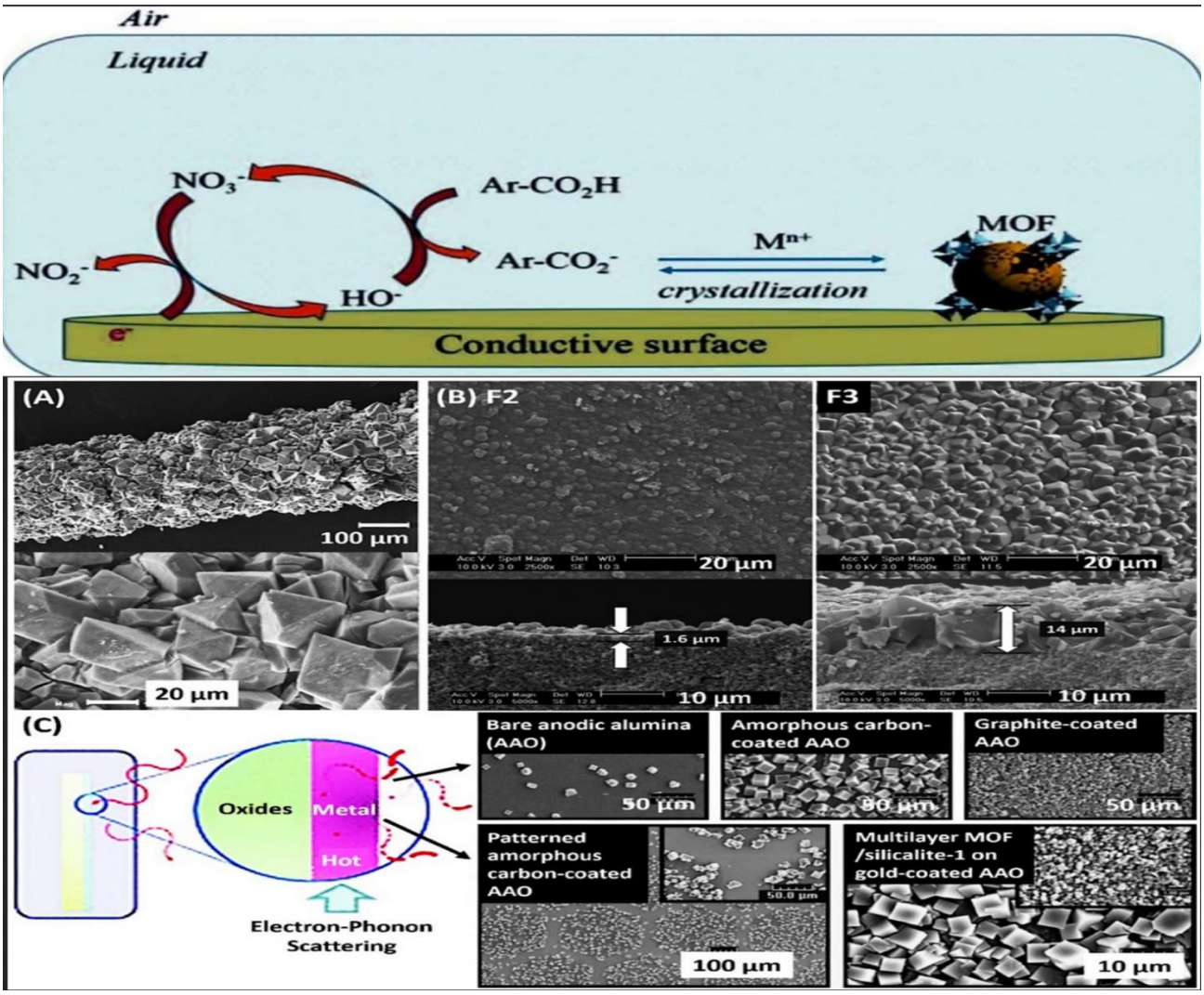

Fig. 9. Research on the cathode deposition mechanism of MOFs is reproduced from Ref. [51] with permission from Elsevier, Copyright 2018.

2. Catalytical Properties of MOFs:

They discover that the Phillips catalyst is part of a large dependence on polyethylene in the community and that they have been involved in research efforts aimed at developing catalysts that are homogeneous for the polymerization of ethylene; the catalysts they are developing are based on Cr. Ziegler–Natta catalysts are also emerging as a hot spot, with titanium and zirconium as focus points [10]. Metallocene and Ziegler Natta catalysts work for the polymerization of ethylene [11]. Ghobakhloo *et al* in 2022 have designed a novel Cu (II)-supported nano catalyst with stable and reusability without appreciable loss of activity in cyclized addition reactions that include Knoevenagel condensation–Michael. Aza-Micheal addition CuBTC reusable and retainable crystallinity MOF a substitute of amines responded in 2 to 24 h

over 4 runs with no loss of the catalytic activity provided more promising result with aliphatic amines up to 98% yield [52]. The majority of the others played important roles in the polymerization of associated dienes such 1,3-butadiene or in the synthesis of isotactic polypropylene [53], and mostly originated from the transition metals that are in the first row. Although, several current studies have exhibited the adsorption activity of MOFs for unsaturated hydrocarbons a team of researchers reported a catalyzed disulfide addition reaction of Ni-MOF-74 for gaseous acetylene with superb selectivity in catalysis mechanism with prime advantage of recycling and easier separation possibility monitoring with FT-IR, XRD, EDX and SEM approaches [54]. There are numerous polymerization reactions that take place in the condensed phase (liquid or solid) substrates, and other coordination polymerization reactions that are implying gas-phase substrates [12]. These include radical-based processes, such as RAFT (reversible addition-fragmentation chain), ATRP (light-induced atom transfers radical polymerization), and ROP (ring-opening polymerization) [55]. These processes add co-polymerization and broaden the substrate's scope to include cyclic esters, acrylamides, and monomeric methacrylates. These radical-type reactions typically involve photoactive organic compounds and redox-sensitive transition metallic elements like Fe, Cu, or Ti. There are many publications on polymerization catalysts and many developments have taken place but it is a challenging task to preserve all of them. Guironnetand co-workers in the recent past tried it in their thorough analysis of recent trends in polymerization catalysis [56]. MOFs are thought to have high porosity and metal sites. Microwave-assisted radical polymerization of methylmeth acrylate is catalyzed by MOFs. The number of MOFs-907, co-initiators, organic solvents, and polymerization time are examples of catalysis-related parameters that need to be taken into consideration [5].

2.1. Methmethyl Acrylates

Polymethyl methacrylate is used in the dental industry. The low weight materials with high stability are PMMA [10]. The benefits of polymerization are extended with any advances in MOF-based catalysis for polymerization of methylmeth acrylate. For the methyl methacrylates ’polymerization, different methods of polymerizations are used like Atomic Radical Polymerization, Photopolymerization and Microwave assisted radical polymerization [11]. The most important method of polymerization is microwave assisted radical polymerization [12]. Methylmeth acrylate gets polymerized in the presence of catalyst MOFs-907.The polymerized product of PMMA is dependent on the concentration of Catalyst, initiator concentration as well as concentration of solvent DMF. If the Concentration of DMF is less, high yield product will be obtained [57, 58].

2.2. Microwave assisted Radical Polymerization of MMA

Activated MOF (3mg) is charged in a flask (10ml) which is also charged with few amounts of DMF, MMA, ethyl α-bromoisobutyrate (EBiB) / ethyl α-bromophenylacetate (EBPA) followed by closing the flask with microwave cap. Before being placed in the microwave system, the mixture in the flask was agitated for 30 minutes at 25 degrees Celsius. The polymerization reaction's synthesis conditions were established in a closed system at 100 °C for 30 minutes with 200 W of electricity.Following this procedure, the polymerization system is prepared. MOF builds up once the reaction is finished and is repeatedly soaked in dichloromethane. PMMA, the reaction's product, crystallizes out in a methanol solution. At room temperature, the PMMA should ideally dry. Conditions including reactant concentration, temperature, power, and reaction time will be examined for their effects [59].

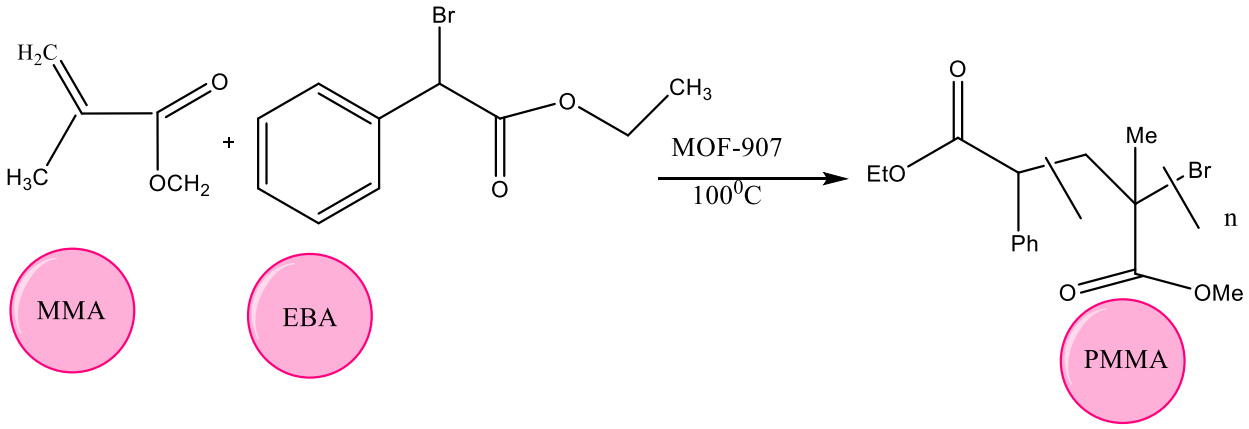

Scheme No. 1: Microwave assisted Radical Polymerization of MMA

In the past, the researchers have used two types of co-initiators – ethyl alpha –Bromophenyl Acetate (EBPA) and ethyl alpha-Bromoisobutyrate (EBiB). By using EBiB, 68% of PMMA is synthesized while by using EBPA, only 43% PMMA product is synthesized.Thus, it can be concluded that EBiB is the most crucial initiator among all initiators which can yield maximum amount of PMMA. DMF is a solvent for use in the monolithic formulation process. It produces a high-yield product with less. Compared to Ni-Vu-74(II) or HKUST-1 types of Ni, Cu based MOFs, Fe-based MOFs have significantly stronger Lewis acid active sites.

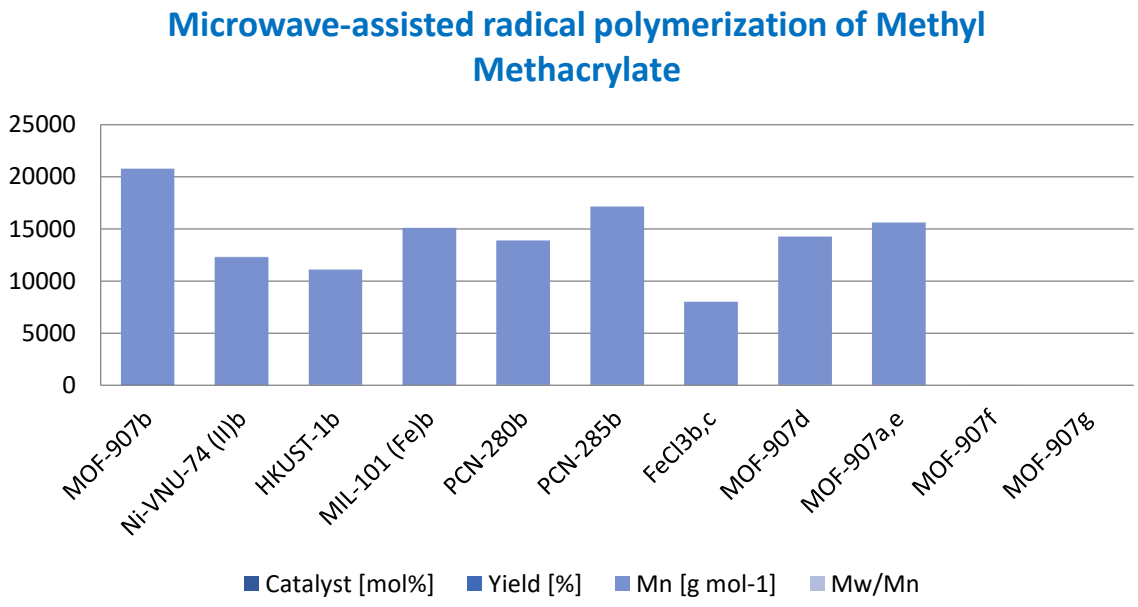

Graph 1: Microwave assisted radical polymerization of Methyl Methaacrylate.

3. Applications of Metal organic frameworks

The functionality of MOFs (metal-organic frameworks) is critical to explore their structural along with chemical diversity for large number of potential applications [60]. Metal-based catalytic reagents, however, have an irreplaceable role in the chemical industry particularly in synthesis [61].

3.1. In the removal and adsorption of metal ions

Food processing, industrial progress, and materials science all depend on the Determination and analysis of ions of metals [10]. The porous materials' unique pore structure and superior adsorption qualities make them useful for metal ion removal and adsorption as well as inspection and identification [11]. This part will focus on the utilizing permeable composite components in order to evaluate a few typical metal ions of various metal ion kinds, including radioactive metal ions, d,f blocks, and alkaline earth metals. The alkali and alkaline metal ions Na, K, Ca, Mg, and Li are the most typical. The modification of a porous composite material to detect alkali metal ions is one of the main areas of research [12]. Because of the alkaline earth metals' large ion diameter, minimal density, and strong valence bond, the number of the coordination and bond effect with the donor, such as the carboxylic acid group, increase with increasing ion diameter [55]. For the production of stable alkaline earth MOFs, this is beneficial. In addition, alkaline earth metal ions have little toxicity and are very biocompatible. They may also successfully stop secondary

pollution brought on by heavy ions made up of metals by acting as fluorescent probes in biological systems [5]. A phosphate MOFs alginic acid hydrogel that uses brown algae to adsorb Liþ and Mg2þ was proposed by Park and coworkers. Adsorption properties analysis indicated that the main functional groups responsible for the adsorption of Liþ and Mg2þ were carboxylic acid and phosphonate groups. This led to the development of an effective ion recovery technology and a novel selective adsorption method for the separation and identification of magnesium and lithium ions [62].

3.2. Metal organic frameworks use in heavy metal ions

Metal ions can seriously harm many of the human body's organs because of their poisonous effects. Heavy metal ions can be adsorbed, removed, and analyzed using the MOF material, which is a composite MOF material with a specific pore structure and good adsorption properties [15, 63].

3.2.1. Ion of a divalent heavy metal

The most common metal ions are bivalent ions of heavy metals, such as Cu^{+2}, Pb^{+2}, Cd^{+2}, Hg^{+2}, and Ni^{+2}, which are necessary for extensive metal ion detection research [10]. Cu^{+2} ions pollution is mostly caused by the steel sector, metal processing, smelting and mining of copper-zinc ores, and the production of technology [11]. Ui O-66 MA is a dual amenable sensor to detect Cu (II) and H_2S in the aquatic systems with high selectivity and sensitivity undergo Micheal addition turn on fluorescent behavior with respective detections limits of 2.6 nM and 3.3 nM indicating development of multirole MOF sensor on routed in combinatorial principles [64]. The other MOFs (UiO-66-EDA) have also been synthesized using the Michael addition reaction as a Zr-based ethylenediamine multirole reagent for the adsorption of ions of heavy metal Cd^{+2}, Cu^{+2}, and Pb^{+2} from water. The maximum removal capacities of these MOFs were 217.39 milligram per gram, 208.33 milli gram per gram, and 243.90 milli gram per gram, respectively, due to electron sharing, electrostatic forces, and covalent forces between the metallic ions and the MOF (UiO-66-EDA) with different functional groups on its surface. Additionally, the stability of the produced UiO-66-EDA MOF in this exothermic and spontaneous in nature adsorption investigation was demonstrated by thermodynamic parameters that were monitored, such as ΔS (standard entropy changes), ΔH (standard enthalpy changes), and free energy changes (ΔG) [65]. Copper ion pollution in the atmosphere is mostly caused by the smoke and dust that smelting produces. Numerous recent studies have examined the acknowledgment and absorption of Cu^{2+} ions by ordinary porous materials [66]. For example, ZIF-8 nanoparticles were prepared on a large scale and grown in-situ on ZIF-8/PAN-NF membranes made of electrospun polyacrylonitrile (PAN) nanofiber Cu2þ showed good dynamical

absorption and standard filtering performance compared with the ZIF8/PAN nanofiller, according to Peng and coworkers. Copper was eliminated at a rate of 29.2% during the adsorption phase and 34.1% over four minutes [67]. The development of a thin ZIF-8 modified zeolite imidazole in salt (ZIF-8) forward osmosis film was also reported by Qiu and colleagues [68] on a crosslinked matrix of 1,3,5-benzenetricarboxylic acid chloride (TMC) and polyethyleneimine (PEI). The improved PDA layer made it possible for the nanofiller and the selective layer to have a good affinity. Compared to the original thin membrane composite membrane, ZIF-8@PDA demonstrated excellent water selectivity and higher water flux. Additionally, the altered membrane demonstrated a high rejection rate for heavy metal ions (Cu2 þ, Ni2þ, and Pb2þ). The human body's typical lead (Pb^{2+}) concentration is 0.1 mg L^{1}. Anemia and harm to the nervous system might result from exceeding this standard due to excessive Pb2þ in the water. Active steps to discharge lead should be taken after the blood lead level exceeds the standard [69].

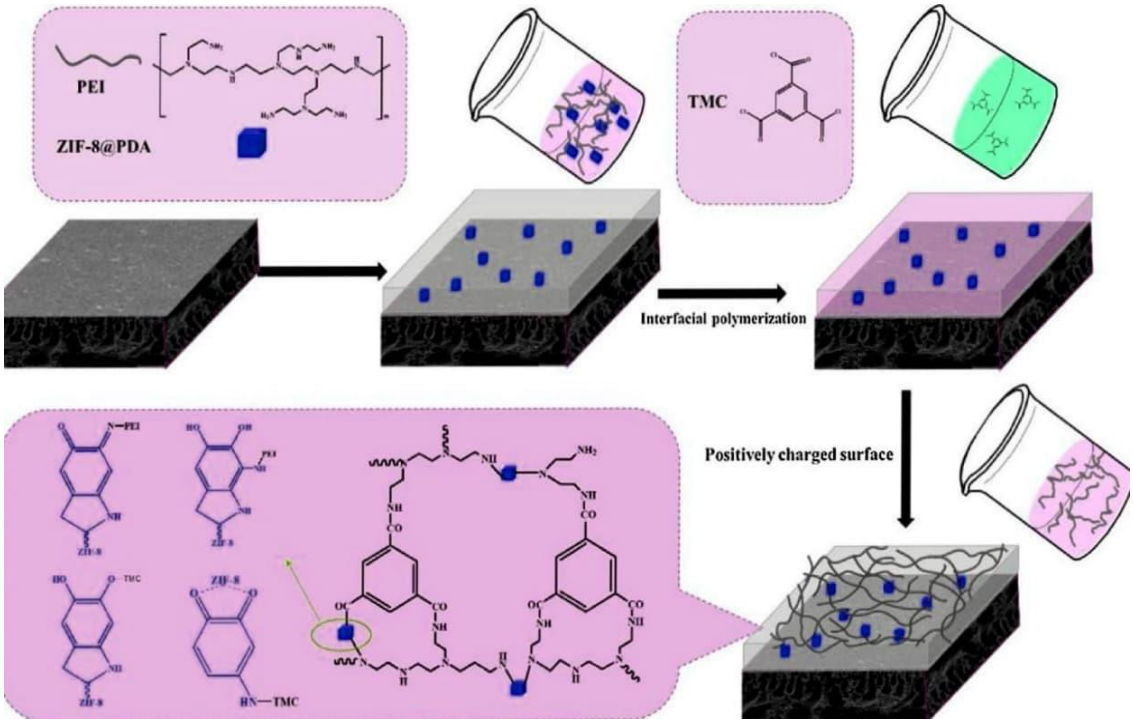

Figure 10. Schematic diagram of the preparation of ZIF-8@PDA modified TFN membrane is reproduced from Ref. [53] with permission from Elsevier, Copyright 2019.

3.3. Using Metal organic frameworks to radioactive ions

Numerous radioactive materials are unavoidably discharged into the environment as a result of the heavy use of coal, oil, and other fossil fuels [10]. Radionuclides such as uranium ,europium and strontium ions not only have a long half-life, high atmospheric mobility, water stability, and non-degradability

characteristics, but they also have extremely high toxicity and adverse effects that lead to a number of illnesses [11]. Thus, it is extremely important that the radioactive wastewater is properly treated prior to discharge into the environment. to detect and identify radioactive ions [12], It is essential to use materials with pores as solid adsorbents through chemical control. Uranium is a commonly used radioactive metal element and a fuel used for nuclear reactions. It is one of the most hazardous metal elements due to its high toxicity and poor degradability. the researchers Liu and colleagues synthesized MOFs with the azo functional group using the solvothermal method, and they tested uranium batch adsorption using MOFs and thermodynamics. The findings showed that the MOF's adsorption capability for uranium (U) ions in waste water was 312.32 mg/g, indicating that it is a suitable uranium adsorbent [59]. Using the same 3D framework, Song and colleagues conducted a series of studies on uranyl adsorption on iso network MOFs. The various adsorption processes were shown in studies using the Freundlich and Langmuir adsorption isotherms. The eOH and eNH_2 groups easily achieved a desorption rate of more than 70% and shown greater uranium adsorption than other groups, and the U-loaded MOFs can be eluted in addition to eNO_2. With 0.1 mol/L nitric acid, the highest desorption rate of 11.29% was noted. The results obtained demonstrate the significant U(VI) adsorption ability of MOF materials modified with particular organic groups in aqueous conditions, and functionalizing the porous materials will boost the capacity for adsorption when compared to the original material.

As uranium (U) ion research progresses, maintaining consistent adsorption performance in a complex matrix environment is more crucial than the material's adsorption performance. Apart from uranium ions, other radioactive ions such europium (Eu), strontium (Sr), cesium (Cs), and iodine (I) must also be efficiently identified and adsorbed [62]. As seen in Fig. 11, Chang and coworkers used a cutting-edge in-situ "green" radiation approach to develop a novel Prussian blue/natural porous material frameworks nanocomposite. The generated adsorbent demonstrates strong dispersibility characteristics and a porous structure, and it is demonstrated to be effective for Cs adsorption in an aqueous solution. The method can be modified to create other comparable porous adsorbents and is straightforward, effective, and safe for the environment. The necessary adsorption material stability was successfully attained by this technique, and the functionality's synergistic improvement has some practical significance [62].

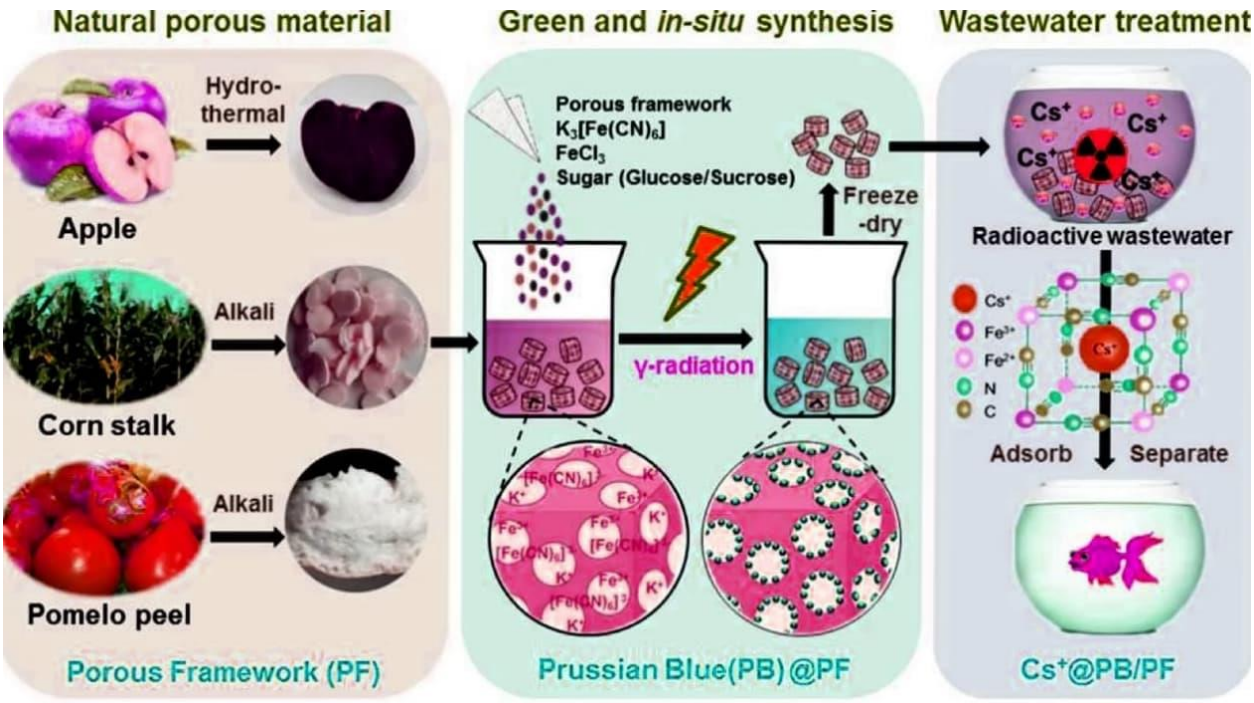

Fig 11: Schematic diagram of in situ green production strategy for Prussian blue/natural porous framework nanocomposites for radioactive Cs removal is reproduced from Ref. [63] with permission from Springer Nature, Copyright 2018.

3.4. Metal organic frame works for Photocatalysis

Metal organic frameworks can be considered as a new platform, and can organize various components to realize the functions of photoresponse, which has gained more interests in application for artificial photosynthesis [10]. Compared to traditional photocatalysts, MOFs possess structural diversity and tailor ability, which makes them have some unique advantages in photocatalysis [11]. irst, MOFs' extremely porous and crystalline structure can allow substrates and products to diffuse readily through their channels that are open and shorten the charge carriers' transportation length to the porous area for reactions, thereby lowering the electron-hole conventional volume recombine [12]. Second, structural flaws that may create recombination centers [55] can be prevented due to the high crystallinity. Third, the high density of the catalytic sites on the substrates placed in well-defined porous MOFs structure makes the enriched substrates available, and this is another advantage of this kind of system [5]. The diversity and tunability of MOFs' structure, in particular, is their greatest advantage over other inorganic materials: the performance of MOF photocatalysts can be adjusted for target structures by choosing the fine-tuning particular functional groups and/or right building blocks of MOFs. The latest developments in MOFs for light-driven energy conversion processes, such as conventional organic reactions, carbon dioxide

reduction, and splitting water, will be the main topic of this section. The degradation of organic pollutants has been the main focus of the early research on MOF photocatalysis. Guo and his colleagues recently examined the relevant studies.

3.5. Metal organic frameworks for Photocatalytic Water Separation

Two half-reactions participate in water splitting, which are water reduction, which yields hydrogen gas, and water oxidation, which yields oxygen. The initial and primarily reported reaction by MOF photocatalysts is the latter of these two half reactions, according to Fateeva and colleagues *at el* [67] , By integrating photosensitizer $Ru(bpy)_3^{2+}$ into the porous MOF [Ru2(p-BDC)2]n (p-BDC = p-benzenedicarboxylate), which is utilized to photoreduce a water to hydrogen, Mori and his coworkers reported MOFs as cocatalysts of sorts. When the -NH_2 group is added to the UiO-66 framework, the resultant NH_2-UiO-66 is a photo-catalyst that, when exposed to UV light, can clearly increase the activity of H_2 production in a aqueous methanolic solution and expand the absorption band to the visible region. In a similar vein a Ti-containing metal organic framework (NH_2-MIL125(Ti)) was shown to be a visible-light sensitive photocatalyst for a typical hydrogen evolution using Pt NPs as the standard cocatalyst and a triethanolamine (TEOA) as the electron sacrificing agent The consequences of coating NH_2-MIL-125 (Ti) with various noble metallic elements gold and platinium on photocatalytic activity under visible light irradiation in saturated carbon dioxide with TEOA present have been studied. In addition, amine functionalized MIL101(Cr) has been reported to be used for photocatalytic generation of hydrogen from water [12]. The longest wavelength is only roughly 500 nm because of the weak visible sensitivity of BDC-amine, despite the fact that MOF modified with -amine groups has been established to make hydrogen from water splitting using light that is visible. Developing MOFs with a broad light response spectrum that spans the visible spectrum is greatly desired[5]. As they absorb almost the entire visible-light spectrum, porphyrins are useful and interesting organic building blocks for the design of porphyrinic-based MOFs for photocatalysis applications. In light of this, a water-stable Al-porphyrinic MOF has a When applied as a photocatalyst for hydrogen gas production by breaking down water under visible light (VL) exposure to sunlight, it has an overall turnover number of 8.16 and a quantum yield of 4.82% Besides the extent of light absorption, charge effectiveness is important in photocatalysis. Throughout the photocatalytic process, catalysts containing elements like POMs, metal complexes, and noble metal NPs may promote more effective charge separation. Lin and colleagues have presented PT@MOF composite containing Pt NPs in MOF cavities. The Pt@ MOF composites showed outstanding productivity and a high turnover number (TON) as photocatalysts for hydrogen evolution. Jiang, Zhang, and colleagues have

created a photocatalyst that uses Pt NPs as electron acceptors in an UiO-66-NH_2 framework to effectively produce $H2$ from water splitting when exposed to visible light, as shown in Fig. 12b

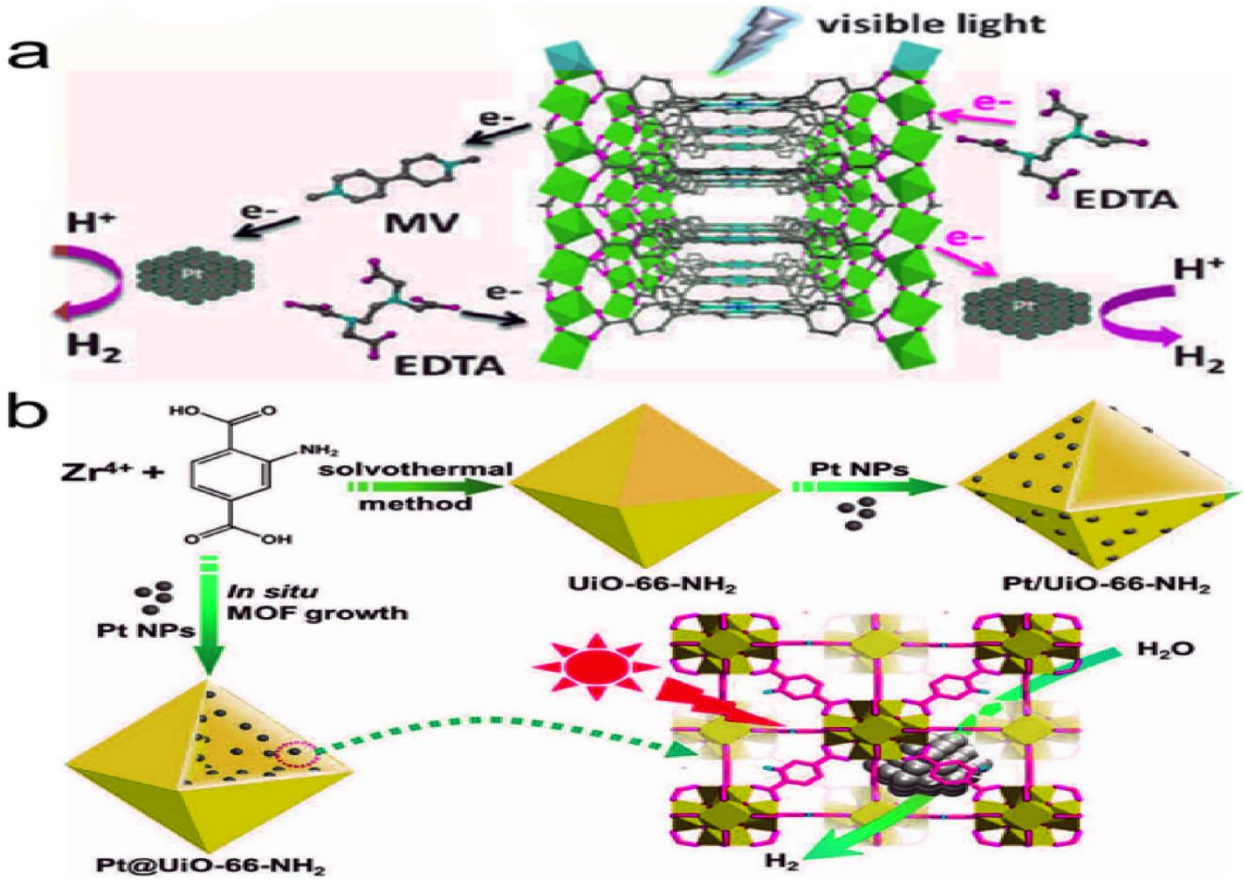

Fig12 a) water-stable Al-porphyrinic Metal organic framework as a photocatalyst for hydrogen prpduction from water separation under visible light b**)** photocatalyst of UiO-66-NH_2 incorporated with Pt NPs as electron acceptors for efficient hydrogen production from water separation under visible. Fig. 12 a and 12 b are Reproduced from Ref. [72] under the Creative Commons CC BY License.

3.6. Metal organic frameworks for Electrocatalysis

An additional option for the storage and conversion of renewable energy is the electrocatalytic system, which primarily consists of ORR, OER/HER, and electrochemical carbon dioxide reduction[10]. A novel synthesis for effectively prerpared chiral amine, amide and Ni consisting Zr-MOF DUT <136 ≥ MOFs respectively1111 by metalation and redox reaction inspired by C:N bond versatile derivatization to check catalytic activity for modified systems on a variety of asymmetric organic conversions as Micheal addition, Friedle-Crafts alkylation, Ni-catalyzed C-C coupling and aldol reaction[70]. However, catalysts of Platinium,Iridium and Ruthium metals are typically required to cover the inherently large kinetic obstacles in electrochemical processes[11]. However, noble metals' limited availability and high cost limit

their use in industry[12]. Finding earth-abundant substitutes with superior activity and stability is crucial. Metallic-containing compounds, transition metal/metal oxides, heteroatom doped carbon materials, etc. are a few examples. Organic ligands that contains carbon,hydrogen, oxygen and nitrogen with first Fe, Co, Ni, Cu, Mn, etc.typically compose the majority of MOFs [55]. MOFs have numerous benefits as non-noble metal electrocatalysts, such as a wide surface area, uniform distribution of open active centers, adjustable pore size and channels, and a designable structure [5]. However, the low conductivity and electrochemical instability of pure MOFs generally limit their electrocatalysis[18]. In order to increase their conductivity, Metal organic frame works have also been combined with conductive materials like carbon nanotubes as well as graphene [19]. Additionally, metal organic frame works were used as perfect sacrificial templates to produce a variety of nanostructured materials with great stability and conductivity, including metal oxides, porous carbons, metal (oxides)/carbon composites, and other metal-containing compounds like metal carbides and metal nitrides[5]. Some of the advantages of pure MOFs, such their high surface area, tunable porosity, and ability to be changed with additional heteroatoms and metal/metal oxides, may be present in the materials generated from MOFs[22]. In addition to significantly lengthening the range of catalytic applications, these MOF derivatives have some significant disadvantages compared to unmodified MOFs [16]. For example, in electrochemical reactions, nanostructures made with MOFs show significantly more durability than pristine MOFs, even under sensitive reaction conditions such highly acidic or basic solutions. Metal organic frame based nanomaterials used in electrocatalysis have received increasing interest and development in recently due to these advantages [69].

Challenges, Limitations, Outcomes of MOFs materials

From the recent years, MOFs have attracted huge interest of researchers worldwide because of their larger number of applications in various fields. However, at present numerous challenges and limitations are concerned includes laborious synthesis, analysis procedures, poor electrical characteristics and low solubilities [1] toxicity, degradation and reuse/recycle/regenerate[2] membrane-based MOFs need improved stability for the practical separation parameters for instance pressure and temperature [71]. The modification of size, morphology, structural arrangement, porosity, backbone framework of multicomponent MOFs is essential to achieve their excellent performance in water [4]. However, the MOFs main disadvantage is its toxicity of metal and linker, stability, size dispersity, colloidal and chemical stability, drug loading and releasing practice etc.. [5]. Furthermore, the challenge of MOFs that is currently unattainable is stability in catalysis[14]. In parallel, there are many problems related to the stability of MOF, including the issue of comparing stability between MOF and other porous fabricated materials like zeolites, porous carbons and mesoporous silica etc. which are more or less stable [7]. The

challenges that are more major for MOFs are: Selectivity, foulings, deactivation, accessibility to active sites, MOF interaction, surface area, synthesis complexity, and environmental toxic hazards. It is important to emphasize the re-use, re-cycle, regenerate and degradation of MOFs. The necessary step for the preparation of large-scale MOFs is synthesis protocol and theoretical prediction (a), preferably the reaction medium should be water (b), the organic linkers should be biodegradable, biocompatible and bio-inspired (c) and bulk organic solvents should be avoided for environment sustainability and safety (d) [8]. To overcome this, there is a need of continuous trans-disciplinary efforts from the outset, and of course, a gathering of the chemists, pharmacologists, clinicians, physicists and biologists involved in the preparation of the various MOFs.

Future Horizon

In the coming future, the synthesis of highly stable MOFs seems like a workable dream that may leads to diverse ends with respect to their applications. MOFs or variants of MOFs with stable and intellectual design with properties of each individual component, for example, can provide excellent performance for the specific applications [1]. As the synthesis of MOFs and their derivatives can be done using numerous technologies by controlling size, shape and porosity parameters. In spite of these efforts, however, there are still several shortcomings that hinder the effectiveness of designed MOFs, primarily low chemical stability, low capacity, low selectivity and high barrier to recycling and regeneration [71]. Moreover, the performance is crucial factor in various applications like catalytic processes and greater need to synthesis larger number of MOFs and their derivatives in coming days [3]. However, many more speculations about the morphology and structures for the MOFs would be prepared with cheap materials [72]. By studying the characteristics of MOFs in various properties, new materials will emerge and probably benefit from the advantages in broad range prospectives [3]. MOFs' degradation and recycling properties are also promising for environmental research to realize a benign and green future [5]. With respect to discarding and waste handling, there is a lot of work to be done with MOFs as there are no legal regulations present [6]. MOFs materials would also be improved in future using the faster-futuristic machine learning and AI methods to cater to the needs of contemporary solutions [7]. Finally, everything should be directed towards future research, not towards one dimension or another dimension to solve problems and limitations with MOFs synthesis and applications to improve human beings.

Conclusion

Metal-organic frameworks are a category of materials in which atoms are arranged in regular pattern consisting of periodic networks of nodes, including metals, connected by bridging features between self-

assembling organic molecules. This review summarizes the mechanochemical process, the primary growth method, the 2ndry growth approach, and the different types which may be in the form of powder/membrane structures and production methods of metal organic frame works materials. The most recent advancements in MOFs for different metal ion enrichment adsorption, analytical detection, and other catalytic applications are then highlighted. Then we discussed the microwave method of radical polymerization of methylmeth acrylate in detail. Future trends in MOF materials were examined, along with technical issues that need to be resolved. Additionally, other MOF applications have been researched.

Funding: Funding is inappropriate for this research study.
Data availability: The statistics supporting the outcomes of this research are accessible upon reasonable request from the first author.

Declarations

Ethical approval: Not applicable
Consent to participate: Not applicable
Consent to publish: All authors have given consent to publish.
Competing interest: The authors have no competing interests to declare.

References

1. Bui, N.T., et al., *A nature-inspired hydrogen-bonded supramolecular complex for selective copper ion removal from water.* 2020. **11**(1): p. 3947.
2. Choi, S., X. Liu, and Z.J.A.P.S. Pan, *Zinc deficiency and cellular oxidative stress: prognostic implications in cardiovascular diseases.* 2018. **39**(7): p. 1120-1132.
3. Zhao, S., et al., *Water-compatible surface imprinting of 'Saccharin sodium'on silica surface for selective recognition and detection in aqueous solution.* 2015. **144**: p. 717-725.
4. Darbha, G.K., et al., *Selective detection of mercury (II) ion using nonlinear optical properties of gold nanoparticles.* 2008. **130**(25): p. 8038-8043.
5. Gao, Y., et al., *Recent advances and applications of magnetic metal-organic frameworks in adsorption and enrichment removal of food and environmental pollutants.* 2020. **50**(5): p. 472-484.
6. Eddaoudi, M., et al., *Zeolite-like metal–organic frameworks (ZMOFs): design, synthesis, and properties.* 2015. **44**(1): p. 228-249.
7. Ranjan, R. and M.J.C.o.M. Tsapatsis, *Microporous metal organic framework membrane on porous support using the seeded growth method.* 2009. **21**(20): p. 4920-4924.
8. Kent, C.A., et al., *Energy transfer dynamics in metal− organic frameworks.* 2010. **132**(37): p. 12767-12769.
9. Tan, Y.-X., F. Wang, and J.J.C.S.R. Zhang, *Design and synthesis of multifunctional metal–organic zeolites.* 2018. **47**(6): p. 2130-2144.
10. Park, H.B., et al., *Maximizing the right stuff: The trade-off between membrane permeability and selectivity.* 2017. **356**(6343): p. eaab0530.
11. Deng, Y., et al., *Metal-organic framework membranes: Recent development in the synthesis strategies and their application in oil-water separation.* 2021. **405**: p. 127004.
12. Zhang, Y., et al., *Challenges and recent advances in MOF–polymer composite membranes for gas separation.* 2016. **3**(7): p. 896-909.
13. Yaghi, O.M.J.J.o.t.A.C.S., *Reticular Chemistry Construction, Properties, and Precision Reactions of Frameworks*. 2016, ACS Publications. p. 15507-15509.
14. Eddaoudi, M., et al., *Porous metal− organic polyhedra: 25 Å cuboctahedron constructed from 12 Cu2 (CO2) 4 paddle-wheel building blocks.* 2001. **123**(18): p. 4368-4369.
15. Wang, C.-C., et al., *Photocatalytic organic pollutants degradation in metal–organic frameworks.* 2014. **7**(9): p. 2831-2867.
16. Lin, R.-B., Z. Zhang, and B.J.A.o.C.R. Chen, *Achieving high performance metal–organic framework materials*

through pore engineering. 2021. **54**(17): p. 3362-3376.
17. Zhang, J., Y. Tan, and W.-J.J.M.A. Song, *Zeolitic imidazolate frameworks for use in electrochemical and optical chemical sensing and biosensing: a review.* 2020. **187**(4): p. 234.
18. Denny, M.S., et al., *Metal–organic frameworks for membrane-based separations.* 2016. **1**(12): p. 16078.
19. Friščić, T., C. Mottillo, and H.M.J.A.C. Titi, *Mechanochemistry for synthesis.* 2020. **132**(3): p. 1030-1041.
20. Gao, M., et al., *Recent advances in metal-organic frameworks/membranes for adsorption and removal of metal ions.* 2021. **137**: p. 116226.
21. Li, W.J.P.i.M.S., *Metal–organic framework membranes: Production, modification, and applications.* 2019. **100**: p. 21-63.
22. ZareKarizi, F., M. Joharian, and A.J.J.o.M.C.A. Morsali, *Pillar-layered MOFs: functionality, interpenetration, flexibility and applications.* 2018. **6**(40): p. 19288-19329.
23. Titi, H.D.J.-L.J.C.S., *Howarth AJ Nagapudi K. Friščić T.* 2020. **11**: p. 7578-7584.
24. Sun, J.-K., M. Antonietti, and J.J.C.S.R. Yuan, *Nanoporous ionic organic networks: from synthesis to materials applications.* 2016. **45**(23): p. 6627-6656.
25. Brekalo, I., et al., *Manometric real-time studies of the mechanochemical synthesis of zeolitic imidazolate frameworks.* 2020. **11**(8): p. 2141-2147.
26. Xia, Q., et al., *State-of-the-art advances and challenges of iron-based metal organic frameworks from attractive features, synthesis to multifunctional applications.* 2019. **15**(2): p. 1803088.
27. Joharian, M. and A.J.J.o.S.S.C. Morsali, *Ultrasound-assisted synthesis of two new fluorinated metal-organic frameworks (F-MOFs) with the high surface area to improve the catalytic activity.* 2019. **270**: p. 135-146.
28. Hu, Z. and D.J.C. Zhao, *Metal–organic frameworks with Lewis acidity: synthesis, characterization, and catalytic applications.* 2017. **19**(29): p. 4066-4081.
29. Nikseresht, A., et al., *TMU-16-NH2: A metal–organic framework as an efficient, green, and heterogeneous catalyst for the Michael addition annulations for the synthesis of a new series of 2, 4-Diphenylpyrido [4, 3-d] pyrimidines.* 2024. **44**(6): p. 3771-3786.
30. Wu, D., et al., *L-proline functionalized pillar-layered MOF as a heterogeneous catalyst for aldol addition reaction.* 2020. **119**: p. 108052.
31. Moghadaskhou, F., et al., *Fabrication and characterization of a novel catalyst based on modified zirconium metal-organic-framework for synthesis of polyhydroquinolines.* 2023. **13**(1): p. 16584.
32. Zhan, D., et al., *Structures and Catalytic Properties of two New Squaramide-decorated Cd-MOFs.* 2022. **648**(9): p. e202200064.
33. Seyedpour, S.F., A. Rahimpour, and G.J.J.o.M.S. Najafpour, *Facile in-situ assembly of silver-based MOFs to surface functionalization of TFC membrane: A novel approach toward long-lasting biofouling mitigation.* 2019. **573**: p. 257-269.
34. Lu, K., et al., *Ionothermal synthesis of five keggin-type polyoxometalate-based metal–organic frameworks.* 2019. **58**(3): p. 1794-1805.
35. Zhou, X., et al., *Mechanochemistry of metal–organic frameworks under pressure and shock.* 2020. **53**(12): p. 2806-2815.
36. Yoo, Y., et al., *Fabrication of MOF-5 membranes using microwave-induced rapid seeding and solvothermal secondary growth.* 2009. **123**(1-3): p. 100-106.
37. Yuan, J., et al., *Fabrication of ZIF-300 membrane and its application for efficient removal of heavy metal ions from wastewater.* 2019. **572**: p. 20-27.
38. Hootifard, G., et al., *Fe3O4@ iron-based metal–organic framework nanocomposite [Fe3O4@ MOF (Fe) NC] as a recyclable magnetic nano-organocatalyst for the environment-friendly synthesis of pyrano [2, 3-d] pyrimidine derivatives.* 2023. **11**: p. 1193080.
39. Gangu, K.K., et al., *A review on contemporary metal–organic framework materials.* 2016. **446**: p. 61-74.
40. Li, W., et al., *Metal− organic framework composite membranes: Synthesis and separation applications.* 2015. **135**: p. 232-257.
41. Li, X., et al., *Metal–organic frameworks based membranes for liquid separation.* 2017. **46**(23): p. 7124-7144.
42. Sun, D., et al., *Tetraaniline-modified Co-MOF-PDA for anti-corrosive reinforcement of waterborne epoxy coating.* 2024. **685**: p. 133250.
43. Van Vleet, M.J., et al., *In situ, time-resolved, and mechanistic studies of metal–organic framework nucleation and growth.* 2018. **118**(7): p. 3681-3721.
44. Wang, H., et al., *Membrane adsorbers with ultrahigh metal-organic framework loading for high flux separations.* 2019. **10**(1): p. 4204.
45. Chernikova, E. and E.J.P.S. Sivtsov, Series B, *Reversible addition-fragmentation chain-transfer polymerization: Fundamentals and use in practice.* 2017. **59**(2): p. 117-146.
46. Lee, H.-C., et al., *Synergic effect between nucleophilic monomers and Cu (II) metal–organic framework for visible-light-triggered controlled photopolymerization.* 2017. **29**(21): p. 9445-9455.

47. Nguyen, H.L., et al., *A complex metal-organic framework catalyst for microwave-assisted radical polymerization.* 2018. **1**(1): p. 70.
48. Park, S.H., et al., *Selective lithium and magnesium adsorption by phosphonate metal-organic framework-incorporated alginate hydrogel inspired from lithium adsorption characteristics of brown algae.* 2019. **212**: p. 611-618.
49. Zinicovscaia, I., et al., *Metal ions removal from different type of industrial effluents using Spirulina platensis biomass.* 2019. **21**(14): p. 1442-1448.
50. Kumar, A., M. Rachamalla, and A.J.M.O.F.f.W.C.R. Adarsh, *Case Studies (Success Stories) on the Application of Metal-Organic Frameworks (MOF s) in Wastewater Treatment and Their Implementations; Review.* 2023: p. 151-176.
51. Van Goethem, C., et al., *The role of MOFs in thin-film nanocomposite (TFN) membranes.* 2018. **563**: p. 938-948.
52. Bhattacharjee, S., A.A. Shaikh, and W.-S.J.C.L. Ahn, *Heterogeneous aza-Michael addition reaction by the copper-based metal–organic framework (CuBTC).* 2021. **151**(7): p. 2011-2018.
53. Qiu, M. and C.J.J.o.h.m. He, *Efficient removal of heavy metal ions by forward osmosis membrane with a polydopamine modified zeolitic imidazolate framework incorporated selective layer.* 2019. **367**: p. 339-347.
54. Degtyareva, E.S., K.S. Erokhin, and V.P.J.C.C. Ananikov, *Application of Ni-based metal-organic framework as heterogeneous catalyst for disulfide addition to acetylene.* 2020. **146**: p. 106119.
55. Zhang, Z., et al., *Metal–organic frameworks (MOFs) based chemosensors/biosensors for analysis of food contaminants.* 2021. **118**: p. 569-588.
56. Li, Y.S., et al., *Controllable synthesis of metal–organic frameworks: From MOF nanorods to oriented MOF membranes.* 2010. **22**(30): p. 3322-3326.
57. Liu, S., et al., *Adsorption equilibrium and kinetics of uranium onto porous azo-metal–organic frameworks.* 2016. **310**(1): p. 353-362.
58. Liu ShuJuan, L.S., et al., *Adsorption equilibrium and kinetics of uranium onto porous azo-metal-organic frameworks.* 2016.
59. Miensah, E.D., et al., *Zeolitic imidazolate frameworks and their derived materials for sequestration of radionuclides in the environment: A review.* 2020. **50**(18): p. 1874-1934.
60. Nayab, S., et al., *Reversible Diels–Alder and Michael addition reactions enable the facile postsynthetic modification of metal–organic frameworks.* 2021. **60**(7): p. 4397-4409.
61. Beiranvand, M., D. Habibi, and H.J.S.R. Khodakarami, *A novel pillar-layered MOF with urea linkers as a capable catalyst for synthesis of new 1, 8-naphthyridines via the anomeric-based oxidation.* 2024. **14**(1): p. 27727.
62. Chang ShuQuan, C.S., et al., *In situ green production of Prussian blue/natural porous framework nanocomposites for radioactive Cs+ removal.* 2018.
63. Wang ChongChen, W.C., et al., *Photocatalytic organic pollutants degradation in metal-organic frameworks.* 2014.
64. Yang, X.-L., et al., *Selective dual detection of H2S and Cu2+ by a post-modified MOF sensor following a tandem process.* 2021. **403**: p. 123698.
65. Ahmadijokani, F., et al., *Ethylenediamine-functionalized Zr-based MOF for efficient removal of heavy metal ions from water.* 2021. **264**: p. 128466.
66. Gomes Silva, C., et al., *Water stable Zr–benzenedicarboxylate metal–organic frameworks as photocatalysts for hydrogen generation.* 2010. **16**(36): p. 11133-11138.
67. Fateeva, A., et al., *A water-stable porphyrin-based metal–organic framework active for visible-light photocatalysis.* 2012. **124**(30): p. 7558.
68. Xiao, J.D., et al., *Boosting photocatalytic hydrogen production of a metal–organic framework decorated with platinum nanoparticles: the platinum location matters.* 2016. **55**(32): p. 9389-9393.
69. Li, R., et al., *Integration of an inorganic semiconductor with a metal-organic framework: a platform for enhanced gaseous photocatalytic reactions.* 2014. **26**(28): p. 4783-4788.
70. Nguyen, K.D., et al., *New 1D chiral Zr-MOFs based on in situ imine linker formation as catalysts for asymmetric CC coupling reactions.* 2020. **386**: p. 106-116.
71. Qiao, L., L. Zhao, and K.J.C.E.J. Du, *Construction of hierarchically porous chitin microspheres via a novel Dual-template strategy for rapid and High-capacity removal of heavy metal ions.* 2020. **393**: p. 124818.
72. Liu, J., et al., *Simple synthesis of magnetic porous organic cages for adsorption of triphenylmethane dyes in aquatic products.* 2020. **158**: p. 105275.

Journal of Computational and Experimental Science (JCES)
ISSN Print: XXXX | ISSN Online: XXXX
Volume 1, Number 1, 2026, Pages 76-88
Journal Home Page: https://journals.airsd.org/index.php/jces

Hybrid Plasmonic Modes In Graphene-Loaded Waveguide Surrounded By Insb And Magnetized Plasma Layers

Sanam saleem[1], Maham Nadeem[1], Abdul Ghaffar[1*], Muhammad Umair[1*]

[1] Department of Physics, University of Agriculture, Faisalabad, Pakistan

ARTICLE INFO

Article History:
Received: April 15, 2026
Revised: May 17, 2026
Accepted: June 05, 2026
Available Online: June 11, 2026

Keywords:
Plasmonic Modes, Graphene, Waveguide, Magnetized Plasma, Temperature Sensitive Material

Corresponding Author:
Muhammad Umair
Email: rumair.uaf@gmail.com
Abdul Ghaffar
Email: aghaffar16@uaf.edu.pk

ABSTRACT

In this paper, hybrid plasmonic modes are theoretically investigated in a graphene-loaded waveguide surrounded by indium antimonide (InSb) and magnetized plasma layers operating in the GHz frequency regime. The dispersion relation is derived using transfer matrix technique and the conductivity of graphene is modeled using the Kubo formalism. Hybrid plasmon modes are observed due to the presence of anisotropic plasma. The influence of material parameters such as chemical potential (μ_c), cyclotron frequency (ω_c), plasma frequency (ω_p), relaxation time (τ), number of graphene layers (N), and temperature (T) on effective mode index (EMI) and graphene's conductivity are numerically analyzed. Numerical results show that the variations in graphene's chemical potential and relaxation time significantly influence the EMI and cutoff frequencies. Higher chemical potential (μ_c) increases the cutoff frequency and enhances plasmonic coupling. Furthermore, tensorial permittivity of magnetized plasma parameters i.e., cyclotron frequency and plasma frequency play crucial role in modulating the dispersion curves and shift the plasmonic frequencies. The temperature-dependent permittivity of InSb provides an additional degree of freedom for tuning electromagnetic (EM) wave propagation. These findings may have potential applications in tunable plasmonic devices, optical devices related to surface plasmon polaritons (SPPs) by using plasma, and thermal photonic devices.

Introduction

With the rapid advancement in optical techniques, there is a continuous exploration for the integration of highly efficient photonic technologies intended for data transmission and communication systems [1]. These optical technologies include silicon photonics, lithium niobate photonics, indium phosphide photonics, and plasmonics [2, 3]. The rate of data transmission increases by reducing the element size of the photonic devices up to the nanometer (nm) scale. However, it becomes very difficult for conventional photonic devices to reduce the element size up to nanometer scale due to diffraction limit of light [4]. Plasmonics has emerged as a highly promising solution by the excitation of surface plasmon polaritons (SPPs), for next generation electronic-photonic integration, due to its ability to confine and manipulate light below the diffraction limit. These exceptional features of SPPs allow the integration of ultra-compact devices with high speed data transfer capacity, low energy consumption, and enhanced bandwidth. SPPs have become a promising candidate for light sources to control the propagation and dispersion of light at nanometer scale [5]. SPPs are characterized by strong field confinement close to the interface [6, 7].

Subwavelength confinement of SPPs offers an effective way to promote photonics and chip electronics technology in which light signals propagate in nanophotonic devices at optical frequency regime. Plasmonic technology undergoes a revolution by the emergence of 2D optical materials that offers new ideas to explore photonic and electronic properties [8]. Graphene has attracted significant scientific attention due to its exceptional physical properties, exhibiting promising potential for applications in optoelectronic and nano-electronic devices. Graphene exhibits ultra-high electron mobility, gate-variable optical conductivity, and ultrafast relaxation time for photo-excited carriers [9]. Graphene also possesses incredible optical properties such as strong light-matter interaction, high speed and broadband operation etc [10]. Graphene is an outstanding candidate for designing tunable optical devices that operates in both optical and GHz frequency ranges due to its tunable conductivity and charge carrier density. Moreover, the tunable conductivity of graphene opens new doors for tunable optical sensors, tunable GHz absorber, and tunable metamaterials [11, 12]. Graphene provides a way for controlling the optical bistability by appropriately varying the applied voltage [13]. Graphene plasmon polaritons show strong field confinement as well as relatively long propagation distance as compared to plasmon polaritons in noble metals [14]. A lot of research has been conducted on graphene and isotropic materials. However, isotropic materials lack polarization sensitivity and less control over dispersion characteristics.

The efficiency of graphene-based devices can be enhanced by integrating them with magnetized plasma. Plasma, when integrated with graphene exhibits exceptional characteristics. Generally, plasma is considered to be unmagnetized when no external magnetic field is applied [15] but as the external magnetic field is applied, an anisotropic behavior is induced in plasma. This behavior is used to manipulate the SPPs, offering a greater control compared to unmagnetized plasma [16]. Numerous theoretical investigations have highlighted the role of plasma medium to study the characteristics of SPPs [17-26]. Xu et al. analyzed experimentally and theoretically the wavelength of SPPs at the dielectric-plasma interface [27]. Shahmansouri et al. examined the collective excitation of SPs in a massless Dirac plasma by using a relativistic quantum fluid model [28]. Furthermore, plasma-based waveguide offers a novel approach to nanophotonic devices. Plasmonic modes in graphene-loaded waveguide surrounded by InSb and magnetized plasma layers have not been explored in the existing literature.

The objective of this study is to theoretically model graphene-loaded waveguide surrounded by magnetized plasma and indium antimonide (InSb) for thermal control of SPPs. Indium antimonide (InSb), a small bandgap semiconducting material has emerged as a temperature sensitive material in the field of plasmonics and nano-photonics, which can significantly guide the SPPs at various temperatures [29]. Optical properties of InSb are highly responsive to temperature variations, making it an ideal candidate for GHz technology [29-31]. Furthermore, InSb can be fabricated with standard fabrication techniques which make it easier to incorporate into practical devices. In the present study, we will investigate the impact of material parameters by plotting dispersion relation to compute effective mode index (EMI) and graphene's conductivity in the interested frequency regime. The proposed geometry will allow strong light-matter coupling, enhance field confinement, and tunable plasmon modes which will lead towards highly efficient optical devices.

Methodology

The theoretical modelling of the graphene-loaded waveguide surrounded by magnetized plasma and InSb is presented in this section. Figure 1 illustrates the propagation of EM waves along z-direction.

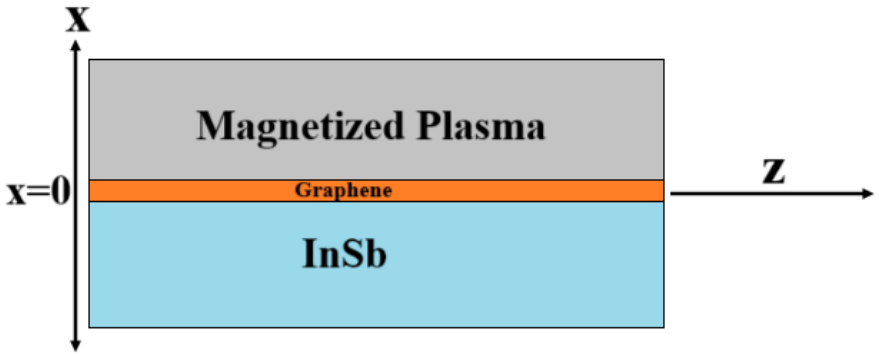

Figure 1: schematic view of graphene-loaded waveguide surrounded by InSb and magnetized plasma.

Graphene's conductivity is modelled using the Kubo formula.

$$\sigma(g) = \frac{ie^2(\omega - j2\tau)}{\pi\hbar^2} \times \left[\frac{1}{(\omega - j2\tau)^2} \int_0^\infty \xi_{en} \times \left(\frac{\partial f_d(\xi_{en})}{\partial \xi_{en}} - \frac{\partial f_d(-\xi_{en})}{\partial \xi_{en}} \right) d\xi_{en} - \int_0^\infty \frac{f_d(-\xi_{en}) - f_d(\xi_{en})}{(\omega - j2\tau)^2 - 4\left(\frac{\xi_{en}}{\hbar}\right)^2} d\xi_{en} \right] \quad 1$$

$f_d(\xi_{en}) = \left(e^{(\xi_{en} - \mu_c)/K_B T} + 1\right)^{-1}$ is the Fermi-Dirac distribution. where μ_c, τ, T, e, K_B, ω, ξ_{en} and $\hbar$ are chemical potential, relaxation rate, temperature, charge on electron, Boltzmann's constant, operating frequency, energy, and reduced Plank's constant, respectively [32].

Magnetized plasma has the following constitutive relations:

$$D = \varepsilon_0 \bar{\bar{\varepsilon}} E \quad 2$$

$$H = 1/\mu_0 B \quad 3$$

μ_0 and ε_0 represent the permeability and permittivity of free space, respectively, and $\bar{\bar{\varepsilon}}$ is the tensorial permittivity tensor for anisotropic plasma.

$$[\bar{\bar{\varepsilon}}] = \begin{bmatrix} \varepsilon_1 & -i\varepsilon_2 & 0 \\ i\varepsilon_2 & \varepsilon_1 & 0 \\ 0 & 0 & \varepsilon_3 \end{bmatrix} \quad 4$$

Where, ε_1, ε_2 and ε_3 represent the tensorial permittivity of plasma medium as reported in [19] and $\varepsilon_1 = \varepsilon_0\left(1 - \frac{(\omega_p)^2}{(\omega)^2 - (\omega_c)^2}\right)$, $\varepsilon_2 = \varepsilon_0\left(\frac{\omega_c * (\omega_p)^2}{\omega * ((\omega)^2 - (\omega_c)^2)}\right)$, $\varepsilon_3 = \varepsilon_0\left(1 - \frac{(\omega_p)^2}{(\omega)^2}\right)$, $\omega_p = \sqrt{\frac{ne^2}{m\,\varepsilon_0}}$, $\omega_c = \frac{eB}{m}$. ω_c, ω_p represent the cyclotron frequency and plasma frequency [17]. $e, B, m, n,$ and ε_0 represent the electron charge, magnetic field, electron mass, number density of electrons, and permittivity of free space, respectively [33]. The wave equation for H_z and E_z in the magnetized plasma are as follows [16]:

$$[\nabla^2 E_{z1}\ \nabla^2 H_{z1}] + [U_1\ iU_2\ iU_3\ U_4][E_{z1}\ H_{z1}] = 0 \quad 5$$

Where,

$$\nabla = \hat{e}_x \frac{\partial}{\partial x} + \hat{e}_y \frac{\partial}{\partial y} + \hat{e}_z \frac{\partial}{\partial z} \quad 6$$

$$U_1 = -\left(\frac{\beta^2 \varepsilon_3}{\varepsilon_1} - \omega^2 \mu_0 \varepsilon_3\right) \quad 7$$

$$U_2 = \frac{\omega \mu_0 \beta \varepsilon_2}{\varepsilon_1} \quad 8$$

$$U_3 = -\beta \omega \varepsilon_2 \frac{\varepsilon_3}{\varepsilon_1} \quad 9$$

$$U_4 = \frac{(\omega^2 \mu_0 \varepsilon_1^2 - \omega^2 \mu_0 \varepsilon_2^2)}{\varepsilon_1} - \beta^2 \quad 10$$

Where, β and μ_0 denote the propagation constant and permeability of free space, respectively. Model fields for magnetized plasma are given as:

$$E_{z1} = (A_1 e^{-q_1 x} + A_2 e^{-q_2 x}) e^{-i\beta z} \quad 11$$

$$H_{z1} = i(A_1 \alpha_1 e^{-q_1 x} + A_2 \alpha_2 e^{-q_2 x})\, e^{-i\beta z} \quad 12$$

The remaining magnetized plasma field components can be derived from [34].

$$E_t = ia\nabla_t E_z + b\nabla_t E_z \times a_z + c\nabla_t H_z + id\nabla_t H_z \times a_z \quad 13$$

$H_t = e\nabla_t E_z + if\nabla_t E_z \times a_z + ia\nabla_t H_z + b\nabla_t H_z \times a_z$ 14

Where a, b, c, d, e and f are given by [16]

$a = \frac{U_3\omega\mu_0\varepsilon_2 - U_4\beta\varepsilon_3}{\varepsilon_1(U_1U_4+U_2U_3)}$ 15

$b = -\frac{U_3\omega\mu_0}{U_1U_4+U_2U_3}$ 16

$c = -\frac{U_1\omega\mu_0\varepsilon_2+U_2\beta\varepsilon_3}{\varepsilon_1(U_1U_4+U_2U_3)}$ 17

$d = -\frac{U_1\omega\mu_0}{U_1U_4+U_2U_3}$ 18

$e = -\frac{U_3\beta}{(U_1U_4+U_2U_3)}$ 19

$f = \frac{U_4\omega\varepsilon_3}{(U_1U_4+U_2U_3)}$ 20

The eigenvalues are:

$k_1 = \sqrt{\frac{1}{2}(U_1+U_4)+\frac{1}{2}\sqrt{(U_1-U_4)^2-4U_2U_3}}$ 21

$k_2 = \sqrt{\frac{1}{2}(U_1+U_4)-\frac{1}{2}\sqrt{(U_1-U_4)^2-4U_2U_3}}$ 22

The associated eigen functions describe the hybrid nature of SPPs:

$q_1 = \sqrt{\beta^2 - {k_1}^2}$ 23

$q_2 = \sqrt{\beta^2 - {k_2}^2}$ 24

α_1 and α_2 describe hybrid mode factors [17].

$\alpha_1 = \frac{U_1-{q_1}^2}{U_2}$ 25

$\alpha_2 = \frac{U_1-{q_2}^2}{U_2}$ 26

InSb EM fields components are given as:

$E_{y2} = A_3\, e^{\gamma_1 x}$ 27

$H_{y2} = A_4\, e^{\gamma_1 x}$ 28

$E_{z2} = \frac{i\gamma_1}{\omega\varepsilon_{InSb}}(A_4 e^{\gamma_1 x})$ 29

$H_{z2} = -\frac{i\gamma_1}{\omega\mu_0}(A_3 e^{\gamma_1 x})$ 30

Where, $\varepsilon_{InSb} = \varepsilon_\infty - \frac{\omega_p^2}{\omega^2+i\gamma\omega}$, ω_p describe the plasma frequency, $\omega_p = \sqrt{\frac{nq^2}{0.015\varepsilon_0 m_e}}$, $q = -1.60\times10^{-19}C$ charge on electron, $m_e = 9.11\times10^{-31}$ kg electron mass, relative permittivity $\varepsilon_\infty = 15.68$, damping constant $\gamma = \pi\times10^{11}\ rad\ s^{-1}$, carrier density $n = 5.76\times10^{20}T^{\frac{3}{2}}exp(-\frac{E_g}{2K_BT})$, where E_g is the bandgap of value $E = 0.26eV$ and K_B is Boltzmann constant, $K_B = 8.62\times10^{-5}\ eV\ K^{-1}$. $\gamma_1 = \sqrt{\beta^2-\omega^2\varepsilon_{InSb}\mu_0}$ is permittivity of InSb medium [29].

In all calculation $e^{-i\beta z}$ is omitted. A_1, A_2, A_3 and A_4 are amplitudes constant. Using anisotropic plasma and InSb fields components following boundary conditions are applied.

$\hat{x}\times(H_1 - H_2) = \sigma E$ 31

$\hat{x}\times(E_1 - E_2) = 0$ 32

Where, σ is the graphene's surface conductivity

The obtained dispersion relation is:

$$i\Big(\gamma_1\big(\mu_0\omega q_1(f+b\alpha_1)\alpha_2-(b^2+df)(-i\mu_0\sigma\omega+\gamma_1)q_1q_2(-\alpha_1+\alpha_2)-\mu_0\omega q_2\alpha_1(f+b\alpha_2)\big)-(\varepsilon_{InSb}\omega+i\sigma\gamma_1)\big((-i\mu_0\sigma\omega+\gamma_1)q_1(b-d\alpha_1)+\mu_0\omega(\alpha_1-\alpha_2)-(-i\mu_0\sigma\omega+\gamma_1)q_2(b-d\alpha_2)\big)\Big)=0 \quad (33)$$

Results and Discussion

In this section, numerical analysis of proposed planar structure is analyzed in the interested frequency region. The numerical analytical results are discussed by using dispersion relation 33. The results are examined by computing dispersion curves, effective mode index (EMI), and conductivity of graphene as a function of GHz frequency to observe the behavior of SPPs. Two types of SPPs modes i.e., lower, and higher mode confirm hybrid nature of plasma medium. In all calculations the numerical parameters are set as: ω_c=6 *THz*, ω_p=2×10^{13}Hz, T=280K, τ=8ps and μ_c=0.3*eV*. Figure 2 presents the EMI as the function of incident wave frequency (GHz), for different values of chemical potential (μ_c). The chemical potential in graphene controls the position of the Fermi level, which in turn affects the charge carrier concentration [35-38]. In lower frequency mode, the EMI increases rapidly with frequency for all values of the chemical potential. For highest chemical potential i.e., μ_c=0.9 *eV*, EMI increases more steeply and reaches higher values, implying stronger coupling and enhanced mode confinement. At lowest chemical potential μ_c=0.1 *eV*, the increase in the EMI is less pronounced, meaning weaker coupling and less confinement. At lower frequencies, the chemical potential directly impacts the carrier density in graphene, which governs the plasma frequency. At higher frequencies, the chemical potential has less influence on the effective mode index. This is because the graphene behavior shifts from plasmonic response to more dielectric-like response. The increase in effective mode index becomes less sensitive to changes in chemical potential as the frequency rises above the plasmon resonance. In the high-frequency region, the plasmonic effects diminish, and the graphene's behavior is more influenced by its dielectric properties rather than its conductivity. As a result, the EMI starts to stabilize. Hence graphene's response at these higher frequencies is less dependent on chemical potential. Lower mode is beneficial for plasmonic devices, communication systems, and GHz sensors, where the chemical potential in graphene can be tuned to control mode confinement and enhance signal propagation. In case of higher propagating mode, as the frequency increases, the EMI increases with the increase in incident wave frequency. Figure 3 depicts the variation in EMI versus incident wave frequency under different values of relaxation time. In case of lower propagating mode, for lowest value of relaxation time, the EMI increases quickly and reaches higher values as reported in [39, 40]. This is because shorter relaxation times lead to higher carrier scattering rates, which results in stronger plasmonic effects and thus a stronger mode confinement. As the relaxation time is increased, the dispersion curves moves towards lower frequency region. In case of higher propagating mode, the EMI increase with increasing relaxation time but the effect of relaxation time disappears at higher frequency values indicating non-physical region which has no significance in scientific community. Additionally, higher relaxation time shift the dispersion curves to lower cutoff frequencies in both propagating modes which is validated from the literature [38].

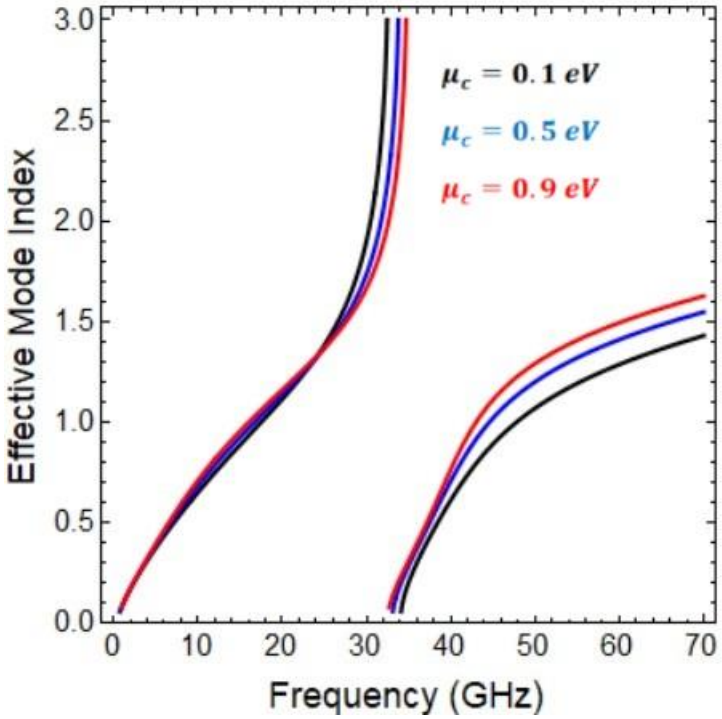

Figure 2: Influence of graphene's chemical potential on EMI versus GHz frequency.

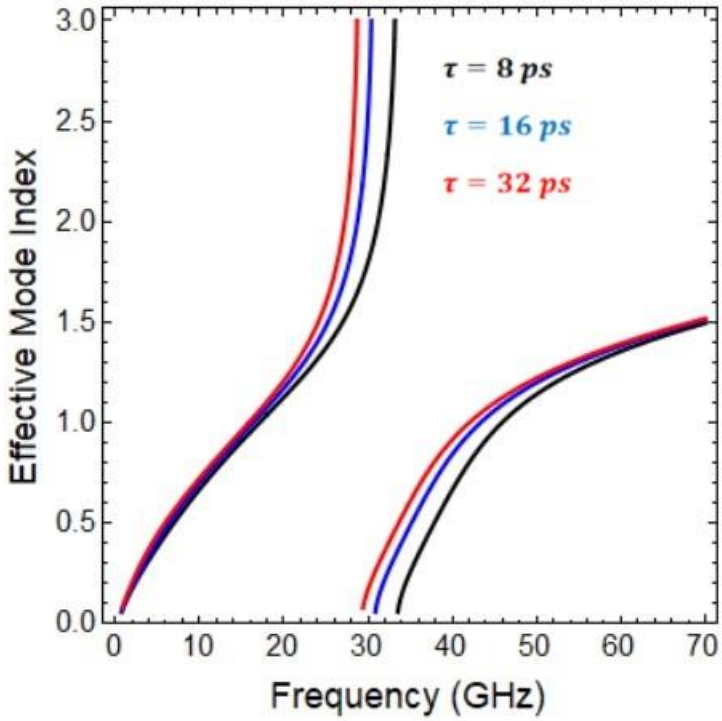

Figure 3: Influence of graphene's relaxation time on EMI versus GHz frequency.

The dependence of EMI on number of graphene layers as a function of incident wave frequency is depicted in figure 4. In case of lower mode, the EMI increases steeply with frequency for all values of N. For N=1, the increase in the EMI is the steepest, indicating stronger coupling and tighter mode confinement. Because single layer graphene has higher surface-to-volume ratio, which results in stronger plasmonic effects enable high-speed communication systems like fiber optics or microwave photonics and increasing N changes the modal coupling and field distribution. The electromagnetic waves interact more strongly

with the charge carriers in the graphene, leading to better mode confinement and higher effective mode index. The EMI increases with increasing incident wave frequency as the number of graphene layer increase. For upper propagating mode, the EMI increases as a function of incident wave frequency as the number of graphene layers is increased. It is also observed that the frequency band start squeezing as the number of graphene layers are increased. These tunable features of graphene may be useful for future fabrication of nano-photonic devices in the plasmonic community [41].

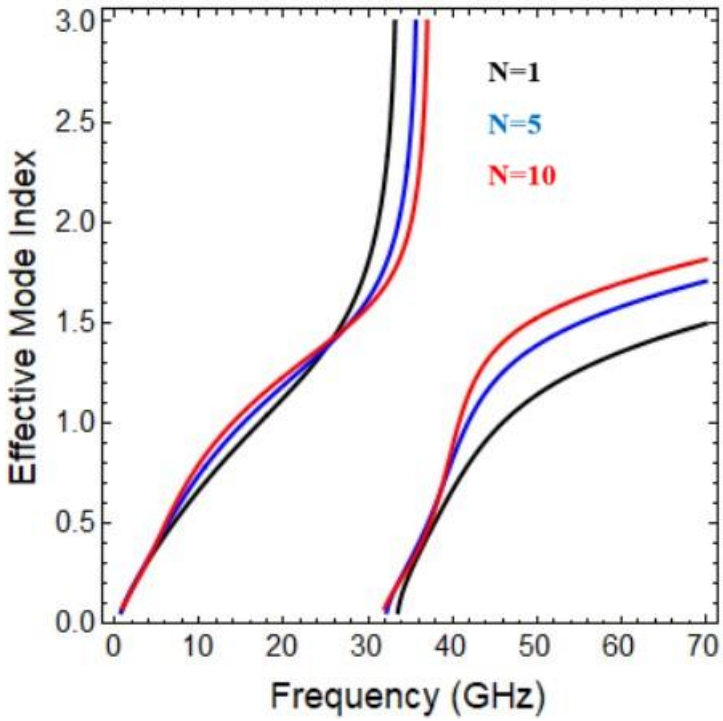

Figure 4: Influence of graphene's layers on EMI versus GHz frequency.

The influence of plasma frequency on EMI versus incident wave frequency is analyzed in figure 5. For lower propagating mode, the EMI increases with frequency for all values of ω_p, indicating that the plasmonic modes became more confined. Increasing plasma frequency modifies the tensor permittivity components which strengthen electromagnetic confinement. It is observed that when the plasma frequency increases, EMI increases and the curves move towards lower frequency regime. The plasma frequency is a function of number density of electrons which exhibits significant role in tunable plasmon modes. It is of peculiar of interest to note that at lower frequencies (below ~20 GHz), the EMI increases slowly. Consequently, at lower frequencies, the plasma's effect on the waveguide is less significant, and the wave propagates more freely. When the frequency increases over 20 GHz, there is drastic increase in EMI. This shows that the plasma influence becomes more pronounced as the frequency increases, leading to stronger confinement of SPPs. The EMI increases with increasing plasma frequency as a function of incident wave frequency for higher propagating mode. The understanding of the behavior of plasmonic modes is crucial to design plasmonic waveguides. These results offer promising potential for designing tunable high frequency waveguides and are consistent with literature [40]. Figure 6 illustrates the effect of cyclotron frequency on EMI as a function of incident wave frequency. In lower propagating mode, the EMI curves rises rapidly at low cyclotron frequency. As the cyclotron frequency rises, the corresponding EMI curve increases smoothly with increasing wave frequency and the propagating mode bandgap start squeezing. Moreover, the effect of cyclotron frequency disappears after 30 GHz and the region become non-significant region. The EMI start decreasing with increasing value of incident wave frequency, as the

cyclotron frequency increases. This behavior is crucial for GHz plasmonic applications where precise control of wave propagation is important for improving the device performance.

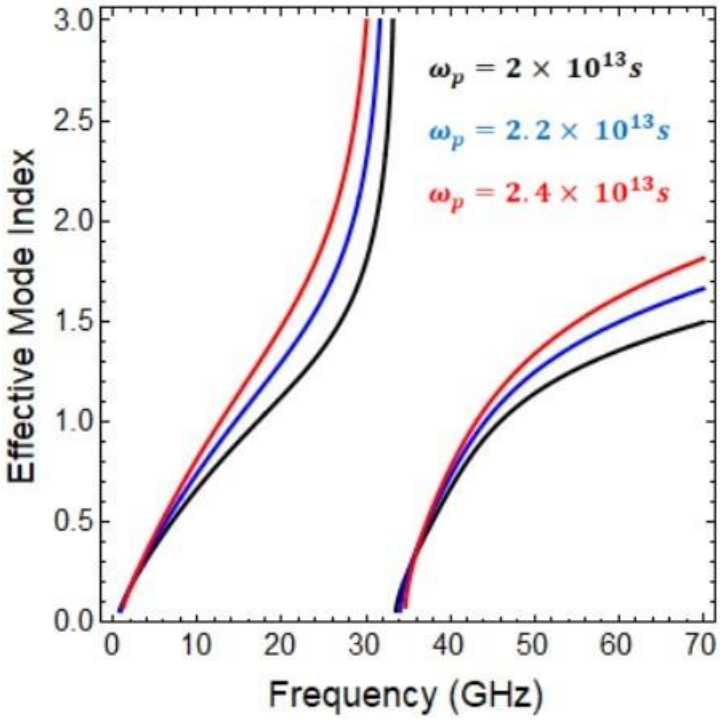

Figure 5: Influence of plasma frequency on EMI versus GHz frequency.

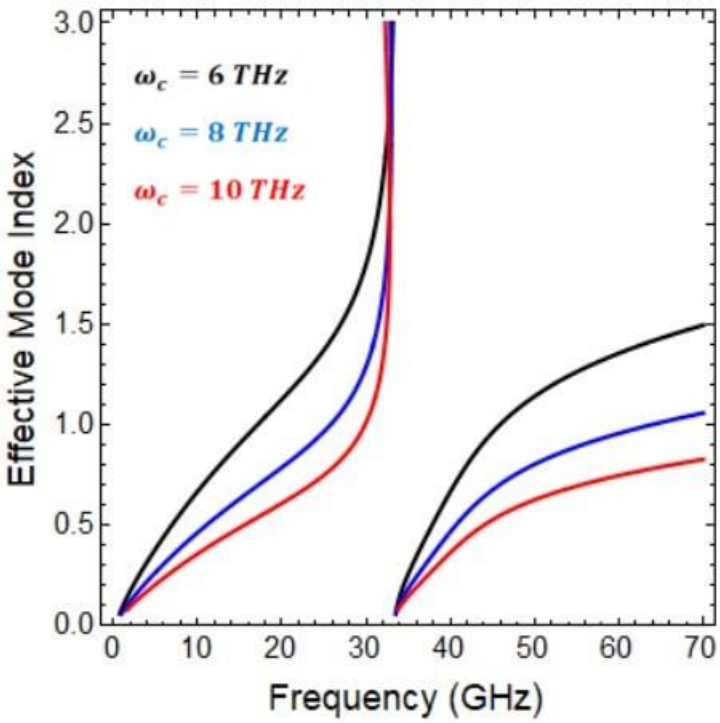

Figure 6: Influence of cyclotron frequency on EMI versus GHz frequency.

The influence of InSb temperature on EMI as a function of incident frequency is illustrated in figure 7. In lower propagating mode, as the temperature of InSb increases, the corresponding EMI curve shifts towards higher frequency region. Temperature variation modifies the carrier concentration and mobility in InSb, which in turn alters its plasma frequency and effective permittivity. The temperature of InSb exhibits

strong influence on upper propagating mode, EMI increases as the temperature increases and the bandgap starts squeezing. This behavior is important for thermo-plasmonic applications where the temperature dependence of plasmonic properties is critical. Higher values of temperature lead towards strong plasmon coupling and higher energy excitation in plasmonic devices, which affect their performance in applications, such as sensing and imaging. This temperature sensitivity plays an important role in system efficiency and response. The variation in surface conductivity of graphene versus GHz waves frequency under different plasma frequencies is analyzed in figure 8. As the plasma frequency of the magnetized plasma increases, there is a sharp increase in conductivity and the curves shifts towards lower frequency region. Additionally, the frequency band of both modes begins to squeeze as the plasma frequency increases. The conductivity of graphene sharply decreases near the plasma frequency of the magnetized plasma, making it valuable for applications such as graphene-based metamaterials. The dependence of graphene's conductivity under different cyclotron frequencies is studied in figure 9. As the cyclotron frequency increases, the conductivity increases and curves shifts towards higher frequency region. This is because the interaction between the electrons in graphene and the electromagnetic field becomes more pronounced at higher cyclotron frequencies. Plasma characteristics have strong influence on the modulation and propagation of hybrid SPPs for the proposed geometry which can be utilized for potential applications such as nanophotonic and optoelectronic devices in GHz frequency regime. Figure 10 demonstrated how InSb temperature influences the interaction between the incident wave and the graphene's conductivity. As the temperature of InSb increases, it influences the graphene's conductivity by affecting the electron mobility and the interaction between graphene and electromagnetic waves. Higher temperatures typically lead to increased electron scattering, which reduces the conductivity of graphene. Based on numerical results, it can be inferred that temperature-sensitive sensors can be developed by leveraging the variation in graphene's conductivity to detect temperature changes in the surrounding environment.

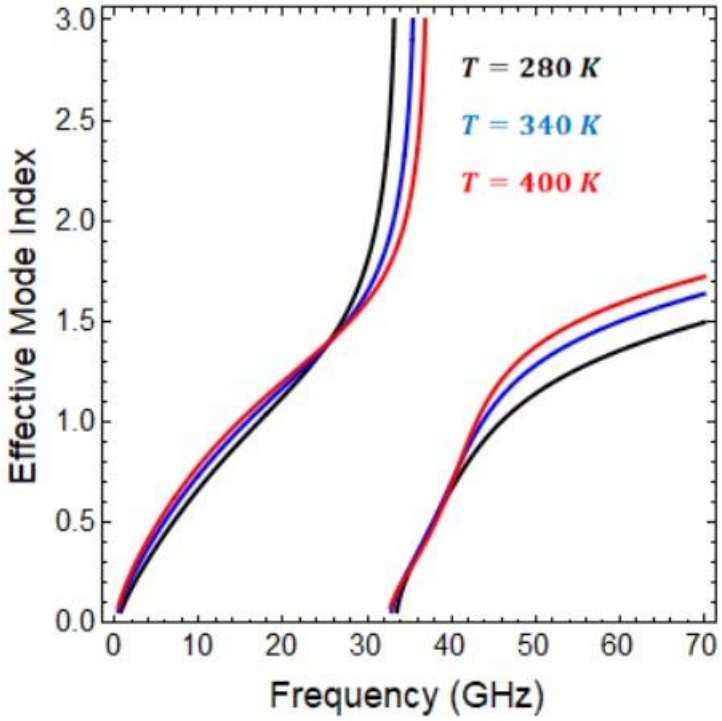

Figure 7: Influence of InSb temperature on EMI versus GHz frequency.

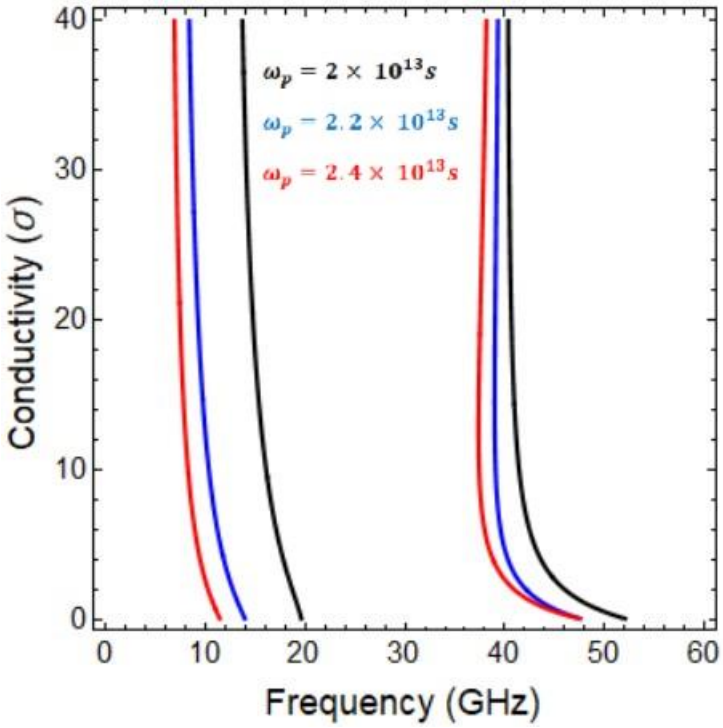

Figure 8: Influence of plasma frequency on graphene's conductivity versus GHz frequency.

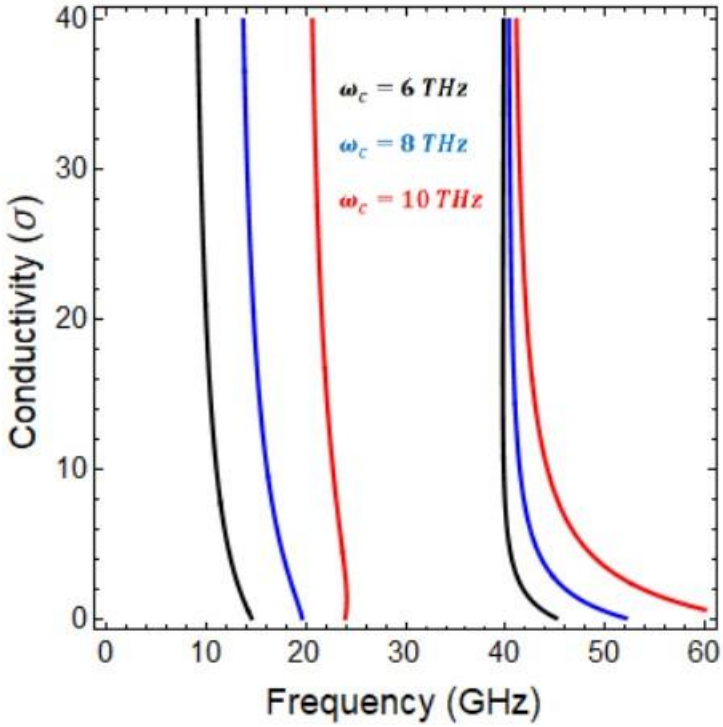

Figure 9: Influence of cyclotron frequency on graphene's conductivity versus GHz frequency.

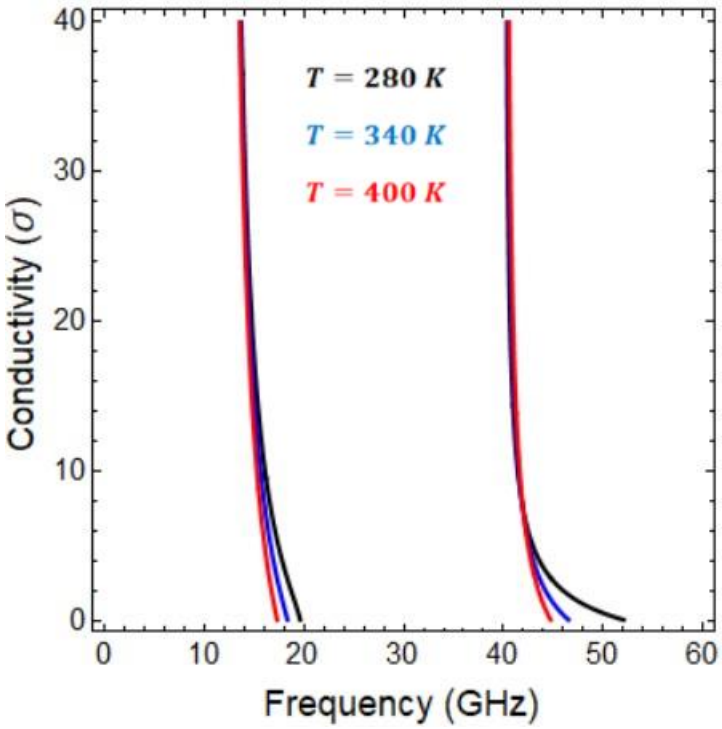

Figure 10: Influence of InSb temperature on graphene's conductivity versus GHz frequency.

Conclusion

This study presented a theoretical model to analyze the hybrid plasmonic modes in graphene-loaded waveguide surrounded by InSb and magnetized plasma. The extended wave theory is used to derive the electromagnetic (EM) field components and transfer matrix technique is used to obtain the dispersion relation. The conductivity of graphene is modeled using Kubo formula. The influence of chemical potential, relaxation time, number of graphene layers, plasma frequency, cyclotron frequency, and InSb temperature on effective mode index and graphene's conductivity is analyzed numerically. Based on the numerical results, the material parameters reveal significant insights into the SPPs properties. Due to the anisotropic nature of the magnetized plasma, two plasmon modes (lower and upper modes) are observed which exhibit different behaviors in lower and higher frequency regions. Moreover, the influence of material parameters on effective mode index and graphene's conductivity highlights the sensitivity of SPPs in the interested frequency regime. The present work offers promising potential for application in high performance and tunable plasmonic devices, including optical modulators, tunable plasmonic antennas, GHz sensors, and thermal photonic devices.

Funding: Funding is inappropriate for this research study.
Data availability: The statistics supporting the outcomes of this research are accessible upon reasonable request from the first author.

Declarations

Ethical approval: Not applicable
Consent to participate: Not applicable
Consent to publish: All authors have given consent to publish.
Competing interest: The authors have no competing interests to declare.

References

1. Li, K., et al., *Electronic–photonic convergence for silicon photonics transmitters beyond 100 Gbps on–off keying.* Optica, 2020. **7**(11): p. 1514-1516.
2. Chen, P.-K., et al., *Adapted poling to break the nonlinear efficiency limit in nanophotonic lithium niobate waveguides.* Nature Nanotechnology, 2024. **19**(1): p. 44-50.
3. Haffner, C., et al., *All-plasmonic Mach–Zehnder modulator enabling optical high-speed communication at the microscale.* Nature Photonics, 2015. **9**(8): p. 525-528.
4. Li, K., et al., *An integrated CMOS–silicon photonics transmitter with a 112 gigabaud transmission and picojoule per bit energy efficiency.* Nature Electronics, 2023. **6**(11): p. 910-921.
5. Elshaari, A.W., et al., *Hybrid integrated quantum photonic circuits.* Nature photonics, 2020. **14**(5): p. 285-298.
6. Schröter, U. and A. Dereux, *Surface plasmon polaritons on metal cylinders with dielectric core.* Physical Review B, 2001. **64**(12): p. 125420.
7. Zhang, J., L. Zhang, and W. Xu, *Surface plasmon polaritons: physics and applications.* Journal of Physics D: Applied Physics, 2012. **45**(11): p. 113001.
8. Umair, M., et al., *Tunability of plasmon modes at uniaxial chiral–black phosphorus planar structure.* Plasmonics, 2024: p. 1-9.
9. Novoselov, K.S., et al., *Electric field effect in atomically thin carbon films.* science, 2004. **306**(5696): p. 666-669.
10. Castro Neto, A.H., et al., *The electronic properties of graphene.* Reviews of modern physics, 2009. **81**(1): p. 109-162.
11. Liu, M., et al., *A graphene-based broadband optical modulator.* Nature, 2011. **474**(7349): p. 64-67.
12. Bonaccorso, F., et al., *Graphene photonics and optoelectronics.* Nature photonics, 2010. **4**(9): p. 611-622.
13. Xiang, Y., et al., *Tunable optical bistability at the graphene-covered nonlinear interface.* Applied Physics Letters, 2014. **104**(5).
14. Xiao, S., et al., *Graphene-plasmon polaritons: From fundamental properties to potential applications.* Frontiers of Physics, 2016. **11**(2): p. 117801.
15. Umair, M., et al., *Modelling of Surface Plasmon Polaritons (SPPs) in Magnetized Plasma-Graphene-PEMC Interfaces.* Plasmonics, 2025: p. 1-8.
16. Umair, M., et al., *Plasmonic modes of metallic slab in anisotropic plasma environment.* Plasmonics, 2023. **18**(5): p. 1857-1864.
17. Ali, M., et al., *Study of hybrid surface Plasmon modes in metallic circular waveguide filled with magnetized plasma.* Waves in Random and Complex Media, 2022. **32**(1): p. 449-462.
18. Ali, R., B. Zamir, and H. Shah, *Transverse electric surface waves in a plasma medium bounded by magnetic materials.* Results in physics, 2018. **8**: p. 243-248.
19. Alkanhal, M.A., et al., *Propagation of hybrid surface waves in ferrite anisotropic plasma planar structures.* Optik, 2021. **229**: p. 166255.
20. Ivanov, S. and N. Nikolaev, *Magnetic-field effect on wave dispersion in a free semiconductor plasma slab.* Journal of Physics D: Applied Physics, 1999. **32**(4): p. 430.
21. Shaban, M., et al., *Plasmonic characteristics of LiF filled slab waveguide in isotropic plasma environment.* Plasmonics, 2024: p. 1-7.
22. Shaban, M., et al., *Tunable characteristics of light plasmon coupling in Lithium Fluoride (LiF) sandwiched waveguide structure bounded by plasma and graphene layers.* Plasmonics, 2024: p. 1-7.
23. Umair, M., et al., *Transverse electric surface waves in ferrite medium surrounded by plasma layers.* Journal of the European Optical Society-Rapid Publications, 2020. **16**: p. 1-6.

24. Umair, M., et al., *Dispersion characteristics of hybrid surface waves at chiral-plasma interface.* Journal of Electromagnetic Waves and Applications, 2021. **35**(2): p. 150-162.
25. Yaqoob, M., et al., *Electromagnetic scattering from perfect electromagnetic conductor cylinders placed in magnetized plasma medium.* Optoelectronics and Advanced Materials-Rapid Communications, 2014. **8**(November-December 2014): p. 1150-1156.
26. Zamir, B. and R. Ali, *Characteristics of TE surface waves in a plasma medium bounded by nonlinear metamaterials.* Journal of the Korean Physical Society, 2018. **72**: p. 1166-1173.
27. Xu, X., et al., *Visual phenomena of surface plasmon polaritons at the dielectric-plasma interface.* Applied Physics Letters, 2008. **92**(1).
28. Shahmansouri, M., R. Aboltaman, and A. Misra, *Surface plasmons in a semi-bounded massless Dirac plasma.* Physics Letters A, 2018. **382** (32): p. 2133-2136.
29. Yaqoob, M., et al., *Thermally tunable electromagnetic surface waves supported by graphene loaded indium antimonide (InSb) interface.* Scientific Reports, 2023. **13**(1): p. 18631.
30. Sajid, M., et al., *Modeling of graphene wrapped indium antimonide nanowire as thermo-optical waveguide.* Materials Research Express, 2025. **12**(3): p. 036201.
31. Zhang, C., et al., *Design of a highly sensitive terahertz temperature and refractive index composite sensor based on an InSb–Ag composite grating.* Journal of the Optical Society of America B, 2024. **41**(2): p. 411-420.
32. Falkovsky, L. and A. Varlamov, *Space-time dispersion of graphene conductivity.* The European Physical Journal B, 2007. **56**: p. 281-284.
33. Umair, M., et al., *Characteristics of Plasmon Mode at Anisotropic Plasma–Black Phosphorene Interface.* Plasmonics, 2024: p. 1-8.
34. Gong, J., *Electromagnetic wave propagation in a chiroplasma-filled waveguide.* Journal of plasma physics, 1999. **62**(1): p. 87-94.
35. Arif, M., et al., *Dispersion properties in uniaxial chiral–graphene–uniaxial chiral plasmonic waveguides.* Plasmonics, 2024: p. 1-10.
36. Mahal, A., et al., *Characteristics of Photon–Plasmon Coupling in Uniaxial Chiral Filled Slab Waveguide Bounded by Graphene Layers.* Plasmonics, 2025. **20**(3): p. 1473-1480.
37. Shaban, M., et al., *Light Plasmon Coupling in Graphene-Wrapped Cylindrical Waveguide Filled with Lithium Fluoride (LiF).* Plasmonics, 2025: p. 1-8.
38. Umair, M., et al., *Hybrid plasmon modes at chiroferrite-graphene interface.* Plasmonics, 2024. **19**(4): p. 2193-2199.
39. Azam, M., et al., *Dispersion characteristics of surface plasmon polaritons (SPPs) in graphene–chiral–graphene waveguide.* Waves in Random and Complex Media, 2021: p. 1-12.
40. Umair, M., et al., *Plasmonic characteristics of monolayer graphene in anisotropic plasma dielectric.* Plasmonics, 2024. **19**(3): p. 1165-1171.
41. Umair, M., et al., *Light plasmon coupling in planar chiroplasma–graphene waveguides.* Plasmonics, 2023. **18**(3): p. 1029-1035.

Journal of Computational and Experimental Science (JCES)
ISSN Print: XXXX | ISSN Online: XXXX
Volume 1, Number 1, 2026, Pages 89-103
Journal Home Page: https://journals.airsd.org/index.php/jces

OPTIMIZATION PERFORMANCE OF CYBERSECURITY WITHIN MULTI-MODAL CLOUD HEALTHCARE INDUSTRY BASED ON DEEP LEARNING TECHNIQUES

Muhammad Irfan Balouch[1], Syed Sohail Ahmed Shah[1*], Salman Qazi[1], Sana Nisar Shaikh[1]
[1] *Department of Computer Science, Faculty of Computing & Information Technology, Government College University Hyderabad*

ARTICLE INFO

Article History:
Received: April 28, 2026
Revised: May 10, 2026
Accepted: May 25, 2026
Available Online: June 18, 2026

Keywords:
Cybersecurity, Healthcare, Internet of Things (IoT), multi-modal, and cloud architectures

Corresponding Author:
Syed Sohail Ahmed Shah
Email:
sohailahmed.shah@gcuh.edu.pk

ABSTRACT

In next-generation medical systems, the amount of Internet of Things (IoT) devices, edge computing infrastructure, and multi-modal cloud architectures has increased significantly, making healthcare cybersecurity a global concern. Although healthcare organizations invest a lot in storing security measures, they are far more susceptible to the sophisticated cyber threats. More than 90% of them have experienced at least one cyberattack over the past few years, and between 2013 and 2023, ransomware attacks in the healthcare industry have seen a surge to unprecedented heights. There is an important gap in the current literature: current cybersecurity frameworks don't offer a unified, scalable, and efficient solution for securing real-time flows of data across the different layers of the IoT, across the shore (edge) clouds, and across the center (core) clouds in a multi-domain healthcare environment. The current models are either computation intensive or domain specific, with multi-modal healthcare architecture being under-protected. This study introduces a novel hierarchical Deep Neural Network (DNN) framework that can identify and block malicious activities in multi-area healthcare data flows. The framework is inspired by transfer learning, utilizing pre-trained edge cloud models and fusion is to an optimized center cloud model. A Capability List (CP List) access control mechanism is built-in to implement fine-grained data access policies. The proposed model is tested on the structured dataset of healthcare network security incidents from the simulated environments in 2024. The experimental results show that the proposed hierarchical DNN architecture can achieve the accuracy of 95% to 100% for training and testing in the unknown attack. Taking an average of 26.2% less training time than the independently trained center cloud models, the model needs just 6-8 epochs to train, whereas the standalone edge cloud model requires 35-40 epochs. The research has validated that the combination of hierarchical deep learning and cloud-based security systems can greatly improve threat detection and decrease computational load. To protect sensitive patient data, the use of hierarchical AI-driven security is recommended, as well as the standardization of multi-layer access control across all IoT, edge and cloud environments for policymakers and healthcare administrators.

1. INTRODUCTION

In the context of Information Technology (IT) and cloud computing, cybersecurity is one of the most critical issues facing organizations in a digitally integrated environment, especially in the healthcare industry. Cybersecurity is the application of technologies, processes, and organizational practices to protect computer systems, networks, programs, and data from unauthorized access, damage, theft, or disruption. Within the healthcare sector, it involves safeguarding Electronic Health Records (EHRs), communications between medical devices, clinical decision-making applications, and the substantial amounts of patient-sensitive information flowing across multi-cloud environments with IoT integration.

Cloud computing, with its five key building blocks: on-demand computing, elasticity, rapid adaptation, geographic independence, and cybersecurity, has ushered in a paradigm shift in the collection, storage, processing, and sharing of healthcare data. Cloud-based solutions are increasingly becoming a staple in the healthcare industry, with their three main service models, Infrastructure as a Service (IaaS), Platform as a Service (PaaS), and Software as a Service (SaaS), each presenting unique security challenges in shared resource environments, data sovereignty, and access control. The increased reliance on IoT medical devices, wearables, remote-monitoring sensors, and edge computing nodes compounds the security challenge by extending the attack surface beyond network perimeters to distributed, typically resource-constrained endpoints.

The larger picture of healthcare cybersecurity is characterized by a rapidly changing threat landscape, in which cyberattacks are becoming increasingly sophisticated and prevalent. In 2020, the United States spent $4.1 trillion on health care, accounting for 19.7% of its GDP, yet many medical errors are preventable and can be exacerbated by cyber incidents, which are a primary driver of patient harm. More than 90% of healthcare organizations have been victims of a cyberattack at least once, with a 71% increase in attacks from 2020 to 2023. Healthcare had the highest number of ransomware insurance claims among all economic sectors from 2013 to 2023, underscoring its importance as a high-value target for attackers. Healthcare systems are becoming multi-domain, multi-layer environments where the traditional perimeter security approach is simply not enough due to the convergence of cloud, IoT, and big data. They have edge computing nodes, known as shore clouds, which process data close to the source to minimize latency and facilitate real-time clinical response, and central clouds for storing large-scale data, data analysis, and administrative work. The interdependence of these layers introduces intricate dataflow paths that are highly vulnerable to man-in-the-middle attacks, payload tampering, unauthorized data exfiltration, and service disruption.

Despite the extensive research in the areas of cloud security, IoT protection, and intrusion detection, a fundamental research challenge remains: the lack of a single cybersecurity framework using Deep Learning that supports the security needs of IoT gateways, shore cloud environments, as well as central cloud infrastructures, and is computationally efficient and scalable. Current frameworks tend to focus on a single level of security and apply the same approach to endpoint security, network-level intrusion detection, or cloud access control, but do not offer a unified approach capable of detecting unknown, multi-vector attacks across the multi-domain healthcare pipeline. Moreover, current DNN-based ID models require large amounts of training data and long training times to be applied directly in resource-constrained central cloud environments, which is unsafe for real-time deployment. The research questions of this study are as follows: (1) What is the design of a hierarchical DNN architecture to correctly identify malicious activities in multi-domain healthcare dataflows? (2) How to shorten the training time for the center cloud model with high detection accuracy using transfer learning technology? (3) What are the methods for implementing the Capability List-based access control mechanism to ensure fine-grained access control policies in multi-area cloud healthcare systems?

The research is crucial as it addresses the dual challenges of efficiency and accuracy in healthcare cybersecurity. The proposed hypothesis is that a hierarchically structured DNN framework, in which pre-trained edge cloud models can be aggregated into an optimized center cloud model, can achieve high detection accuracy (95%–100%) with much less training time than training a single cloud model at the center. The aims of this research are three-fold: to design a reference architecture for next generation healthcare cyber security architectures, to design a healthcare risk model to clearly describe IT and OT (IT/Operational Technology) threats and their mitigations within multi-domain healthcare systems, and to propose a novel hierarchical DNN strategy that provides cyber security for patient dataflows between IoT devices, Healthcare Edge Clouds, and Healthcare Center Clouds. The approach includes the design of the

deep learning model, supervised learning with data augmentation, weighted cross-entropy loss functions to address class imbalance, and a CP List-based access control system. The outcome of the project is expected to be a trained model with accuracy >95%, reduced training overhead, and a validated access control architecture that can serve as a reference model for deployment in real-world healthcare settings. The current research has several novel contributions to cybersecurity in healthcare. It first introduces a novel hierarchical DNN structure that leverages multi-layer transfer learning between the edge and center cloud tiers, a gap that has not been studied systematically to date in healthcare IoT. Second, it introduces a fine-grained policy enforcement layer built into the cloud security architecture that provides a role-based access control mechanism by encoding the identifiers of users (UID), files (FID), and access rights (AR) in the policy layer. Third, it presents a cross-entropy loss function strategy with weight to address the class imbalance in healthcare threat datasets and enhance the model generalization, and reduce the bias toward the majority threat categories. Finally, it delivers an extensive threat model for the multi-domain health care space, from the IoT, edge, into the cloud layer, to guide future standards and policy frameworks in health IT security. All these contributions contribute to the theory and practice of AI-driven cybersecurity in the next generation of healthcare systems.

2. LITERATURE REVIEW

2.1 Global Theories and Foundations of Cybersecurity in Cloud Healthcare

Cybersecurity in cloud computing has its theoretical basis in several areas, such as information security theory, distributed systems architecture, machine learning, and cryptography. As described by Smith (2023) in Comprehensive Cybersecurity: Protecting the Digital Enterprise, this is the basic model of cloud security, which states that a successful cybersecurity strategy must cover all security layers at once, including network, endpoint, threat detection and incident response. The holistic paradigm is especially salient for multimodal healthcare systems, which have an attack surface made up of diverse, geographically distributed elements. The National Cybersecurity Center's Cybersecurity Framework Initiative (2024) translates this theoretical holism into practical principles and best practices: Risk Assessment, Incident Response Planning, Employee Education Training, and more; offers a systematic methodology that organizations can implement to systematically lower their vulnerability profile. Complementing this framework, Davis (2024) has strengthened the theoretical argument for AI in cyber security, proposing that machine learning algorithms, notably with the aid of deep neural networks, are the most promising method to maneuver threats, speed up reaction times, and foresee new vulnerabilities in intricate and ever-changing environments where human monitoring is insufficient. This theoretical framework is aligned closely with the current study's approach of DNN based detection, which places the research in the context of the scientific community that believes AI is the next major challenge in adaptive cybersecurity.

From the narrow scope of IoT and cloud healthcare security, Thompson (2023) has identified the specific vulnerability profile of IoT medical devices, which are commonly resource-limited, relied upon standard communication protocols, and directly involved in patient care, making them especially appealing to adversarial actors. Thompson suggests more complete security architectures, which include device level hardening and network level anomaly detection, both of which are implemented in this research. In Network Security Essentials, White & Brown further explore how the configuration of firewalls, intrusion detection systems, and secure network architecture design should each be understood as a part of a comprehensive security strategy, not as individual security solutions. In a recent study in Cloud Security Quarterly, Lawson and Myers (2024) explored vulnerabilities on the cloud side, suggesting that alongside other methods of risk reduction in cloud environments, cloud data encryption, access control, and regular security audits would be complementary. In the field of advanced encryption theory, Patel and Singh (2024) explore the concepts of symmetric and asymmetric encryption, as well as the benefits of encrypting

data at rest and in transit for providing a baseline level of security even in the face of a breach at the network level. This body of work provides the theoretical foundation for the design of the integrated DNN based security architecture presented in this study, which combines the DNN with a CP List.

With the increasing convergence of machine learning and cybersecurity, there are significant amounts of literature that have been created directly to support the methodology used in this research. In the AI & Cybersecurity Review (2024), Kramer and Li have comprehensively shown that machine learning algorithms are far more effective at identifying new attacks that haven't been previously seen than traditional rule-based IDS systems, a trait which is essential to the healthcare threat landscape, where adversarial actors are constantly refining their attack strategies. This is echoed by Johnson and Gupta (2024), who report the rapid evolution of new attack vectors against cloud-based healthcare infrastructure requiring the need for continuous monitoring and adaptive machine-learning-based defenses, not just advantages. The Global Cybersecurity Insights Annual Report (2024) backs these statements with detailed threat data across all sectors, showing that healthcare remains the top sector for attacks and that AI-based detection tools achieve the highest accuracy in controlled testing. Hamilton's (2023) historical analysis of the evolution of cyber threats in the Global Security Review provides valuable context as he showed that every new generation of cyber threats has outpaced the corresponding generation of defensive cyber technologies and tools, making the continuous improvement of AI-based tools like the hierarchical DNN developed in this research an operational need for healthcare organizations to safeguard patient information and ensure clinical continuity. The literature cited in this work collectively supports the research hypothesis that a hierarchically structured AI-based security framework would be an improvement over current security frameworks, with the present study's contribution being the specific application of hierarchical transfer learning to the multi-domain healthcare cloud environment.

2.2 Research Gap Addressed

The literature reviewed is comprehensive, but all of it is lacking in providing a solution to the problem of having multiple tiers of healthcare systems that include an IoT, a shore cloud and a center cloud element in one single, unified system. Most previous research focus only a single tier (IoT device security, edge computing security, or cloud-based central security) and are unable to offer a validated, end-to-end architecture that can detect threats in real time throughout the entire multi-domain pipeline. In addition, the literature on healthcare security lacks a systematic study of using hierarchical transfer learning in the training process of large DNN models directly in the central cloud environment. This work fills the above gaps in the literature by introducing a novel hierarchical DNN architecture that combines the advantages of transfer learning, weighted loss functions, and CP List-based access control, and embeds them into a deployable security framework for multi-modal cloud healthcare systems.

3. DATA AND METHODOLOGY

3.1 Theoretical Background

The theoretical approach for this research is based on the combination of deep learning, cloud computing security architecture, and access control theory. Deep Neural Networks (DNNs) are multilayered computational models inspired by biological neural networks that can learn hierarchical representations of features from raw input data by performing successive non-linear transformations (Agarwal, A., 2020). From a cybersecurity perspective, DNNs can be used as pattern-recognition engines that perform statistical anomaly detection in network traffic, payload structure, and metadata, matching existing or emerging attack vectors (Malik, 2019). The hierarchical DNN architecture proposed in this study is an extension of the standard DNN model that uses transfer learning: each edge cloud model is trained with threat data that is locally available, the learned weight configurations are merged and aggregated to create a cloud model in the central cloud that carries the generalized threat representations learned at the edge

(Smith, 2023). This aggregation scheme requires only 35-40 training epochs at the central cloud, but still maintains the detection performance, which is a significant improvement on the computational efficiency of the central cloud.

The capability List (CP List) access control mechanism is based on the theory of Role-Based Access Control (RBAC) and attribute-based cryptography (Johnson, 2024). The CP List model links each data object to a structured record with data to represent the User Identifier (UID), File Identifier (FID), and Access Rights (AR) and allows fine-grained, attribute-driven authorization decisions made at the cloud service provider level (Initiative, 2024). The Data Owner (DO) has the power to specify and change access rights (Joshi, B. D., & Ahn, G.-J. , 2010). The Cloud Service Provider (CSP) enables read operations and privilege management based on the current CP List entries. This architecture is designed to remove the need for trusted third parties and provide transparent and verifiable access control to all cloud service models (Davis, 2024). The cryptographic protection layer uses symmetric encryption using block-based encoding: binary bits are first converted to ASCII characters and then the dataset is segmented into blocks of different sizes (2-bit, 4-bit, or 8-bit bit blocks) and the blocks are encrypted (Modi, C. , 2019). The more bits in the block, the greater number of different keys, the more unpredictable and the more strong the privacy protection, a fundamental principle of security, that is confirmed by classical information-theoretic analysis (White, 2023).

3.2 Data and Variables

The information for this study comes from a structured network security incident dataset created specifically to track multidimensional aspects of cybersecurity incidents in a cloud-integrated healthcare environment (Thompson, 2023). This dataset is designed to be representative of realistic incident scenarios for the multi-area healthcare system architecture, including IoT devices (medical sensors), shore cloud (edge computing) nodes, and center cloud (central storage and analytics) environments (Insights, 2024). The dataset is especially relevant because it represents the four major attack categories in the healthcare threat landscape literature: malware at endpoint devices, unethical attempts to access server level infrastructure, data breach events at mobile endpoint devices, and ransomware attacks on workstations (Franklin, 2024).

The data reflects simulated incidents during June 2024, meaning that it reflects the current threat environment (Cisco, 2019). Temporal metadata is included in each incident record, along with endpoint identifiers and classifications of endpoint types, a categorization of incident types, the detection method used, severity level designation, enumeration of affected systems, assessment of data compromise, measurement of service downtime, response time, mitigation measures implemented, and resolution time (Patel, D., & Singh, K., 2024). Each incident record contains temporal metadata (date and time), endpoint identifiers and classifications of endpoint types, a categorization of the incident types, the detection method, severity level designation, affected systems enumeration, assessment of data compromise, measurement of service downtime, response time, mitigation measures implemented, and resolution time, as well as a summary of the post incident analysis and a status indication of preventive measures implemented, and user awareness training status (Labovitz, C., Iekel-Johnson, S., McPherson, D., Oberheide, J., & Jahanian, F., 2010). This complete set of variables allows the DNN model to learn from the characteristics of the attacks as well as from response and mitigation patterns, helping both detection and response optimization (Harris, B., 2023).

3.3 Variable Identification

Table 1 presents the complete variable identification framework, classifying each variable as dependent or independent and specifying its role in the DNN training and evaluation pipeline.

Variable	Abbreviation	Type	Role	Data Source
Detection Accuracy	DA	Dependent	Primary outcome: proportion of correctly classified incidents	Model Output
Training Loss	TL	Dependent	Weighted cross-entropy loss across training epochs	Model Output
Training Time (Epochs)	TTE	Dependent	Number of epochs to converge in the center cloud	Model Output
Incident Type	IT	Independent	Categorical: Malware, Unauthorized Access, Data Breach, Ransomware	Dataset
Endpoint Type	ET	Independent	Categorical: Workstation, Server, Mobile Device	Dataset
Severity Level	SL	Independent	Ordinal: Low, Medium, High, Critical	Dataset
Detection Method	DM	Independent	Categorical: IDPS, Firewall, EDR, Encryption	Dataset
Response Time	RT	Independent	Continuous (minutes): Time to initial incident response	Dataset
Service Downtime	SD	Independent	Continuous (minutes): Duration of service unavailability	Dataset
Preventive Measures	PM	Independent	Binary/Categorical: Measures in place before the incident	Dataset
User Awareness Training	UAT	Independent	Binary: Yes/No for security training completion	Dataset
Block Size	BS	Independent	Categorical: 2-bit, 4-bit, 8-bit encryption block size	Cryptographic Layer
Edge Cloud Model Weight	ECMW	Independent	Continuous: Pre-trained weight vectors from edge models	Pre-training Phase

Table 1: Variable Identification and Classification

3.4 Data Sources and Time Span

Table 2 summarizes the data sources, variables, abbreviations, time span, and data repositories used in this study.

Data Source	Variables Provided	Abbreviation	Time Span	Data Bank / Repository
Simulated Healthcare Network Security Dataset	Incident type, endpoint, severity, response metrics	HNSD	June 2024	GC University Hyderabad Research Lab
Global Cybersecurity Insights Annual Report	Threat landscape, attack frequencies, sector-level incidence	GCIAR	2020–2024	Geneva: Cybersecurity International
National Cybersecurity Framework Initiative	Best practices, risk categories, control benchmarks	NCFI	2024	Washington D.C.: National Cybersecurity Centre
Cloud Security Alliance (CSA) Guidelines	Cloud security domains, control specifications	CSA	2019–2024	Cloud Security Alliance
Healthcare Ransomware Claims Data	Ransomware incident frequency, sector distribution	HRCD	2013–2023	Insurance Sector Aggregate Reports
DNN Training Output Logs	Accuracy curves, loss curves, epoch convergence data	DTOL	2024 (Experimental)	Research Laboratory Environment

Table 2: Data Sources, Variables, and Repositories

3.5 Methodological Framework

The methodology involves four interdependent phases: (1) Datasets construction and preprocessing, (2) Design and pre-training of a hierarchical DNN model at the edge-cloud, (3) Assembly of the center cloud model by weight aggregation, and (4) Evaluation with and without data augmentation (Lawson, G., & Myers, J., 2024). Raw incident records are processed in preprocessing to be converted to ASCII character strings and then into fixed-size binary bits (Devi, G., Manogaran, G., Sundarasekar, R., Chilamkurti, N., & Varatharajan, R., 2018). The DNN has a multi-dimensional input layer to accept feature vectors of the incident, two hidden layers to learn complex inter-feature relations and anomalous patterns, and an output layer that outputs threat classifications (categorical) and anomaly probability scores (Norton, C., 2023).

To address class imbalance in the incidents, the loss function used during training is weighted cross-entropy (Ukil, A., et al., 2013). The standard cross-entropy loss for a single training example x_i with label y_i is:

$$L_{xess}(x_i) = -(y_i \cdot log(f(x_i)) + (1 - y_i) \cdot log\ (1 - f(x_i)))$$

The overall average cross-entropy loss over the complete training set D of size N is expressed as:

$$L_{xess}(D) = -(1/N)\ (\Sigma_{positive}\ log(f(x_i)) + \Sigma_{ne}{}^{g}{}_{ative}\ log\ (1 - f(x_i)))$$

To address class imbalance, a weighted cross-entropy formulation is applied:

$$L_{lxess}(x) = -(w_p \cdot y \cdot log(f(x)) + w_n \cdot (1 - y) \cdot log\ (1 - f(x)))$$

where w_p and w_n are weighting coefficients assigned to positive (attack) and negative (normal) examples, respectively, calibrated to balance the contribution of minority and majority classes in the loss computation (Cyber Defense Magazine, 2024). The edge cloud training phase employs 35–40 epochs per edge model to ensure sufficient convergence with locally available data (Fazlullah, et al., 2017). The aggregated center cloud model is then fine-tuned over only 6–8 epochs, leveraging the transferred

knowledge to rapidly adapt to the comprehensive multi-domain threat environment while achieving accuracy benchmarks of 95–100% (Edwards, V. , 2024).

Information is added to the unbalanced center cloud training distribution to augment the training process in the final phase of training in the center cloud using an Image Data Generator paradigm adapted to tabular incident data, to create synthetic variations of underrepresented incident types to further balance the training distribution and improve generalization of the model to unseen attack types (Schwartz, L. , 2023). The Capability List (CP List) integration is a layer of middleware between the cloud security architecture and the CP List, and contains entries validated each time they are accessed, via a Pseudorandom Number Generator (PRNG) based mechanism that is hard to predict adversarially (Kramer, T., & Li, Y. , 2024).

4. RESULTS

4.1 Network Security Incident Dataset

Table 3 shows the main network security incident logs collected and used for training and evaluating the DNN. Each record contains information about the incident identifier, the incident type, temporal metadata, endpoint information, the response, and the mitigation outcomes (Na, H., Park, J.-Y., & Huh, E.-N. , 2010). The dataset covers the four major types of health care cyberattacks in the literature: malware, unauthorized access, data breaches, and ransomware. Within these categories, there is substantial variation in how quickly some detection systems respond and resolve, both of which indicate the effectiveness of the detection system (Tariq, I., 2019). Malware events had the shortest detection time (10 minutes) and resolution time (40 minutes) compared to other malware events, highlighting that the existing AV and firewall technology is mature (Gaurav Pal, D., et al., 2012). By comparison, ransomware cases took the longest to resolve (240 minutes), highlighting the operational disruption and forensic challenges posed by this attack vector (Mahdavinejad, M. S., et al., 2018). Healthcare organizations need to focus on ransomware-specific response plans and dedicated recovery infrastructure to minimize downtime (Malik, M. N. , 2012).

ID	Incident Type	Date/Time	Endpoint ID	Endpoint Type	Resp. Time (min)	Resolution (min)
001	Malware	2024-06-01 10:30	EP-1001	Workstation	10	40
002	Unauthorized Access	2024-06-05 14:45	EP-1002	Server	15	120
003	Data Breach	2024-06-10 09:00	EP-1003	Mobile Device	5	180
004	Ransomware	2024-06-15 11:20	EP-1004	Workstation	20	240

Table 3: Network Security Incident Dataset

The economic justification for these findings is simple: different types of attacks cost the healthcare organization different amounts, depending on how much they can get into, the impact of the loss of certain resources, and the difficulty of recovery (Talib, M., 2010). Workstation-level malware can be disruptive, but it is limited to individual endpoints and can be addressed through Workstation Quarantine and Antivirus Remediation (Hamilton, R., 2023). Unauthorized access to servers poses a greater risk, as it can

lead to exposure of administrative credentials and lateral movement within the healthcare network (Rosa, S. L., & Kadir, E. A., 2018). Mobile device data breaches have legal consequences in healthcare data privacy laws and regulations (Monica, M., 2012). Ransomware attacks that encrypt critical healthcare data for ransomware payments for decryption keys are the most expensive threat to operate and deserve a higher priority for detection (and a priority that is accelerated by AI).

4.2 Response and Mitigation Outcomes

Table 4 shows an overview of the incidents categorized by mitigation measures, post-incident analysis, preventive status, and user training status (Martinez, F., 2024). They show that endpoints without user awareness training took a longer time to respond to an incident and caused a high amount of operational disruption, while those with training responded more quickly and effectively mitigated (Sirohi, A., & Agarwal, A. , 2015). This discovery directly supports the policy implication that all healthcare staff should undergo mandatory, routine cybersecurity training – a worthwhile preventive investment (Lee, Y., & Lee, Y. , 2013). The proposed DNN detection framework is anticipated to augment human awareness training by enabling automated, real-time threat detection, regardless of individual human operators' training status, thereby reducing response time (Bennett, A., 2023).

Resp. Time	Mitigation Measure	Resolution Time	Post-Incident Analysis	Preventive Measures	User Training
10 min	Quarantine File	40 min	Malware detected and quarantined	Antivirus, Firewall	Yes
15 min	Block User Account	120 min	Unauthorized access attempt blocked	EDR, Access Control	No
5 min	Wipe Device	180 min	Data breach contained; forensic analysis ongoing	Encryption, User Training	Yes
20 min	Reimage Device	240 min	Ransomware attack mitigated; device reimaged	Antivirus, Regular Backups	Yes

Table 4: Response and Mitigation Outcomes by Incident Type

4.3 DNN Model Performance: Training and Test Accuracy

The key performance metrics of the proposed hierarchical DNN under two training conditions, (A) without data augmentation and (B) with data augmentation using the Image Data Generator, are presented in Table 5. The findings show that the model performs well under both conditions, achieving training and test accuracies in the range of 95% to 100% across all categories, with test accuracy improving slightly with data augmentation for the less frequently occurring incident categories (Walters, P., & Zhou, X., 2023). The average training time of the center cloud model at the same epoch is 26.2% of the epoch required for the model to converge when training is performed individually, as predicted by the theory of the hierarchical transfer learning strategy (Panel, 2024). Policy implication: Health care providers using AI-powered cybersecurity solutions must implement hierarchical edge-center AI training architectures to reduce computing costs and enable quicker deployment of new threat models as the attack surface evolves (Turner, D. , 2024).

Metric	Without Augmentation	With Augmentation	Improvement
Training Accuracy	95.2%	97.8%	+2.6%
Test Accuracy	96.4%	99.1%	+2.7%
Training Epochs (Center Cloud)	7 epochs	8 epochs	~6–8 range maintained
Training Epochs (Edge Cloud)	35–40 epochs	35–40 epochs	Baseline (unchanged)
Training Time Reduction	25.8%	26.2% (avg)	+0.4%
False Positive Rate	3.2%	1.6%	−1.6% (improvement)
Weighted Cross-Entropy Loss	0.087	0.054	−0.033 (improvement)

Table 5: DNN Model Performance Metrics

The trade-off between the model's generalization and the quality of the training data that underlies these performance results is fundamental (Donovan, M., 2024). The increase in test accuracy (+2.7%) further validates that synthetic data generation is a viable solution to the scarcity of labeled data in healthcare security, a frequent challenge where real incident data is often sensitive and inaccessible (Security Solutions Web , 2024). The impact of reducing the false positive rate from 3.2% to 1.6% is especially clinically relevant because false positives in healthcare security systems create unnecessary alerts and divert healthcare professionals' time from patient care, adding indirect healthcare costs to the direct expenses of these systems.

5. DISCUSSION

The findings from this study are substantive and lead to six main findings that collectively contribute to the knowledge of AI-based cybersecurity in multimodal cloud healthcare environments. The existing literature and research hypotheses are discussed for each finding and the implications for healthcare organizations and policymakers are discussed.

The hierarchical DNN framework delivers consistently high training and test accuracy within the range of 95% to 100%, thus proving the research hypothesis that a transfer-learning enhanced architecture can achieve the same or better detection performance when compared to center cloud models trained independently. This finding is in line with the theory proposed by Kramer and Li (2024), which states that machine learning algorithms are better suited for detecting new attack patterns than rule-based intrusion detection systems, and directly applied to the multi-domain healthcare environment. High accuracy range shows that the hierarchical aggregation of edge cloud weights does not lose much threat-detection knowledge in transferring it to the center cloud, allowing for accurate classification of attack categories not seen before in the center cloud.

Second, the proposed framework reduces the training time of center cloud by 26.2% on average, taking merely 6-8 center cloud training epochs to reach the same performance as standalone edge cloud models need 35-40 epochs to do so. The computational advantage has practical consequences such as the ability to deploy new threat models quickly when new attack variations emerge, lower cloud computing costs for

new model training, and being able to implement continuous learning architectures where new threat models can be pushed to the cloud on an almost real-time basis as new incidents are reported. This is in line with the larger body of research on the efficiency of pre-training on domain-specific data, which also portends a significant reduction in the learning load for target-domain models.
Third, adding the CP List access control mechanism offers a structured, verifiable and role-based access control layer on top of the DNN detection mechanism. The CP List is a representation of the access rights of a user encoded into UID-FID-AR, thereby removing the need for trusted third-party authentication intermediaries used in many current cloud healthcare access control implementations. This architectural autonomy is especially useful in multi-cloud healthcare settings where information moves across a range of administrative realms with possible divergent trust policies. The CP List's ability to allow fine-grained access differentiation, granting the Data Owner the right to modify data while the Cloud Service Provider applies read operations, addresses the data sovereignty issue identified by Lawson and Myers (2024) as a key security weakness in cloud applications.

Fourth, by minimizing the maximum false positive rate, the use of a weighted cross-entropy loss function brings down the false positive rate from 3.2% to 1.6% for the DNN. This is important as false-positive alerts have two costs: in the healthcare setting, investigative resources are wasted on false-positive alerts and in the security realm, alert fatigue creates a negative effect on the ability to respond to real incidents. The weighted loss approach, therefore, enhances the performance of the statistical models as well as the effectiveness of operational security.

Fifth, there is a consistent inverse relationship between the sophistication of the prevention measure used and the time to detect, contain and resolve an incident, as incidents at endpoints with multi-layered preventative infrastructure (antivirus, firewall, EDR, encryption, user training) consistently show faster detection, containment, and resolution times than those at endpoints with limited or absent preventative measures. This finding reinforces the work by Franklin (2024) which identified preparedness and post-incident analysis as key factors to consider when evaluating response effectiveness and supports quantitative evidence of the policy recommendation that healthcare organizations should focus on multi-layer preventive architectures, rather than reliance on response detection, alone.

Sixth, compared to the non-data-augmented training, the data augmentation strategy using an Image Data Generator makes an accuracy gain of 2.7% on the test set, while reducing the weighted cross-entropy loss by 0.033 units. This finding confirms that synthetic data generation is a promising and computationally efficient technique to overcome the limitation of having too few labelled instances in the healthcare cyberattack field, which has hindered the creation of high-performance supervised learning models. The application of the AI security model is that even in the absence of large, external validated labeled datasets, healthcare data can be artificially expanded and balanced via data augmentation and used in the training of the AI security model for deployment.

6. CONCLUSION

6.1 Summary of Key Findings

The key findings are summarized below. The key findings are summarized below:
In this research work, a novel hierarchical Deep Neural Network (DNN) framework for cybersecurity optimization in multi-modal cloud healthcare environments has been proposed, implemented, and evaluated. This framework fills a missing void in the literature by enabling a single, efficient, and secure security framework for the protection of IoT devices, the shore cloud nodes (edge computing), and the center cloud nodes (central storage). This research was conducted to summarize the key findings as follows.

The core hypothesis of transferring pre-trained edge cloud model weights to center cloud model to get high threat detection accuracy without full independent training at the center cloud level was consistently verified by the hierarchical DNN architecture under all the experimental conditions. The 26.2% reduction in training time achieved with hierarchical weight aggregation shows that the two goals of computational efficiency and detection performance are not mutually exclusive and help counterbalance an important tension in the current cybersecurity literature. The Capability List (CP List) access control mechanism successfully enforces fine-grained and role-specific authorization policies in multi-cloud healthcare environments, offering a practical implementation of attribute-based access control (ABAC) that does not require trusted intermediaries to be centrally trusted. The use of weighted cross-entropy loss functions significantly reduced the false positive rate from 3.2% to 1.6% compared to standard training, highlighting substantial improvements in the operational utility of AI-based security systems in real healthcare environments. The use of the Image Data Generator consistently improved results across all metrics, further indicating that generating synthetic data is a useful strategy to address the problem of limited labeled data in the healthcare cybersecurity domain. The comparative analysis of incident response and resolution times by attack category provided quantitative evidence that multi-layered preventive infrastructure, in conjunction with mandatory user awareness training, can significantly affect the operational consequences of cyberattacks on healthcare organisations.

6.2 Policy Implications

This research's results have a number of direct policy implications for healthcare organizations, regulators, and technology policymakers. Healthcare organizations should require the use of hierarchical AI security solutions as a standard part of their cybersecurity portfolio, as a first step. The proposed DNN architecture's ability to achieve detection accuracy above 95% and training overhead less than 100 while maintaining a moderate number of trainable parameters renders it operationally viable for healthcare organizations, regardless of their size and available resources. Regulatory frameworks for cybersecurity in the healthcare sector, including those set by national cybersecurity centres, should include this hierarchical detection method as a best practice and, for situations where sensitive patient data is handled, as a minimum technical requirement.

Second, policymakers should create standardized data governance frameworks that enable healthcare organizations to share anonymized cyberattack incident data for model training without compromising their obligations to protect patient privacy. Overall, the results of this study highlight the need for more data to improve the performance of AI models in healthcare cybersecurity, as well as the potential of federated learning architectures and privacy-preserving data-sharing protocols to both increase the available training data for AI models and ensure compliance with healthcare data protection regulations. Healthcare regulatory agencies need to issue specific directives on responsible data-sharing practices in the context of a cybersecurity attack and introduce new legal structures that encourage data sharing and the exchange of threat intelligence across the healthcare sector and jurisdictions.

Third, empirical evidence that user awareness training is associated with significantly faster incident response and containment times supports the need for mandatory, regularly updated cybersecurity training for all health care personnel. Healthcare policymakers should mandate that security awareness training programs are offered by healthcare organizations and that there is verifiable evidence of a comprehensive security awareness training program. Training programs should be integrated into the cybersecurity cost center, just as investments in technical infrastructure are, to more accurately calculate the return on investment associated with human-centered security measures.

6.3 Limitations

However, the study has its limitations, and these need to be addressed to ensure that the study findings can be appropriately interpreted and future research directions. The main constraint is the size of the data

set used for model training and testing: the incident dataset was built from a simulated healthcare network security environment based on incident scenarios from June 2024, rather than real-world operational healthcare data. This method is essential for addressing privacy restrictions on real patient and incident data, but it poses the risk that the simulated data may not accurately reflect the full distributional complexity of real-world cyberattacks in healthcare. Sophisticated, multi-stage Advanced Persistent Threat (APT) attacks, which are increasingly a significant component of major healthcare cyber incidents, may exhibit characteristics not well represented by the four incident types used in this study (malware, unauthorized access, data breach, or ransomware). Moreover, the evaluation has been conducted in a laboratory setting, and the performance outcomes, although very encouraging, may be affected in a real-world healthcare network deployment with diverse hardware, changing network configurations, and traffic dynamics. The CP List access control mechanism was tested in a simulated single-organization cloud environment, and its performance in multi-organization, multi-jurisdictional healthcare environments with multiple cloud providers and regulatory requirements needs further evaluation. Lastly, the research was mostly limited to detection and access control, rather than automated threat response and remediation as this aspect is a critical complement to detection performance in production healthcare security environments.

6.4 Future Research Directions

The results of this study and its limitations suggest several avenues for future research. Second, future research should build on the hierarchical DNN model by incorporating federated learning architectures that enable multiple healthcare organizations to jointly train a common threat detection model without sharing raw incident data. Federated learning would overcome the data scarcity constraint identified in this research and adhere to healthcare data protection policies and regulations, enabling the creation of industry-wide threat detection models with much wider coverage of training data than any single organization could achieve on its own. Second, future research should focus on extending the CP List access control mechanism to accommodate cross-organizational, multi-cloud architectures with multiple competing cloud service providers and heterogeneous regulatory regimes, as well as formal verification techniques to demonstrate the security properties of the extended mechanism in adversarial environments. Thirdly, automated threat response is a logical and essential progression of the detection framework advanced in this research, including dynamic rule updates on the firewall, automated isolation of infected network segments, and AI-based forensic analysis. Research into reinforcement learning-based response optimisation, in which the AI system learns to select the best mitigation for an incident based on the incident type, severity, and historical resolution patterns, would greatly enhance the operational value of an AI-driven cybersecurity system for healthcare. Finally, empirical studies that assess the effectiveness of the proposed framework in real healthcare settings over extended periods, monitor model accuracy, track false-positive trends, and evaluate detection coverage in a changing threat landscape would enable regulatory adoption of AI-based cybersecurity standards in the healthcare sector.

Funding: Funding is inappropriate for this research study.
Data availability: The statistics supporting the outcomes of this research are accessible upon reasonable request from the first author.

Declarations

Ethical approval: Not applicable
Consent to participate: Not applicable
Consent to publish: All authors have given consent to publish.
Competing interest: The authors have no competing interests to declare.

References

1. Agarwal, A. (2020). *Cloud computing data storage security framework addressing data integrity, privacy, and trust.* .IEEE Transactions on Cloud Computing.
2. Bennett, A. (2023). *Application Security Frameworks.* . London: CyberPress.
3. Cisco. (2019). *Global Fixed and Mobile Internet Traffic Forecasts.* . Cisco Systems.
4. Cyber Defense Magazine. (2024). *Guide to Modern Security Protocols.* New York: CDM Publishing.
5. Davis, M. (2024). *The role of artificial intelligence in cybersecurity.* . Tech Innovations Journal, 12(3), 78–92.
6. Devi, G., Manogaran, G., Sundarasekar, R., Chilamkurti, N., & Varatharajan, R. (2018). *Ant colony optimization algorithm with Internet of Vehicles for intelligent traffic control system. Computer Networks.* 29.doi: 10.1016/j.comnet.2018.07.001.
7. Donovan, M. (2024). *Risk management strategies in cybersecurity.* . 23.Risk and Compliance Journal, 19(1), 44–62.
8. Edwards, V. . (2024). *Human factors in cybersecurity.* Human-Computer Interaction and Security, 16(3), 142–159.
9. Fazlullah, et al. (2017). .*State-of-the-art deep learning: Evolving machine intelligence toward tomorrow's intelligent network traffic control systems.* 31.State-of-the-art deep learning: Evolving machine intelligence toward tomorrow's intelligent network traffic control systems. IEEE Communications Surveys & Tutorials. doi: 10.1109/COMST.2017.2707140.
10. Franklin, P. (2024). *Strategies for effective incident response.* 9.Security Management Review, 17(4), 204–223.
11. Gaurav Pal, D., et al. (2012). *A novel open security framework for cloud computing.* . International Journal of Cloud C.
12. Hamilton, R. (2023). *The evolution of cyber threats: A historical perspective.* . 18.Global Security Review, 14(1), 22–44.
13. Harris, B. (2023). *Endpoint Security Solutions.* . .Boston: Tech Innovations Publishing.
14. Initiative, C. F. (2024). *Best Practices for Securing IT Infrastructure.* . Washington, D.C.: National Cybersecurity Centre.
15. Insights, G. C. (2024). *Annual Report on Cyber Threat Landscape.* . .Geneva: Cybersecurity International.
16. Johnson, L. &. (2024). *Latest trends in cybersecurity threats.* .Journal of Information Security, 25(1), 15–35.
17. Joshi, B. D., & Ahn, G.-J. . (2010). *SecureCloud: Towards a comprehensive security framework for cloud computing environments.* IEEE.
18. Kramer, T., & Li, Y. . (2024). *Machine learning applications in cybersecurity.* . .AI & Cybersecurity Review, 8(2), 99–118.
19. Labovitz, C., Iekel-Johnson, S., McPherson, D., Oberheide, J., & Jahanian, F. (2010). . *Internet inter-domain traffic.* . ACM SIGCOMM. doi: 10.1145/1851275.1851194.
20. Lawson, G., & Myers, J. (2024). *Mitigating risks in cloud computing.* . .Cloud Security Quarterly, 14(1), 34–56.
21. Lee, Y., & Lee, Y. . (2013). *41.Toward scalable internet traffic measurement and analysis with Hadoop.* . Computer Communication Review. doi: 10.1145/2427036.2427038.
22. Mahdavinejad, M. S., et al. (2018). .*Machine learning for Internet of Things data analysis: A survey.* . Digital Communications and Networks. doi: 10.1016/j.dcan.2017.10.002.
23. Malik, A. (2019). *Security Guidance for Critical Areas of Focus in Cloud Computing.* . Cloud Security Alliance (CSA), April 2019.

24. Malik, M. N. . (2012). *36.Security framework for cloud computing environment: A review.* . Journal of Emerging Trends in Computing and Information Sciences, 3.
25. Martinez, F. (2024). . *Data security in multi-cloud environments.* . Cloud Computing Security, 6(3), 77–95.
26. Modi, C. . (2019). *Designing an efficient security framework for detecting intrusions in virtual network of cloud computing.* Science Direct, 85, 402–422.
27. Monica, M. (2012). *Enhanced security framework to ensure data security in cloud computing using cryptography.* . Advances in Computer Science and its Applications, 1.
28. Na, H., Park, J.-Y., & Huh, E.-N. . (2010). *Personal cloud computing security framework.* IEEE.
29. Norton, C. (2023). *Understanding cybersecurity regulations.* Regulatory Affairs Journal, 20(2), 58–79.
30. Panel, C. B. (2024). *42.Recommendations for Financial Sector Security.* . Industry Report.
31. Patel, D., & Singh, K. (2024). *Encryption techniques for data protection.* Data Security Journal, 11(1), 45–67.
32. Rosa, S. L., & Kadir, E. A. (2018). *.Abnormal internet usage detection in LAN Islamic University of Riau Indonesia.* . Proceedings of the International Conference on Intelligent Science and Technology (pp. 17–22).
33. Schwartz, L. . (2023). *The impact of cyber-attacks on small businesses.* . 16.Small Business Journal, 31(4), 200–218.
34. Security Solutions Web . (2024). *43.Recent innovations in intrusion detection systems.* . Security Solutions Online.
35. Sirohi, A., & Agarwal, A. . (2015). *Cloud computing data storage security framework relating to data integrity, privacy and trust.* IEEE.
36. Smith, J. (2023). *Comprehensive Cybersecurity: Protecting the Digital Enterprise.* .New York: Tech Press.
37. Talib, M. (2010). *Security framework of cloud data storage based on multi-agent system architecture: Semantic literature review.* . Computer and Information Science, 3.
38. Tariq, I. (2019). *33.Agent-based information security framework for hybrid cloud computing.* . KSII Transactions on Internet and Information Systems, 13(1), 406–434.
39. Thompson, H. (2023). *Cybersecurity in the age of IoT.* .Internet of Things Analysis, 9(2), 112–130.
40. Turner, D. . (2024). *Securing wireless networks.* Wireless Security Digest, 11(2), 58–74.
41. Ukil, A., et al. (2013). *A security framework in cloud computing infrastructure.* A security framework in cloud computing infrastructure. International Journal of Network Security & Its Applications, 5.
42. Walters, P., & Zhou, X. (2023). *vances in biometric security technologies.* 21.Ad. Journal of Biometric Security, 9(1), 31–49.
43. White, S. &. (2023). *Network Security Essentials.* . London: Global IT Publishing.